12-2011

Characterization of the Mechanism of PPARγ-Mediated Neointima Formation in Rodents

Ryoko Tsukahara
University of Tennessee Health Science Center

Characterization of the Mechanism of PPARγ-Mediated Neointima Formation in Rodents

DOI
10.21007/etd.cghs.2011.0324

CHARACTERIZATION OF THE MECHANISM OF PPARγ–MEDIATED NEOINTIMA FORMATION IN RODENTS

A Dissertation
Presented for
The Graduate Studies Council
The University of Tennessee
Health Science Center

In Partial Fulfillment
Of the Requirements for the Degree
Doctor of Philosophy
From The University of Tennessee

By
Ryoko Tsukahara
December 2011

DEDICATION

This dissertation is dedicated to my family:
Tamotsu Tsukahara
Keiji and Mutsuko Fukuda
Yoshihito and Sumiko Fukuda
Yoshitaka and Akiko Tsukahara

ACKNOWLEDGEMENTS

I would like to express my deepest gratitude to my advisor, Dr. Gabor Tigyi, for his guidance, patience, encouragement, and providing me with an excellent atmosphere for doing research. He taught me many things, especially he taught me how to think scientifically and present professionally.

I would also like to thank all past and present members in Dr. Tigyi's lab: Yuko Fujiwara, Billy Valentine, James Fells, Alyssa Bolen, Junming Yue, Diana Liu, Sue-Chin Lee, Nora Nusser, Gyongyi Kiss, Yaohong Wang, Daniel Osborne, Huazhag Guo, and Shuyu E.

I am heartily thankful to my committee members: Dr. Abby Parrill, Dr. Edwards Park, Gadiparthi Rao, and Dr. Polly Hofmann for their support, guidance, and valuable suggestions.

I would like to thank Drs. Chunxiang Zhang and Yunhui Cheng for providing me the animal experiment protocol and the techniques. I would also like to thank Dr. Nikhlesh Singh for his help with the immunohistochemical staining protocol and his advice.

I greatly appreciate the support of J. Paul. Quigley Memorial Scholarship and the Dorothy K. and Daniel L. Gerwin Graduate Scholarship.

Finally, I would like to thank my husband, Tamotsu Tsukahara, for his support and great patience at all times. I also thank my parents, my brother and sister, and my parents-in-law. They were always supporting me and encouraging me with their best wishes.

ABSTRACT

Lysophosphatidic acid (LPA) and its ether analog alkyl glycerophosphate (AGP) elicit arterial wall remodeling when applied intralumenally into the uninjured carotid artery. LPA is the ligand of eight GPCRs and the peroxisome proliferator-activated receptor γ (PPARγ). We pursued a gene knockout strategy to identify the LPA receptor subtypes necessary for the neointimal response in a non-injury model of carotid remodeling and also compared the effects of AGP and the PPARγ agonist rosiglitazone (ROSI) on balloon injury-elicited neointima development. In the balloon injury model AGP significantly increased neointima; however, rosiglitazone application attenuated it. AGP and ROSI were also applied intralumenally for 1 hour without injury into the carotid arteries of LPA_1, LPA_2, $LPA_{1\&2}$ double knockout, and Mx1Cre-inducible conditional PPARγ knockout mice targeted to vascular smooth muscle cells, macrophages, and endothelial cells. The neointima was quantified and also stained for CD31, CD68, CD11b, and α-smooth muscle actin markers. In LPA_1, LPA_2, $LPA_{1\&2}$ GPCR knockouts, Mx1Cre transgenic, $PPAR\gamma^{fl/-}$, and uninduced Mx1Cre×$PPAR\gamma^{fl/-}$ mice AGP- and ROSI-elicited neointima was indistinguishable in its progression and cytological features from that of WT C57BL/6 mice. In $PPAR\gamma^{-/-}$ knockout mice, generated by activation of Mx1Cre-mediated recombination, AGP and ROSI failed to elicit neointima and vascular wall remodeling. Our findings point to a difference in the effects of AGP and ROSI between the balloon-injury- and the non-injury chemically-induced neointima. The present data provide genetic evidence for the requirement of PPARγ in AGP- and ROSI-elicited neointimal thickening in the non-injury model and reveal that the overwhelming majority of the cells in the neointimal layer express α-smooth muscle actin.

Cyclic phosphatidic acid (1-acyl-2,3-cyclic-glycerophosphate, CPA), one of nature's simplest phospholipids, is found in cells from slime mold to humans and has largely unknown function. We find that CPA is generated in mammalian cells in a stimulus coupled-manner by phospholipase D2 (PLD2), and binds to and inhibits the nuclear hormone receptor PPARγ with nanomolar affinity and high specificity through stabilizing its interaction with the corepressor SMRT. CPA production inhibits the PPARγ target-gene transcription that normally drives adipocytic differentiation of 3T3-L1 cells, lipid accumulation in RAW264.7 cells and primary mouse macrophages, and arterial wall remodeling *in vivo*. Inhibition of PLD2 by shRNA, a dominant negative mutant, or a small molecule inhibitor blocks CPA production and relieves PPARγ inhibition. We conclude that CPA is a novel second messenger and a physiological inhibitor of PPARγ, revealing that PPARγ is regulated by endogenous agonists as well as by antagonists.

PPARγ is a nuclear hormone receptor related to many human diseases, including obesity, atherosclerosis, diabetes, and cancers. Recent studies have provided evidence that LPA and its analog AGP activate PPARγ. On the other hand, CPA, similar in structure to LPA, can be generated by PLD2 and negatively regulates PPARγ functions. PPARγ agonists elicit lipid accumulation in macrophages and arterial wall remodeling

when topically applied to the carotid artery in the rat non-injury model. Stimulation of PLD2 protects the carotid artery from PPARγ-mediated neointima formation. Consistent with this, inhibition of PLD2 activity using a PLD inhibitor, 5-fluoro-2-indolyl des-chlorohalopemide, diminishes the protective effect of insulin. Stimulation of PPARγ by AGP leads to the recruitment of circulating vascular progenitor cells into the vessel wall and the cells of the ensuing neointima express the α-smooth muscle actin marker. We summarize our current knowledge about the mechanism of PPARγ elicits in response to the endogenous lysophosphatidic acid analogs LPA, AGP, CPA, and the methodological challenges that one faces when working on the intracellular action of LPA.

TABLE OF CONTENTS

LIST OF FIGURES

LIST OF ABBREVIATIONS

AC	acetylated
ACox-luc	acetyl CoA-oxidase-luciferase
AG	alkyl glycerol
AGP	alkyl glycerophosphate
αSMA	alpha-smooth muscle actin
ATP	adenosine triphosphate
ATX	autotaxin
cAMP	3'-5'-cyclic adenosine monophosphate
Capn3	calpain 3
CD	cluster of differentiation
CDC	cell division cycle
CGP	1-O-octadecyl-2,3-cyclic-glycerophosphate
CI	catalytically inactive
CPA	1-acyl-2,3-cyclic-glycerophosphate
Cre	cre recombinase
Csf1	colony stimulating factor 1
CTGF	connective tissue growth factor
CXCL	C-X-C chemokine ligand
Cyp27a1	cytochrome P450-27a1
DKO	double knockout
DOX	doxycycline
EDG	endothelial differentiation gene
Egr	early growth response
FABP4	fatty acid binding protein 4
FATP	fatty acid transport protein
FFA	free fatty acid
FIPI	5-fluoro-2-indolyl des-chlorohalopemide
G3P	glycerol 3-phosphate
GPAT	glycerophosphate acyltransferase

GPCR	G protein-coupled receptor
Hadh	hydroxyacyl-CoA dehydrogenase
KO	knockout
LBD	ligand binding domain
LC-MS	liquid chromatography mass spectrometry
LDL	low density lipoprotein
LPA	lysophosphatidic acid
LPA_{1-6}	LPA receptor 1-6
LPC	lysophosphatidyl choline
LPS	lipopolysaccharide
lysoPLD	lysophospholipase D
lyso-PtBuOH	lysophosphatidyl butanol
MAPK	mitogen-activated protein kinase
MCP	monocyte chemoattractant protein
MOI	multiplicity of infection
mox-LDL	mild oxidation of LDL
Mx1	myxovirus resistance 1
NCoR	nuclear receptor corepressor
NOS	nitroi oxide synthase
OA	oleic acid
OG	oleoyl glycerol
ORO	oil red O
PA	phosphatidic acid
PBS	phosphate based saline
PC	phosphatidyl choline
PEPCK	phosphoenolpyruvate carboxykinase
PGC-1α	peroxisome proliferator-activated receptor gamma coactivator-1alpha
PGJ_2	prostaglandin J_2
PIP_2	phosphatidylinositol-4,5-bisphosphate
PKC	protein kinase C

PLD	phospholipase D
PMA	phorbol myristate acetate
PPARα, β/δ, γ	peroxisome proliferator-activated receptor alpha, beta/delta, gamma
PPRE	peroxisome proliferator response element
RLU	relative light unit
ROSI	rosiglitazone
RXRα	retinoid X receptor alpha
S1P	sphingosine-1-phosphate
SAR	structure-activity relationship
siRNA	small interfering RNA
SMRT	silencing mediator of retinoid and thyroid hormone receptor
t-BuOH	tertiary-butanol
TLC	thin layer chromatography
TZD	thiazolidinedione
VCAM	vascular cell adhesion molecule
VEGF	vascular endothelial growth factor
VSMC	vascular smooth muscle cell
WT	wild-type
1-BuOH	1-butanol

CHAPTER 1. GENERAL INTRODUCTION

1.1 LPA RECEPTORS AND SIGNALING

1.1.1 The Lysophosphatidic Acid Family

Lysophosphatidic acid (LPA) is a naturally occurring simple phospholipid that functions as a bioactive lipid mediator and a second messenger. It is made up of a glycerol backbone with a hydroxyl group, a phosphate group, and a long-chain saturated or unsaturated fatty acid (Figure 1-1). Different molecular species of LPA, dominated by 16-, 18-, and 20-carbon chains, have been detected in biological fluids and elicit a wide variety of biological actions including cell proliferation, migration, morphologic changes, and survival.

Alkyl glycerophosphate (AGP; Figure 1-1) is an alkyl-ether analog of LPA. It is abundant in brain tissue, found in egg yolk and saliva (Sugiura et al., 1999, Nakane et al., 2001). AGP is a weak agonist of plasma membrane LPA receptors except the LPA_5 receptor. LPA_5 shows a preference for AGP relative to LPA (Williams et al., 2009). Interestingly, AGP also shows a higher potency than LPA at the intracellular LPA receptor peroxisome proliferator-activated receptor gamma (PPARγ) (Zhang et al., 2004, Tsukahara et al., 2010).

Cyclic phosphatidic acid (CPA; Figure 1-1) is a naturally occurring acyl analog of LPA present in mammalian blood and brain. CPA is also a weak agonist of many plasma membrane LPA receptors (Fujiwara et al., 2005, Williams et al., 2009), whereas CPA is an inhibitor of PPARγ (Tsukahara et al., 2010).

1.1.2 Plasma Membrane LPA Receptors and Signaling

LPA activates multiple plasma membrane receptors that belong to the G protein-coupled receptor (GPCR) superfamily (Choi et al., 2010). LPA GPCRs have been identified in two distinct gene families, the endothelial differentiation gene (EDG) family and purinergic GPCR cluster. LPA_1, LPA_2, and LPA_3 belong to the EDG family and share 45-56% amino acid identity with the most divergence at the C-termini (Anliker and Chun, 2004). LPA_4 (P2Y9/GPR23), LPA_5 (GPR92), LPA_6 (P2Y5), GPR87, P2Y10, and GPR35 are closely related to the P2Y purinergic receptor gene cluster (Ishii et al., 2009). Upon LPA stimulation, LPA GPCRs interact with different G proteins (G_s, $G_{i/o}$, G_q and $G_{12/13}$) to activate various downstream pathways, which mediate the diverse cellular effects of LPA.

LPA_1 couples with three types of heterotrimeric G proteins: $G_{i/o}$, G_q, and $G_{12/13}$ (Chun et al., 2010). LPA_1 induces Ca^{2+} mobilization, cell proliferation, cell migration, activation of mitogen-activated protein kinase (MAPK), and activation of Akt and Rho

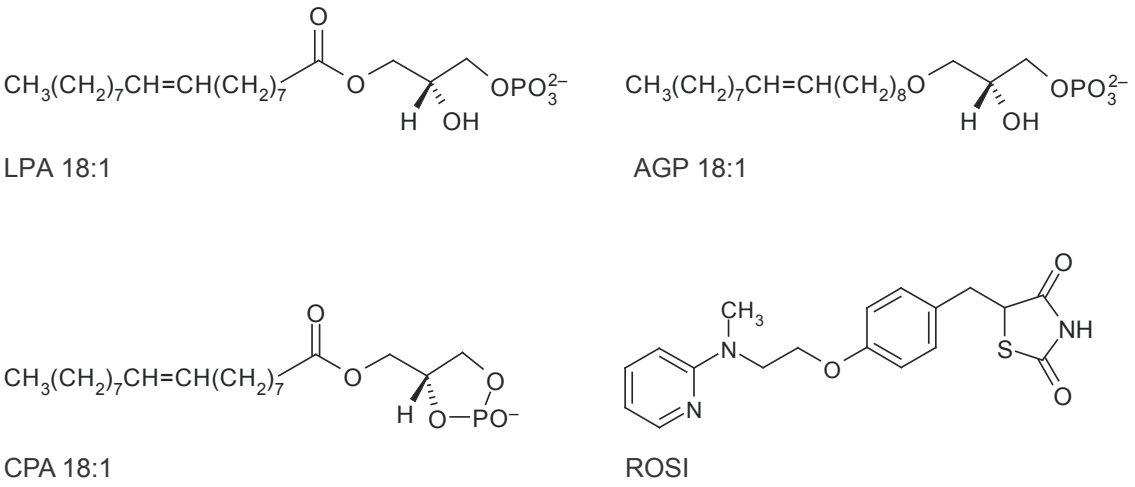

Figure 1-1 Structure of LPA, AGP, CPA, and ROSI

pathways (Anliker and Chun, 2004, Ishii et al., 2004). LPA_1 is widely expressed in mice and humans (Anliker and Chun, 2004, Choi et al., 2010). LPA_1 deficient mice show about 50% perinatal lethality within the first 3 weeks of age and the pups is attributed to an impaired suckling behavior (Contos et al., 2000). Surviving LPA_1 deficient mice have a reduced body size and craniofacial dysmorphism with shorter snouts and more widely spaced eyes (Contos et al., 2000).

LPA_2 also interacts with $G_{i/o}$, G_q, and $G_{12/13}$ (Chun et al., 2010). Hence, some of the LPA_2 signals are similar to LPA_1, such as Ca^{2+} mobilization, proliferation, Akt activation (Choi et al., 2010). LPA_2 also signals via a C-terminal macromolecular complex that includes proteins recruited to its PDZ-motif and LIM-motif (E et al., 2009). LPA_2 is highly expressed in the embryonic brain, testis, kidney, lung, and uterus in mice (Choi et al., 2010). In humans it is detected in the testis, pancreas, prostate, thymus, spleen, and leukocytes (Choi et al., 2010). LPA_2 knockout mice are born normally and show no obvious phenotypic abnormalities (Contos et al., 2002), whereas our group showed these mice have increased sensitivity to radiation (Deng et al., 2007).

LPA_3 can couple to $G_{i/o}$ and $G_{q,}$ and induces Ca^{2+} mobilization, phospholipase C activation, and MAPK activation (Fukushima et al., 1998, Ishii et al., 2000). LPA_3 is highly expressed in testis, kidney, lung, small intestine, heart, thymus, brain, and in the female reproductive system such as the oviduct, placenta, and uterus in adult mice (Choi et al., 2010). It is also found in heart, pancreas, prostate, testis, lung, ovary, and brain in humans (Choi et al., 2010). LPA_3 deficient female mice show delayed and abnormal embryo implantation in the uterus (Ye et al., 2005). LPA_3 knockout along with the lack of $LPA_{1\text{ and }2}$ also contribute to male infertility in aging mice (Ye et al., 2008).

LPA_4 couples to $G_{i/o}$, G_q, and $G_{12/13}$, as well as G_s, and induces Ca^{2+} mobilization, cAMP accumulation, neurite retraction (Ishii et al., 2009). LPA_4 is ubiquitously expressed and specifically abundant in ovary, uterus, and placenta (Ishii et al., 2009). LPA_4 deficient mice display no apparent abnormalities (Lee et al., 2008), whereas an independent study reported that LPA_4 deletion in a different C57BL/6 background mouse showed abnormal embryonic blood and lymphatic vessel formation (Sumida et al., 2010).

LPA_5 couples to G_q and $G_{12/13}$ (Kotarsky et al., 2006, Lee et al., 2006) and induces Ca^{2+} mobilization, neurite retraction, and cAMP accumulation (Ishii et al., 2009, Williams et al., 2009). Unlike other LPA receptors LPA_5 prefers AGP over LPA (Williams et al., 2009) and is broadly expressed in tissues such as brain, small intestine, placenta, spleen, lung, embryonic stem cells (Kotarsky et al., 2006, Lee et al., 2006).

LPA_6 couples to G_s and $G_{12/13}$ (Yanagida et al., 2009). It was reported that 2-acyl-LPA rather than 1-acyl-LPA is more potent ligand of LPA_6 (Yanagida et al., 2009). LPA_6 plays an important role in human hair growth (Pasternack et al., 2008, Shinkuma et al., 2010).

GPR87 is highly expressed in squamous cell carcinomas and lung carcinomas (Gugger et al., 2008). GPR87 was reported to increase Ca^{2+} mobilization using G_{16} fusion

protein system (Tabata et al., 2007). P2Y10 fused with G_{16} can induce Ca^{2+} transients by sphingosine-1-phosphate (S1P) as well as LPA (Murakami et al., 2008). The transcripts of P2Y10 were detected in uterus, prostate, brain, lung, placenta, and skeletal muscle (Murakami et al., 2008).

1.1.3 Intracellular LPA Receptor – PPARγ

Peroxisome proliferator-activated receptors (PPARs) are members of the nuclear hormone receptor superfamily, many of which function as lipid-activated transcription factors (Tontonoz and Spiegelman, 2008). There are three PPAR isoforms that include PPARα, β/δ, and γ. PPARγ, the most extensively studied among the three PPAR subtypes, plays an important role in regulating lipid metabolism, glucose homeostasis, cell differentiation, and motility (Duval et al., 2002, Evans, 2005, Kiec-Wilk et al., 2005). PPARγ has two isoforms, PPARγ$_1$ and γ$_2$. PPARγ$_2$ differs from PPARγ$_1$ only by 30 additional amino acids at the N-terminus, caused by differential promoter usage and alternative splicing (Fajas et al., 1997). PPARγ$_1$ is expressed in almost all tissues, whereas PPARγ$_2$ is highly expressed in only in the adipose tissue (Lehrke and Lazar, 2005). Genetic deletion of PPARγ$_1$ causes embryonic mortality (Asami-Miyagishi et al., 2004). In contrast, deletion of PPARγ$_2$ causes minimal alterations in lipid metabolism (Medina-Gomez et al., 2005). PPARγ heterodimerizes with the retinoid X receptor α (RXRα), and it is the ligand binding domain (LBD) of PPARγ that interacts with its agonists, including LPA (Weatherman et al., 1999). The PPARγ-RXRα heterodimer binds the peroxisome proliferator response element (PPRE) in the promoter region of the target genes. In the absence of ligands, the corepressors nuclear receptor corepressor (NCoR) and silencing mediator of retinoid and thyroid hormone (SMRT) bind to the heterodimer to suppress the target gene activation (Chen and Evans, 1995, Dowell et al., 1999, Yu et al., 2005). Upon ligand binding, PPARγ undergoes a conformational change that facilitates the dissociation of the corepressors and recruits coactivators such as p300 and PGC-1α (Nolte et al., 1998, Yu and Reddy, 2007), resulting in target gene transcription (Lala et al., 1996).

A number of putative physiological agonists of PPARγ have been identified, including 15d-prostaglandin J2 (15d-PGJ2) (Forman et al., 1995), oxidatively modified fatty acids (Nagy et al., 1998, Baker et al., 2005, Li et al., 2008), select species of LPA and AGP (McIntyre et al., 2003, Zhang et al., 2004, Tsukahara et al., 2006), oxidized phospholipids (Davies et al., 2001), and nitrated fatty acids (Li et al., 2008). Among these ligands, AGP stands out with an equilibrium binding constant of 60 nM (Tsukahara et al., 2006) that is similar to that of the thiazolidinedione (TZD) class of synthetic agonists. Interestingly, some of the residues required for PPARγ activation by AGP are different from those required by ROSI. Histidine 323 and 449 within the ligand-binding domain of PPARγ are required for the binding and activation by rosiglitazone (ROSI; Figure 1-1**)** but are not required by AGP. Arginine 288 is an important residue for binding of AGP but not ROSI. Tyrosine 273 is required for activation by both agonists (Tsukahara et al., 2006).

The TZD class of antidiabetics, ROSI, pioglitazone, and troglitazone, are full agonists of PPARγ and have been clinically used to improve insulin sensitivity and lipid metabolism in type 2 diabetics (Froberg and Andersen, 2005, Lautamaki et al., 2005, Negro et al., 2005, Sarafidis et al., 2005). However, despite the beneficial effects of PPARγ on glucose and lipid homeostasis, excessive PPARγ activity can be deleterious. PPARγ agonists promote adipocytic differentiation of 3T3-L1 cells and also stimulate the uptake of low density lipoprotein (LDL) by macrophages, leading to foam cell formation in the arterial wall (Moore et al., 2001).

The cells of the vascular wall expresses LPA_{1-5} receptors as well as PPARγ (Cheng et al., 2009). Topical application of unsaturated LPA species into the non-injured carotid artery of rodents induces arterial wall remodeling (Yoshida et al., 2003), and this response requires PPARγ but not LPA_1 or LPA_2 (Yoshida et al., 2003, Zhang et al., 2004, Cheng et al., 2009) suggesting that LPA-mediated activation of PPARγ can also contribute to vascular wall pathologies.

1.2 LPA IN VASCULAR BIOLOGY

Accumulating evidence has shown that LPA plays an important role in the vascular system including proliferation, migration differentiation of vascular smooth muscle cells (VSMCs) and vascular endothelial cells and the recruitment and trafficking of macrophages and histiocytes (Figure 1-2).

LPA has been identified as a bioactive lipid and is produced in serum after the activation of multiple biochemical pathways linked to platelet activation (Sano et al., 2002, Spector, 2003, Tigyi and Parrill, 2003, Bolen et al., 2011). The concentration of LPA in plasma is in the nanomolar range, whereas it can reach concentrations as high as 10 μM in serum during blood clotting (Baker et al., 2001, Aoki et al., 2002, Baker et al., 2002). LPA production in blood requires autotaxin (ATX), which is a secreted lysophospholipase D that generates LPA from lysophosphatidylcholine (LPC) (Tokumura et al., 2002, Umezu-Goto et al., 2002).

Tokumura et al. reported that crude soybean lecithin contains a vasopressor lipid identified as LPA (Tokumura et al., 1978a, Tokumura et al., 1978b). They demonstrated LPA had hypertensive effects in rats and guinea pigs and hypotensive effects in cats and rabbits (Tokumura et al., 1978b).

LPA increases endothelial permeability via RhoA activation (Schulze et al., 1997, Alexander et al., 1998, van Nieuw Amerongen et al., 2000). LPA activates the endothelial isoform of nitric oxide synthase (eNOS) through the activation of the PI3-K/Akt pathway (Kou et al., 2002). LPA also induces E-selectin, vascular cell adhesion molecule-1 (VCAM-1), and vascular endothelial growth factor-C (VEGF-C) expression in human endothelial cells (Rizza et al., 1999, Lin et al., 2008). Moreover, LPA regulates the expression of pro-atherogenic connective tissue growth factor (CTGF) in human endothelial cells (Muehlich et al., 2004). CTGF is known to mediate migration

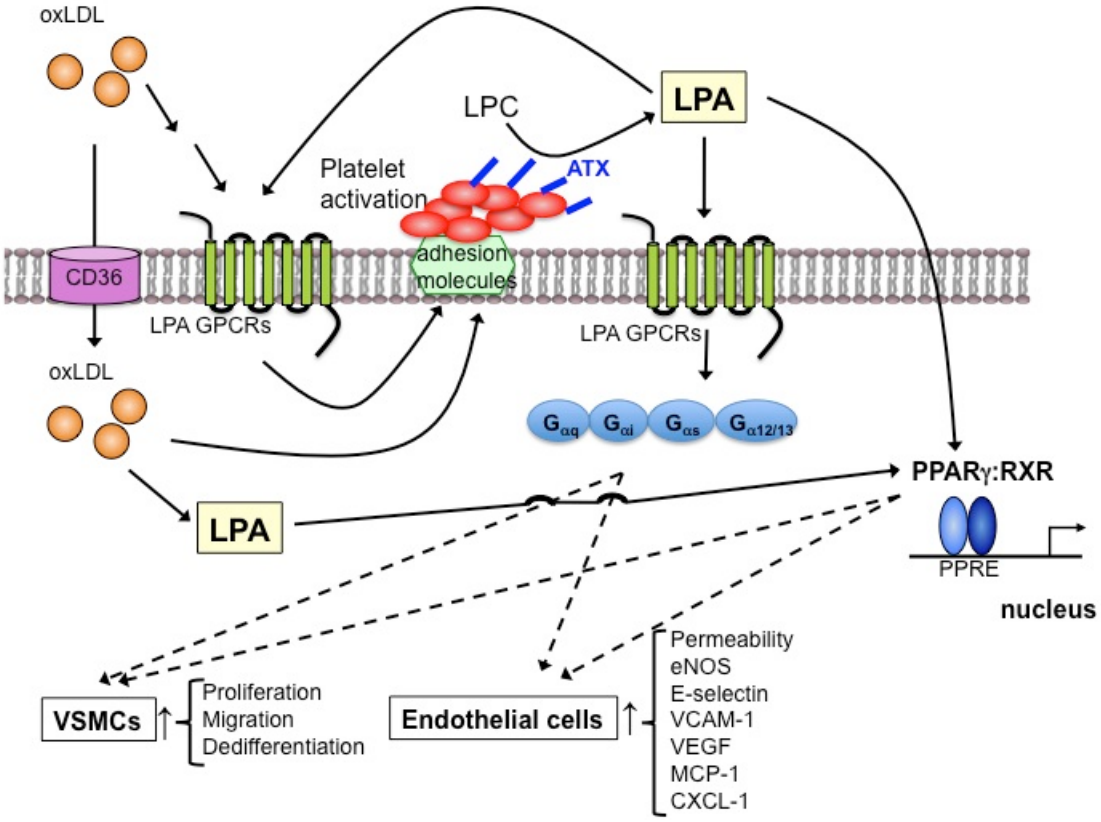

Figure 1-2 The effects of LPA in the vasculature

of monocytes, VSMCs, and activated platelets.

LPA promotes proliferation and migration of VSMCs (Hayashi et al., 2001, Siess, 2002, Kim et al., 2006). Hayashi et al. showed that LPA promotes VSMC dedifferentiation from the contractile phenotype to a secretory phenotype and stimulates VSMC signaling pathways *in vitro* (Hayashi et al., 2001). LPA induces early growth response gene 1(Egr-1), an important transcription factor that activates expression of a set of genes involved in vascular diseases (Cui et al., 2006). Myocyte contractility is regulated by LPA via G_i-mediated mechanism (Cremers et al., 2003). The authors showed that LPA suppressed isoprenaline-induced cell shortening through the activation of LPA_1 and/or LPA_3 in a pertussis toxin sensitive manner.

LPA activates monocytes with low nanomolar concentration (Fueller et al., 2003) and recruits them via inducing monocyte chemoattractant protein-1 (MCP-1) secretion through p38 and JNK pathways in endothelial cells (Lin et al., 2006, Shimada and Rajagopalan, 2010) suggesting the important role in inflammation processes. LPA inhibits conversion of monocytes into migratory cells and keep them in the subendothelium (Llodra et al., 2004). LPA via LPA_1 and LPA_3 induces CXCL-1, which promotes monocyte adhesion to the murine vascular endothelium (Zhou et al., 2011).

Many of the cellular responses elicited by LPA, including platelet activation (Siess et al., 1999, Rother et al., 2003, Haseruck et al., 2004), endothelial cell activation (Siess et al., 1999), proliferation, migration, and phenotypic modulation of VSMCs (Hayashi et al., 2001, Siess, 2002, Kim et al., 2006), can be involved in neointima formation. Oxidative modification of LDL is considered to be an early event in arterial wall remodeling leading to atherosclerosis (Stocker and Keaney, 2004, Asmis et al., 2005); and uptake and oxidation of LDL in the arterial wall is an important mechanism in the pathogenesis of atherosclerosis (Meydani, 2001). It has been shown that LPA is formed during mild oxidation of LDL (mox-LDL) (Siess et al., 1999, Law et al., 2000). In addition, the lipid-rich core of human atherosclerotic plaques, which accumulates oxidized lipids including mox-LDL, contains several species of LPA and AGP (Siess et al., 1999). LPA and AGP accumulated in human atherosclerotic plaques are likely to activate platelets and initiate thrombus formation upon plaque rupture (Rother et al., 2003, Spector, 2003). Following plaque rupture, LPA becomes available to circulating platelets, initiating activation, which in turn may contribute to the induction of thrombosis, leading to myocardial infarction and stroke. Furthermore, a recent report revealed that ATX can bind to platelet integrin receptors through its N-terminal somatomedin B-kike domains (Hausmann et al., 2011) suggesting the possibility that ATX could be localized to the surface of activated platelets, which might concentrate the production of LPA at the sites of vascular injury.

Some clinical studies have shown the correlation between plasma LPA and vascular diseases. Chen et al showed that the serum LPA level was significantly elevated in patients with acute myocardial infarction (Chen et al., 2003).

LPA also plays an important role in vascular development (van Meeteren et al., 2006). ATX-deficient mice die at approximately embryonic day 9.5 with severe vascular formation defects in the yolk sac and enlarged embryonic blood vessels (Tanaka et al., 2006, van Meeteren et al., 2006). Mice that overexpress ATX have elevated plasma LPA levels and show bleeding diathesis, whereas $ATX^{+/-}$ heterozygous mice have almost half the plasma LPA levels and are prone to thrombosis (Pamuklar et al., 2009).

1.3 VASCULAR WALL REMODELING

1.3.1 Neointima Formation Induced by LPA

Neointimal lesions are characterized by accumulation of cells within the arterial wall and are an early step in the pathogenesis of atherosclerosis (Ross, 1999, Baim et al., 2002). Atherosclerosis is the leading cause of death and serious morbidity in the United States (Xu et al., 2010).

Yoshida et al. reported that LPA species containing unsaturated fatty acyl groups 16:1, 18:1, and 18:2 induced neointima formation when injected intralumenally into the rat carotid artery, whereas saturated 16:0 and 18:0 LPA species were inactive (Yoshida et al., 2003). This model comes close to the pathophysiological response seen in humans because mechanical injury is not the cause of the arterial wall remodeling leading to neointimal lesions. In Yoshida's model, LPA was injected through the external carotid artery into a ligated section of the common carotid artery (CCA) that was rinsed free of blood and maintained close to the mean arterial perfusion pressure. There was no mechanical injury or removal of endothelial cells in the CCA. A brief one-hour exposure to unsaturated but not to saturated species of LPA caused neointima development.

Our group found that the LPA-elicited neointima was not mediated by the LPA GPCRs LPA_1 and LPA_2, which are the major LPA receptor subtypes expressed in the vessel wall (Cheng et al., 2009). PPARγ-specific inhibitor, GW9662, abolished the LPA-induced neointima formation, suggesting that arterial wall remodeling elicited by LPA is a PPARγ-mediated response (Zhang et al., 2004). Conversely, the PPARγ-specific agonist ROSI also elicited neointima formation in the same model. Genetic evidence also supports the role of PPARγ in arterial wall remodeling. When conditional knockout $PPAR\gamma^{-/-}$ mice with this receptor knocked out in the endothelial cells, VSMCs, and cells of the macrophage/monocyte lineage were exposed to AGP, LPA, or ROSI no neointima formation or vascular wall remodeling was observed (Cheng et al., 2009).

It is important to note that in a carotid injury model, ROSI diminished the size of the neointima. The opposite effect of ROSI and LPA in these two different models indicates differences in the mechanism underlying vascular wall remodeling in these models (Cheng et al., 2009). These results, combined with the observation that GW9662 abolished neointima in response to ROSI or AGP (Zhang et al., 2004), suggest that

PPARγ is required for LPA-induced neointima formation in the absence of vascular wall injury.

Panchatcharam et al. reported that LPA_1 and LPA_2 receptors play an important role in injury-induced neointima formation (Panchatcharam et al., 2008). They demonstrated that neointima formation induced by mechanical injury was attenuated in $LPA_1^{-/-}LPA_2^{-/-}$ mice compared to wild type mice. In contrast, in our non-injury model, $LPA_1^{-/-}LPA_2^{-/-}$ mice developed neointima in response to LPA treatment (Cheng et al., 2009), suggesting that the mechanism underlying these two models in neointima is fundamentally different.

Moreover, Subramanian et al. reported that LPA_1 and LPA_3 GPCRs play an important role in injury-induced neointima formation (Subramanian et al., 2010). Using a wire-injury model, these authors showed that neointima formation was inhibited by the LPA_1 and LPA_3 inhibitor Ki16425 and that vascular wall remodeling induced by LPA was inhibited by short-term knockdown of either LPA_1 or LPA_3 with small interfering RNA (siRNA) (Subramanian et al., 2010). In sharp contrast with the findings of Subramanian et al., $LPA_1^{-/-}$ mice in our non-injury model develop neointima in response to AGP stimulation. Moreover, although LPA_1 and LPA_3 GPCRs are respectively 12 and 100 times less sensitive to AGP than LPA (Fujiwara et al., 2005), AGP is more potent than LPA in inducing neointima formation (Zhang et al., 2004). Subramanian and colleagues also observed that Mac-2 positive cells accumulated in the neointimal area after vascular injury (Subramanian et al., 2010); in contrast, our non-injury model showed few macrophages in the neointimal region induced by AGP or ROSI (Cheng et al., 2009), suggesting that the cellular elements leading to neointima formation are different between the two models.

Although some clinical studies in diabetic patients have shown a reduction in carotid artery wall thickness after treatment with TZDs (Minamikawa et al., 1998, Haffner et al., 2002), other studies suggested that ROSI increases the risk of myocardial infarction and death from cardiovascular causes (Goldberg et al., 2005, Nissen and Wolski, 2007, 2010), indicating that TZD therapy may actually increase the risk of cardiovascular events. Moreover, in 2010, the U.S. Food and Drug Administration restricted use of ROSI to patients with type 2 diabetes due to the potential for cardiovascular ischemic risks, including heart attack.

1.3.2 The Structure-Activity Relationship (SAR) of Neointima Induction

The different molecular species of LPA contain either saturated or unsaturated fatty acids. Only unsaturated LPA species including oleoyl (18:1), linolenoyl (18:2), and arachidonoyl (20:4) LPA induce neointima (Yoshida et al., 2003, Zhang et al., 2004). In contrast, saturated LPA species including palmitoyl (16:0) and stearoyl (18:0) LPA are inactive in non-injury carotid wall remodeling assay (Yoshida et al., 2003, Zhang et al., 2004). The SAR of neointima induction does not match that of the known LPA GPCRs because saturated LPA activate LPA GPCRs (Zhang et al., 2004). On the other hand,

experiments conducted to determine the SAR for PPARγ activation *in vitro* and the SAR of the neointimal response *in vivo* are closely matched (Zhang et al., 2004). *In vitro*, ROSI, unsaturated LPA and AGP species all activate the peroxisome activator response element-containing acyl-coenzyme A oxidase-luciferase (PPRE-Acox-Luc) reporter construct, whereas all saturated LPA species, CPA, and the related lipid mediator S1P are inactive (Zhang et al., 2004). The similarity of the SAR of neointimal lesions and PPARγ activation support the hypothesis that LPA receptor required for neointima formation is PPARγ (Zhang et al., 2004, Tsukahara et al., 2006).

1.4 THE ROLE OF PPARγ

1.4.1 PPARγ in Vascular Biology

PPARγ plays an important role in the cardiovascular system. PPARγ is expressed in all cell types of the vessel wall (Marx et al., 1998, Delerive et al., 1999, Rangwala and Lazar, 2004), as well as in monocytes and macrophages (Tontonoz et al., 1998). PPARγ expression is upregulated in VSMCs (Law et al., 2000), endothelial cells (Delerive et al., 1999), and macrophages (Tontonoz et al., 1998) in human atherosclerotic plaques and neointimal lesions.

PPARγ expression is also elevated in neointimal lesions after mechanical injury to the endothelium (Law et al., 2000). There are some reports that ROSI suppresses neointima formation after endothelial injury in rodent (Lim et al., 2006, Meredith et al., 2009). Our group found that when AGP was infused to an injured carotid artery, neointima was augmented, although ROSI attenuated neointima induced by mechanical injury (Cheng et al., 2009). Furthermore, in our non-injury model, ROSI induces neointima when applied intralumenally into the carotid artery (Zhang et al., 2004, Cheng et al., 2009). Thus, the mechanisms underlying neointima formation in the chemically-induced neointima model are likely to be different from those in the injury-induced neointima models. It is important to note that circulating LPA makes a complex with serum albumin (Tigyi and Miledi, 1992) and LPA-albumin complex cannot activate PPARγ because the LPAcomplex can not be internalized (Zhang et al., 2004). Therefore, the source of LPA is likely to originate from either the uptake lipid particles such as oxidized LDL (oxLDL) or generated intracellularly.

1.4.2 PPARγ in Macrophages/Monocytes

Macrophages play essential roles in immunity and lipid homeostasis. It has been reported that PPARγ is induced during the differentiation of monocytes into macrophages and is highly expressed in activated macrophages including the foam cells in atherosclerotic lesions (Ricote et al., 1998, Tontonoz et al., 1998). PPARγ is also induced during the differentiation of monocytes into dendritic cells (Figure 1-3) (Gosset et al., 2001, Szatmari et al., 2004).

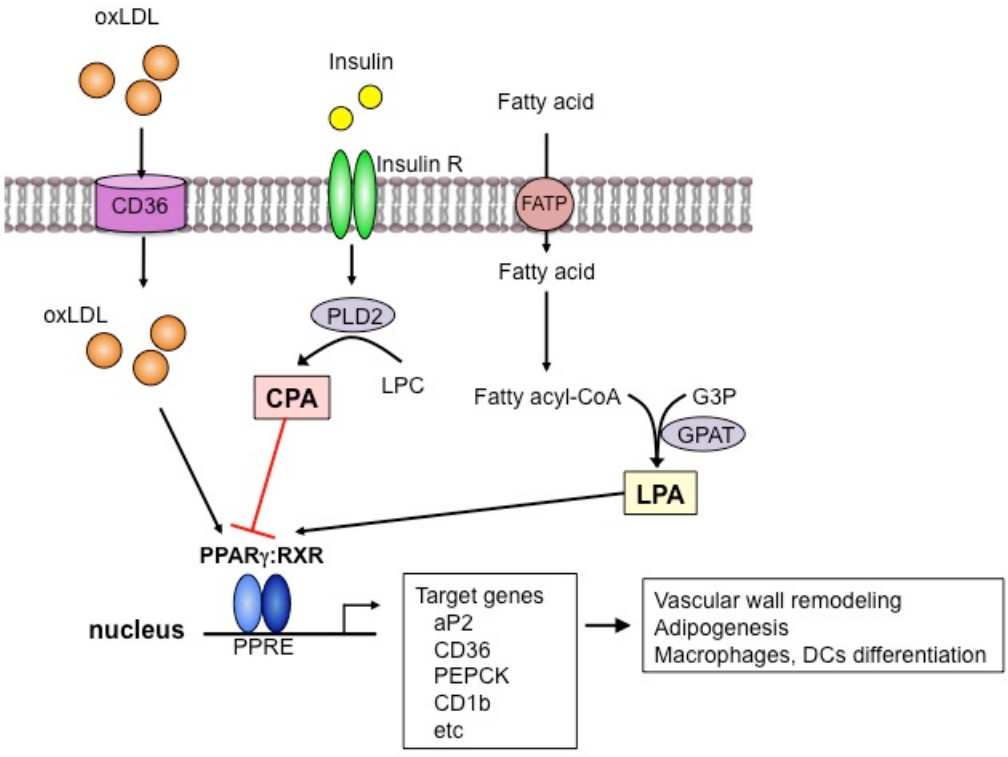

Figure 1-3 Mechanism of PPARγ-mediated effects

CD36 is a scavenger receptor and one of the PPARγ response genes. PPARγ activation upregulates CD36 expression, which results in increased lipid uptake in macrophages (Figure 1-3) (Tontonoz et al., 1998). In macrophages, oxLDL uptake through CD36 results in the development of foam cells. Accumulation of foam cells in the arterial wall is a hallmark of the early atherosclerotic lesion. There is evidence that oxLDL uptake is decreased in PPARγ deficient macrophages due to the loss of CD36 (Moore et al., 2001) suggesting that the activation of PPARγ in macrophages plays an important role atherosclerosis.

Interestingly, it has been shown that macrophages are accumulated in the injury-induced neointima lesions (Subramanian et al., 2010). On the other hand, very few macrophages are detected in neointima lesions induced in non-injury model (Cheng et al., 2009) implying that the roles of macrophages in the two models are different.

Dendritic cells are antigen-presenting cells, which play an important role in stimulating T and B cells. It has been shown that PPARγ promotes antigen-presenting molecule CD1d expression in DCs, and LPA is capable of modulating CD1d expression (Szatmari et al., 2004, Leslie et al., 2008). This line of evidence suggests that LPA may have a critical role in dendritic function through the activation of PPARγ.

1.4.3 PPARγ in Lipid Metabolism

Excess fat is stored as triglycerides in the adipose tissue, and fatty acids are released into the circulation in response to increased energy requirement. If lipid storage capacity of adipocytes is exceeded, adipocytes can no longer regulate the level of free fatty acids (FFAs) in the circulation, which results in the inappropriate deposition of lipids in tissues, including the liver and skeletal muscle (Camp et al., 2002). Accumulation of triglycerides in the liver and the muscle is thought to lead to metabolic dysregulation, especially,to increased levels of triglycerides and FFAs (Camp et al., 2002).

It has been shown that PPARγ plays an important role in regulating glucose metabolism and fatty acid storage (Evans, 2005). Activation of PPARγ in adipose tissue leads to target gene expression including aP2, CD36, PEPCK, which are involved in FFA uptake and triglyceride storage (Rosen and MacDougald, 2006). Consistent with their ability to promote lipid uptake and storage in cultured cells, PPARγ agonists increase adipose tissue mass *in vivo* (Tai et al., 1996).

LPA can be generated intracellularly through multiple pathways and is also an intermediate of fatty acid metabolism. Fatty acids taken up by cells are activated to form fatty acyl-coenzyme A (fatty acyl-CoA). The next biochemical step is the generation of LPA from fatty acyl-CoA and glycerol-3-phosphate by the different forms of glycerophosphate acyltransferase (GPAT; Figure1-3) (Vancura et al., 1991). The LPA generated by GPAT might activate PPARγ leading to upregulation of PPARγ target genes involved in lipogenesis, lipid storage, and adipocyte differentiation (Stapleton et al.,

2011). In addition, CPA, an acyl analog of LPA, is also generated intracellularly by phospholipase D 2 (PLD2) upon the stimulation of insulin, and negatively regulates PPARγ functions (Tsukahara et al., 2010) suggesting that PPARγ functions are regulated by agonists as well as by antagonists.

1.5 CYCLIC PHOSPHATIDIC ACID

1.5.1 CPA Production

CPA (Figure 1-1), an analog of LPA with a five-atom ring linking the phosphate to two of the glycerol carbons, is found in diverse organisms from slime mold to humans (Murakami-Murofushi et al., 2000); its functions are largely unknown. The concentration of CPA in human serum is estimated to be ~0.01 μM, 10-fold lower than that of LPA (Eichholtz et al., 1993, Kobayashi et al., 1999).

Friedman et al. demonstrated that CPA can be formed by a intermediate product through transphosphatidylation reaction with lysophosphatidylcholine (LPC) mediated by a bacterial PLD (Friedman et al., 1996). LPC is a second most abundant phospholipid in serum and a substrate of PLD (Tokumura et al., 1983). Tsuda et al. found that fetal bovine serum has activity to produce CPA, and they identified ATX, a serum lysophospholipase D (lysoPLD), that can produce CPA *ex vivo* in an ether/water two phase buffer system (Tsuda et al., 2006). ATX may not be the only source responsible of CPA in serum. In addition, our group showed that CPA is generated intracellularly from LPC through the activation of PLD2 (Tsukahara et al., 2010).

1.5.2 CPA Receptors

It has been reported that CPA activates $LPA_{1\text{-}5}$ and GPR87 receptors (Fujiwara et al., 2005, Baker et al., 2006, Williams et al., 2009, Tigyi, 2010). CPA activates $LPA_{1\text{-}4}$ receptors with a lower potency than that of LPA (Fujiwara et al., 2005, Baker et al., 2006), whereas CPA activates LPA_5 with a slightly higher EC_{50} concentration than LPA (Williams et al., 2009). GPR87 and P2Y10 are also activated by CPA with lower efficiency than LPA (Tigyi, 2010). In contrast to LPA, CPA does not activate intracellular LPA receptor PPARγ (Zhang et al., 2004, Tsukahara et al., 2010).

1.5.3 Functions of CPA

The concentration of CPA in human serum is estimated to be ~0.01 μM, 10-fold lower than that of LPA (Eichholtz et al., 1993, Kobayashi et al., 1999). Although CPA is structurally similar to LPA and activates LPA GPCRs (Fujiwara et al., 2003, Fujiwara et al., 2005, Williams et al., 2009), CPA shows several unique actions compared to LPA. CPA inhibits cell proliferation in human fibroblast cells whereas LPA stimulates it

(Fischer et al., 1998). CPA directly inhibits Cdc25, leading to dephosphorylation of cyclin-dependent kinase 2 that results in cell cycle arrest (Murakami-Murofushi et al., 2002). Nanomolar concentrations of CPA promote neuron outgrowth and enhance differentiation and survival in cultured embryonic hippocampal neurons (Fujiwara et al., 2003). CPA with an acyl chain inhibits LPA-induced platelet aggregation, whereas CPA with an alkyl chain shows weak platelet aggregation (Gueguen et al., 1999). Although LPA induces transcellular migration, CPA shows inhibitory effect on transcellular migration in rat hepatoma, human lung cancer, and mouse melanoma cells (Mukai et al., 1999). It has been reported that CPA attenuates cancer cell invasion *in vivo* (Ishihara et al., 2004, Uchiyama et al., 2007). Moreover, metabolically stabilized derivatives of CPA suppressed pulmonary metastasis when mouse melanoma cells were injected into C57BL6 mice (Baker et al., 2006).

1.6 PHOSPHOLIPASE D

1.6.1 Functions of PLD

PLD catalyzes the hydrolysis of phosphatidylcholine (PC) and LPC to generate the lipid second messenger phosphatidic acid (PA) or CPA and choline (Frohman et al., 1999). PLD can also catalyze the hydrolysis of LPC to generate LPA, which could be the source of ligand for intracellular LPA receptors. PLD is conserved in cells from bacteria to mammals (Exton, 2002). Mammalian PLD is regulated by many factors, including phosphatidylinositol-4,5-bisphosphate (PIP_2), protein kinase C (PKC), and small G-proteins of the Rho, Ral, and ARF families (Liscovitch et al., 2000, Exton, 2002). PLD plays an important role in a wide variety of cellular responses such as vesicular trafficking (Cockcroft, 1996, Liscovitch, 1996), Golgi function (Yang et al., 2008, Riebeling et al., 2009), cell proliferation, migration, and survival (Plevin et al., 1991, Banno et al., 2001, Zheng et al., 2006, Carrigan et al., 2007).

1.6.2 Mammalian PLD Isoforms

There are two mammalian PLD isoforms, PLD1 and PLD2 (Liscovitch et al., 2000). These isoforms share about 50% amino acid similarity and have a highly conserved HKD domain necessary for catalysis. They also require PIP_2 as a cofactor for activation, however, they exhibit quite distinct regulatory properties (Liscovitch et al., 2000). PLD1 has a low basal activity and responds to members of small G proteins Rho and ARF, whereas PLD2 shows a high basal activity and a little or no response to PLD1 activators (Colley et al., 1997, Exton, 2002). Their distribution is also different. PLD1 is predominantly expressed in Golgi, lysosome, and perinuclear endosome, whereas PLD2 is exclusively expressed at the plasma membrane (Brown et al., 1998, Du et al., 2004). Our recent study showed that PLD2, but not PLD1, can generate CPA from LPC intracellularly in mammalian cells (Tsukahara et al., 2010). Furthermore, we showed that

inhibition of PLD2 by knockdown or dominant negative constructs blocked the protective effect of insulin or other stimulators of this enzyme (Tsukahara et al., 2010).

1.6.3 PLD Inhibitors

Primary alcohols are often used to quench PLD activity *in vitro* studies to confirm PLD effects. PLD catalyses a transphosphatidylation reaction in the presence of primary alcohols like primary butanol, leading to the formation of phosphatidylethanol instead of PA (Munnik et al., 1995). Therefore, primary alcohols inhibit cellular responses elicited by PLD1- and PLD2-produced PA. Secondary and tertiary alcohols cannot be substrates of the transphosphatidylation reaction. 5-fluoro-2-indolyl des-chlorohalopemide (FIPI) is an analog of halopemide, a dopamine receptor antagonist, and identified as an inhibitor of both PLD1 and PLD2 (Monovich et al., 2007, Su et al., 2009). FIPI inhibits PLD-mediated PA production, leading to the inhibition of F-actin cytoskeleton reorganization, cell spreading, and chemotaxis (Su et al., 2009). Recently, we demonstrated that FIPI inhibits PLD2-mediated CPA production in human peripheral mononuclear cells (Tsukahara et al., 2010).

CHAPTER 2. LYSOPHOSPHATIDIC ACID-INDUCED ARTERIAL WALL REMODELING: REQUIREMENT OF PPARγ BUT NOT LPA_1 OR LPA_2 GPCR*

2.1 INTRODUCTION

Lysophosphatidic acid (LPA, 1-acyl-2-hydroxy-sn-glycero-3-phophate) and its ether-linked analog alkyl glycerophosphate (AGP, 1-alkyl-2-hydroxy-sn-glycero-3-phophate) are naturally occurring lipid mediators with growth factor-like effects in almost every mammalian cell type (Siess and Tigyi, 2004). AGP and LPA elicit their biological responses through eight plasma membrane receptors that belong to the GPCR superfamily and intracellularly through the peroxisome proliferator-activated receptor γ (PPARγ) (McIntyre et al., 2003, Tsukahara et al., 2006). AGP and LPA are present in blood plasma (Xiao et al., 2001) and become enriched after minimal oxidative modification of LDL (Rother et al., 2003, Zhang et al., 2004). The lipid rich core in human carotid endarterectomy specimens contains high concentrations of AGP and LPA (Siess et al., 1999) and upon plaque rupture could activate platelet aggregation and lead to atherothrombosis (Rother et al., 2003).

All major cell types of the arterial wall respond to LPA. In endothelial cells, LPA has been shown to regulate the expression of adhesion molecules, proliferation, apoptosis, permeability, motility and cell-to-cell contacts responsible for transendothelial permeability (Rizza et al., 1999, Lin et al., 2006). LPA induces vascular smooth muscle cell (VSMC) contraction, proliferation (Tokumura et al., 1994) and phenotypic transdifferentiation *in vitro* (Hayashi et al., 2001, Zhang et al., 2004). LPA and oxidized LDL inhibit macrophage/dendritic cell egress across endothelial cell monolayers (Angeli et al., 2004, Llodra et al., 2004). LPA also stimulates the formation of platelet-monocyte aggregates, which are considered as an early marker of acute myocardial infarction (Fueller et al., 2003, Siess, 2006).

Yoshida and colleagues were the first to test lumenally applied LPA on the non-injured arterial wall *in vivo* (Yoshida et al., 2003). These authors infused LPA through the external carotid artery of rats into a ligated section of the common/internal carotid artery that was rinsed free of blood and maintained close to the mean arterial perfusion pressure. In this model, which involves no mechanical injury or the removal of endothelial cells in the common carotid artery, after 1-hour exposure to unsatured but not to saturated species of low micromolar LPA leads to neointima development. These authors interpreted their observation as if a yet unknown LPA GPCR activated only by unsaturated species of LPA. However, the structure-activity relationship of neointima induction does not match that of the known LPA GPCRs but matches the structure-activity relationship of PPARγ activation by LPA.

* Adapted with permission. Cheng Y, Makarova N, Tsukahara R, Guo H, Shuyu E, Farrar P, Balazs L, Zhang C, Tigyi G (2009) Lysophosphatidic acid-induced arterial wall remodeling: requirement of PPARgamma but not LPA1 or LPA2 GPCR. Cell Signal 21:1874-1884.

LPA is an agonist of the nuclear transcription factor PPARγ (McIntyre et al., 2003). PPARγ has long been implicated in atherogenesis (Diep and Schiffrin, 2001, Li and Glass, 2002). Many compounds activate PPAR, including the synthetic drug Rosiglitazone (ROSI) of the thiazolidinedione family, oxidized phospholipids, fatty acids, eicosanoids, and oxidized LDL. PPARγ is expressed in macrophages/monocytes, vascular smooth muscle cells, endothelial cells, and is highly expressed in atherosclerotic lesions and hypertensive vascular wall (Diep and Schiffrin, 2001). GW9662, a specific irreversible antagonist of PPARγ (Leesnitzer et al., 2002) completely abolished AGP, LPA and ROSI-induced neointima formation in the rat model (Zhang et al., 2004). Although, these lines of evidence support the role of PPARγ as the receptor responsible for the neointimal thickening elicited by AGP and LPA, the pharmacological evidence does not exclude the possibility that LPA GPCR mediate this response alone or through the indirect activation of PPARγ. Several investigators reported that systemic and chronic administration of ROSI attenuates neointima in models with mechanical injury of the arterial wall which is different from findings reported using the non-injury model (Lim et al., 2006, Lee et al., 2009).

Here we compared the effects of AGP and ROSI on arterial wall remodeling in a balloon injury model with that in the non-injury model and found that these agents elicit model-dependent different responses. We pursued a gene knockout (KO)-based strategy to seek the identification of the LPA receptor subtype(s) necessary for the neointimal response in the non-injury model. We tested AGP and ROSI in LPA_1, LPA_2, LPA_1 and LPA_2 double knockout (DKO), and in inducible conditional PPARγ knockout mice targeted to VSMCs, macrophages and endothelial cells by the Mx1Cre promoter. We also sought to characterize the phenotypic properties of cells involved in LPA-elicited neointimal thickening and found that the overwhelming majority of the cells in the neointimal layer express αSMA characteristic of the VSMC lineage. Our findings showed that $LPA_{1\&2}$ GPCR KO mice behave like wild type (WT) mice whereas, PPARγ KO fail to develop AGP- and ROSI-induced neointimal thickening.

2.2 EXPERIMENTAL PROCEDURES

2.2.1 Reagents

1-O-octadecenyl glycerophosphate (AGP 18:1) was purchased from Avanti Polar Lipids (Alabaster, AL). Rosiglitazone (ROSI) was from ALEXIS Biochemicals, Inc. (Plymouth Meeting, PA). TRIzol Reagent, DNase I, and the ThermoScript RT-PCR System for First-Strand cDNA Synthesis were from Invitrogen (Carlsbad, CA). The RT2 Real-Time SYBR Green/ROX kit was purchased from SuperArray (Frederick, MD).

2.2.2 Quantitative RT-PCR

Total RNA was prepared using TRIzol reagent from mouse common carotid artery from which the adventitia had been peeled off. One μg of total RNA was digested with DNase I and used for the subsequent synthesis of cDNA using the First Strand Synthesis kit as recommended by the manufacturer. The following primer pairs were used: LPA1, (forward) GTCTTCTGGGCCATTTTCAA and (reverse) TCATAGTCCTC TGGCGAACA; LPA2, (forward) GGGCCAGTGCTACTACAACG and (reverse) ACC AGCAGATTGGTCAGCA; LPA3, (forward) GAATTGCCTCTGCAACATCTC and (reverse) ATGAAGAAGGCCAGGAGGTT; LPA4, (forward) TCTGGATCCTAGTCCT CAGTGG and (reverse) CCAGACACGTTTGGAGAAGC; LPA5, (forward) CGCCATC TTCCAGATGAAC and (reverse) TAGCGGTCCACGTTGATG; and GAPDH, (forward) CTGCACCACCAACTGCTTAG and (reverse) GGGCCATCCACAGTCTTC T. The primer sets were designed with a melting temperature of 59–61°C. Amplicon size was 50–200 bases. Amplification was performed for 40 cycles at 94ºC/15 sec and 60ºC /60 sec. Quantitative values were obtained from the threshold cycle value (Ct) as previously described (Guo et al., 2008).

2.2.3 Immunofluorescence Staining

Cryosections dipped in 4% buffered paraformaldehyde were blocked in 10% goat serum and incubated with rat anti-mouse CD31 (anti-PECAM-1 rat monoclonal antibody, 1:400 dilution; RDI Inc.; Concord, MA), or anti-mouse CD11b (anti-Mac-1 rat monoclonal antibody, 1:100 dilution; BD Pharmingen; San Diego, CA), or anti-mouse CD68 (anti-macrosialin rat monoclonal antibody, 1:400 dilution; ABD SeroTec; Oxford, UK) antibodies. Anti-rat fluorescein-conjugated secondary antibody was used at a 1:200 dilution (Vector Laboratories; Burlingame, CA). Cell nuclei were stained with DAPI. The MOM kit (Vector Laboratories) was used for α-smooth muscle actin (αSMA) staining. Briefly, after fixation and permeabilization, tissue sections were incubated with mouse IgG blocking reagent for 1 h, followed by 1:200 diluted anti-αSMA antibody (1:400 dilution; DAKO; Carpinteria, CA) and then 1:200 diluted Texas Red conjugated anti-mouse antibody (1:200 dilution; Vector Laboratories). For the double staining of mouse carotid artery sections, αSMA staining was carried out using the MOM kit on anti-CD11b- or anti-CD68-stained sections. The fluorescence was observed by Nikon Eclipse 80i fluorescence microscope. Merged images for double-stained sections were generated by the NIS-Elements (V2.1, Nikon Instruments) image analysis software.

2.2.4 Rat Carotid Artery Balloon Injury Model

The animal procedures were approved by the Institutional Animal Care and Use Committee at the University of Tennessee and were consistent with the Guide for the Care and Use of Laboratory Animals (National Institutes of Health publication 85-23, revised 1985). Carotid artery balloon injury was induced in male Sprague-Dawley rats (230 to 300 g) anesthetized with ketamine (80 mg/kg) and xylazine (5 mg/kg). Under a

dissecting microscope, the right common carotid artery was exposed through a midline cervical incision. A 2F Fogarty catheter (Baxter-Edwards) was introduced via an arteriotomy via the external carotid artery, and then the catheter was advanced to the proximal edge of the omohyoid muscle. The balloon was inflated with saline and withdrawn three times from under the proximal edge of the omohyoid muscle to the carotid bifurcation. The common and internal carotid arteries were clamped and a 100 µl aliquot of AGP (10 µM), ROSI (10 µM), or vehicle was instilled into the injured segment via a PE-10 catheter and was incubated for 60 min. Subsequently, the catheter was withdrawn and the external carotid artery was ligated with 6-0 silk suture. The clips at the common and internal carotid arteries were released, and blood flow in the common carotid artery was restored. Three weeks after injury the carotids were dissected and processed for histology as described for the mouse specimens above. Each group consisted of six rats.

2.2.5 Transgenic and Knockout Animals

LPA_1 and LPA_2 knockout breeders on C57BL/6 background were generously provided by Jerold Chun (Scripps Institute, CA) and have been characterized previously (Contos et al., 2000, Contos et al., 2002, Yang et al., 2002). $LPA_{1\&2}$ double knockout (DKO) mice were obtained by crossing homozygous LPA_1 males with LPA_2 females. Genotyping of the DKO mice was done as described by Contos et al. coworkers (Contos et al., 2002). The C57BL/6-Mx1Cre mouse line was made available by Dr. Matthew Breyer (Vanderbilt University) that allows the differential, interferon (IFN)-inducible targeting of the Cre recombinase to vascular and renal endothelium, vascular smooth muscle cells and macrophages (Akiyama et al., 2002, Schneider et al., 2003). The Mx1Cre is induced intraperitoneal injection of the IFN-inducer synthetic double-stranded RNA polyinosinic-polycitidylic acid (pIpC, Sigma-Aldrich, St. Louis, MO). Dr. Mark Magnuson (Vanderbilt University) generously provided us a mouse line with exon 2 of PPARγ has been flanked by LoxP sites on the C57BL/6 background (Jones et al., 2002). $PPAR\gamma^{fl/-}$ mice were bred with homozygous Mx1Cre mice to generate mice that are $PPAR\gamma^{fl/-}$×Mx1Cre. Upon Mx1 induction with pIpC in $PPAR\gamma^{fl/-}$×Mx1Cre mice, Cre recombines the single PPARγ allele creating a conditional knockout (Jones et al., 2002, Guan et al., 2005, Jones et al., 2005). These induced conditional KO mice will be referred to as ΔPPARγ. Thus, ΔPPARγ mice allowed the targeted disruption of PPARγ in the three most important cell types – vascular endothelium, VSMC and macrophages (Akiyama et al., 2002, Guan et al., 2005) – involved in vascular remodeling whereas, littermates not induced with pIpC injections served as controls. In addition, Mx1Cre transgenic mice and pIpC-induced $PPAR\gamma^{fl/-}$ mice were also used to examine AGP- and ROSI-induced vascular wall remodeling.

2.2.6 Monitoring PPARγ Recombination

Genotyping of Mx1/Cre×$PPAR\gamma^{fl/-}$ and $PPAR\gamma^{fl/-}$ mice was done as described by Jones et al.(Jones et al., 2002). The position of the genotyping primers and their

respective PCR products is shown in Figure 2-1A and B. Examples of the wild-type (WT) Mx1/Cre×PPARγ$^{fl/-}$ genotype (mouse #23) and PPARγ$^{fl/-}$ genotype (mouse #24) are shown in Figure 2-1C. The following genotyping primers were used: A1, (forward) 5'-TACTTAATGTCATGATGATCTGT-3'; A2, (reverse) 5'-GATAAGACAGCACAA CAATGTTC-3'; B1, (reverse) 5'-GCTCCTGAGTGCTAATATTAAAG-3'; and B2, (forward) 5'-CCATGGACTAATGCTGTAATATTA-3' Cre-specific primers – (forward) 5'-ACCTGAAGATGTTCGCGATTATCT-3' and (reverse) 5'-ACCGTCAGTACGTGA GATATCTT-3' – were used, yielding a 370-bp fragment (Figure 2-1D). Amplification was done using a 200-ng template for 40 cycles (Tag DNA Polymerase; New England Biolabs; Ipswich, MA). Two weeks after pIpC induction of young animals RT-PCR for PPARγ mRNA expression was done using peritoneal macrophages, carotid arteries, or abdominal aorta samples (Figure 2-1D). For PPARγ the 5'-GGAAAGACAACAGACAA ATCACC-3' (forward) and 5'-ATTCAGCTTGAGCTGCAGTTC-3' (reverse) primers were used the amplicon yielding a 558 bp fragment. For quantitative monitoring of pIpC-induced Mx1Cre-mediated recombination of PPARγ, 18 mice were randomly divided into two equal groups. One group was injected i.p. with 250 μl of pIpC (2 mg/ml) on days 1, 3, 5, and 7; the others received vehicle. Two weeks after the last injection, the mice were anesthetized with ketamine and xylazine and injected i.p. with 5 μl of sterile PBS. About 5×10^5-10^6 macrophages per mouse were collected from the peritoneal wash by centrifugation and the common carotid artery and the aorta were dissected. RNA purified using TRIzol was pooled from three mice, yielding three samples (treated separately) from the nine mice. One μg of RNA was digested with DNase I and used for the subsequent synthesis of cDNA, using the First Strand Synthesis kit. The following primer pairs were used: PPARγ, (forward) 5'-CATGCTTGTGAAGGATGCAA-3' and (reverse) 5'-CCCAAACCTGATGGCATT-3'; and GAPDH, (forward) 5'-CTGCACCAC CAACTGCTTAG-3' and (reverse) 5'-GGGCCATCCACAGTCTTCT-3'. Amplification was performed for 40 cycles at 94ºC/15 sec and 60ºC/60 sec. Quantitative values were obtained from the Ct. ΔCt was defined by subtracting the average Ct value of PPARγ from the corresponding Ct value of the GAPDH gene in a given sample. Results were expressed as fold difference (N) in gene expression relative to GAPDH, where $N = 2(\Delta Ct\ pIpC - \Delta Ct\ vehicle)$. In peritoneal macrophages, the PPARγ transcript number decreased by 95% after pIpC induction, whereas in the carotid tissue the decrease was 87% (Figure 2-1E).

2.2.7 Mouse Model of Neointima Induction

The surgical procedure for exposing and cannulating the external carotid artery originally developed by Yoshida et al. (Yoshida et al., 2003) rats was adopted to mice. Briefly, the right carotid arteries of anesthetized adult (8-12 week) and sex-matched mice (20 – 30 g) was surgically exposed. The caudal origin of the common carotid artery was ligated using a vessel clip, followed by exposure and ligation of the internal carotid artery above the bifurcation. The external carotid artery was then exposed and a polyethylene catheter was inserted into the external carotid such that it never reached the common carotid artery, thereby avoiding mechanical injury to this segment of the vessel. The clip occluding the common carotid artery was temporarily released, and the vessel was rinsed

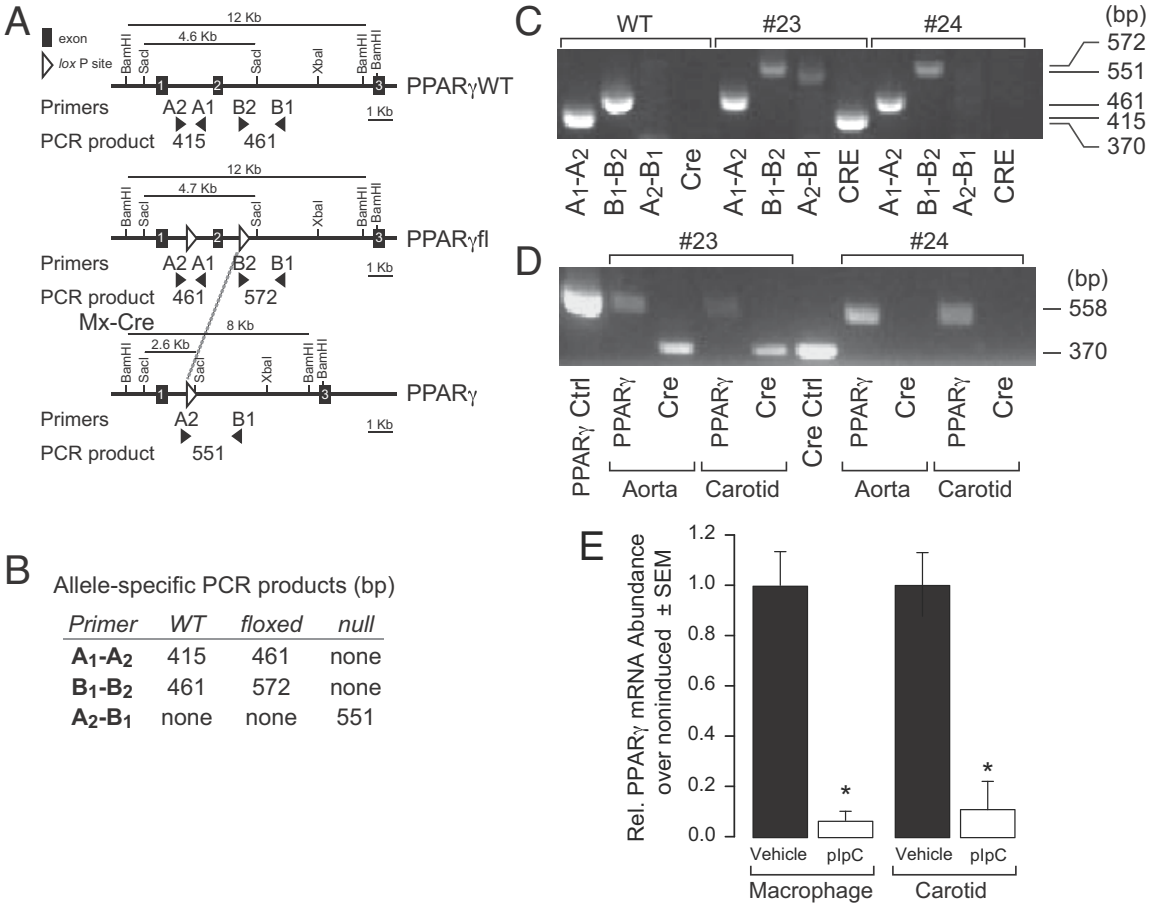

Figure 2-1 Genotyping of PPARγ$^{fl/-}$ and Mx1Cre×PPARγ$^{fl/-}$ mice

(A) Scheme of PPARγ gene arrangement upon Cre-mediated recombination. Note the position and sizes of the different allele-specific primers. (B) Sizes and expected product sizes of allele-specific primers. (C) Genotyping of WT, Mx1Cre×PPARγ$^{fl/-}$ mouse #23, and PPARγ$^{fl/-}$ mouse #24. (D) RT-PCR for PPARγ using carotid and aortic tissues from pIpC-induced ΔPPARγ$^{fl/-}$ (mouse #23) and PPARγ$^{fl/-}$ (mouse #24) mice. Note the diminished 558 bp PPARγ band intensity in mouse #23 compared to mouse #24. (E) Q-PCR using mRNA isolated from peritoneal macrophages and carotid arteries of uninduced vehicle-injected and pIpC-induced ΔPPARγ$^{fl/-}$ mice. Note the substantial but incomplete reduction in PPARγ transcripts in macrophages and carotids.

with a retrograde injection of 100µl physiological saline to remove residual blood. The vessel was again clipped, and 50 µl of treatment solution containing 5µM AGP or ROSI dissolved in 3% DMSO PBS (vehicle) was injected under pressure. After 60 min of incubation, the cannula was withdrawn, the external carotid artery was ligated, and blood flow was restored by removing the clips. Three weeks post surgery the animals were euthanized, and the common carotid artery from the jugular arch to the bifurcation was dissected on both sides, snap frozen in liquid N_2-cooled isopentane and processed for histological analysis. Cryostat sections (~5 µm) were cut and stained with hematoxylin and eosin, Masson's trichrome stain (Richard-Allan Scientific Inc.) or processed for immunohistological staining. Intima-to-media ratios were measured using the NIH Image (version 1.62) software. Groups consisted of four-to-ten animals per treatment or control group. Intima-to-media ratios (mean ± SEM) were compared between the appropriate groups using student's t-test and $p < 0.05$ was considered statistically significant.

2.3 RESULT

2.3.1 Differential Effects of AGP and ROSI on Injury-Induced Neointima

Several literature reports describe the inhibitory effect of the PPARγ agonist ROSI on injury-induced neointima (Lim et al., 2006, Lee et al., 2009). In contrast, in the non-injury model using topical application of ROSI or LPA we and others (Yoshida et al., 2003, Zhang et al., 2004) have found that these PPARγ agonists elicited arterial wall remodeling that includes neointimal growth. To resolve this apparent contradiction, we hypothesized that the mechanisms causing neointima differ between the injury and the non-injury models. Consequently, these agents might exert different effects in these two models. To examine this possibility, we applied a balloon injury model of the rat carotid followed by ROSI or AGP treatments. The injury-induced neointima increased significantly by AGP application following injury ($p < 0.02$, Figure 2-2). However, in agreement with previous reports, ROSI application following balloon injury attenuated neointima formation; although, this attenuation was not statistically significant ($p=0.24$). These observations suggest different mechanisms for AGP and ROSI in this balloon injury model and warn against a direct comparison between this and the non-injury model.

2.3.2 Expression of LPA GPCR Subtypes in the Mouse Carotid

QPCR was used to assess the expression of LPA1-5 GPCR. Transcripts were detected with a rank order of $LPA_1 > LPA_4 >> LPA_2 = LPA_3 > LPA_5$ (Figure 2-3A) in both the carotid and aortic tissue (not shown). LPA_1, LPA_2, LPA_3, and LPA_4 GPCR are 12-, 30-, 100-, and 1.5-times less sensitive to AGP than LPA (Fujiwara et al., 2005, Williams et al., 2009), respectively. In contrast, AGP is more potent than LPA inducing arterial wall remodeling (Zhang et al., 2004). LPA_4 KO mice only became available after the conclusion of the experiments presented herein and were not included in the present

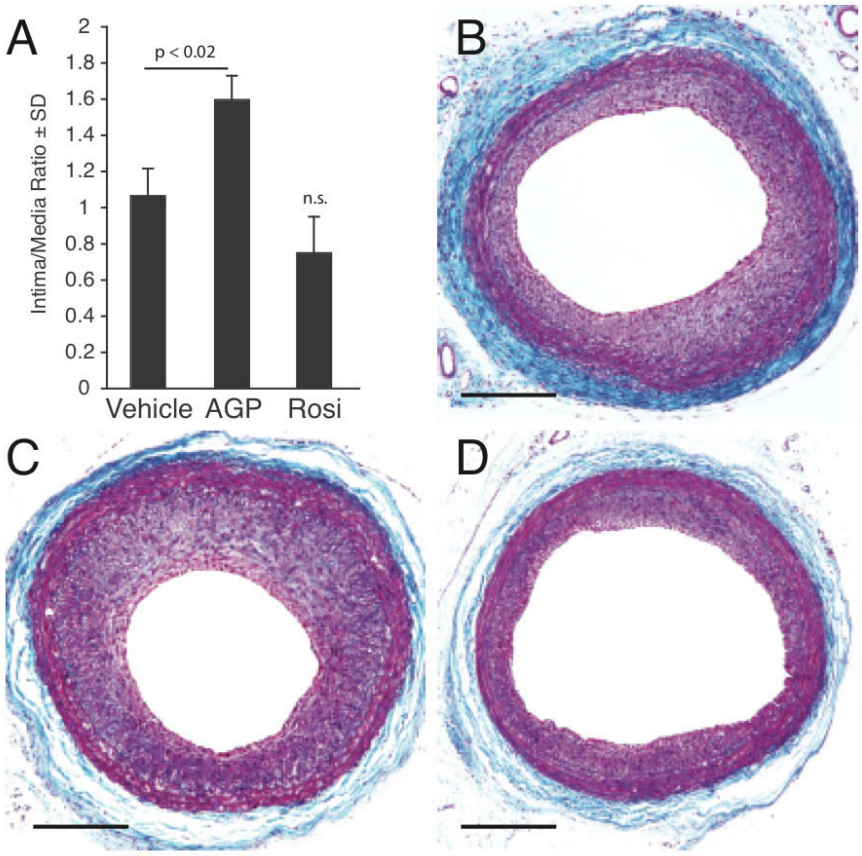

Figure 2-2 Effects of 10 µM AGP or ROSI on neointima induced by balloon injury of the rat carotid artery.

(A) Intima-to-media ratios three weeks after balloon injury followed by a one-hour treatment with vehicle, 10 µM AGP or ROSI. (B, C, and D) Representative cross sections of vehicle-, AGP-, and ROSI-treated carotid arteries. The calibration bar is 200 µm.

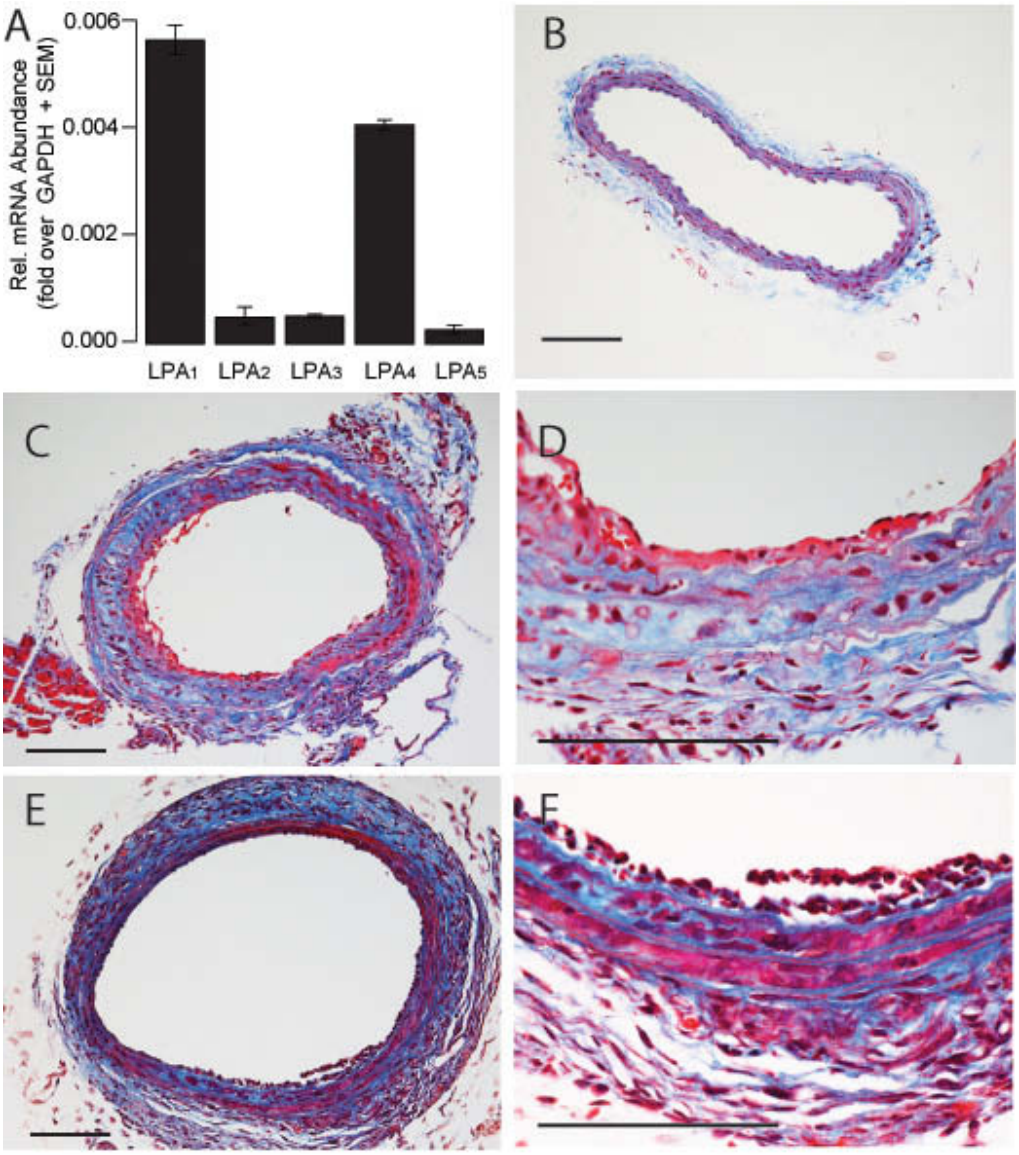

Figure 2-3 AGP and ROSI elicit arterial wall remodeling in C57/BL6 mouse carotids

(A) Quantitative RT-PCR of LPA GPCR expression in the mouse carotid artery. (B) Trichrome-stained cross section of a C57/BL6 mouse carotid treated with vehicle. (C and D) Cross section of a trichrome-stained mouse common carotid artery three weeks after intralumenal application of 2.5 μM AGP. (E and F) Cross section of a mouse common carotid artery three weeks after intralumenal application of 2.5 μM ROSI. Trichrome staining, the bars are 100 μm. Note the multi-layered neointima and changes in the media indicated by the blue stain.

study. Although LPA_3 was reported to prefer unsaturated LPA species over saturated ones (Bandoh et al., 2000), this is not unique to LPA_3 but also found at LPA_1 and LPA_2 (Fujiwara et al., 2005). Due to the 100-fold lesser potency of AGP over LPA at the LPA_3 GPCR combined with the low abundance of its transcripts in the carotid LPA_3 KOs were not included in the study. The ligand selectivity of the LPA GPCR tend to discount but do not exclude the role of these receptors in AGP-induced arterial wall remodeling.

2.3.3 Lumenally Applied AGP and ROSI Elicit Vascular Remodeling in the Uninjured Mouse Carotid Artery

In an effort to examine the contribution of the different cell surface and intracellular LPA receptors to AGP-elicited vascular remodeling we adopted the carotid infusion model to mice. Similarly to our findings in rats (Zhang et al., 2004), infusion of vehicle to the mouse carotid failed to induce remodeling (Figure 2-3B, Figure 2-4A). In contrast, a brief 60 min application of 2.5 μM AGP elicited multilayered neointima (Figure 2-3C). The PPARγ agonist ROSI (2.5 μM) also elicited arterial wall remodeling (Figure 2-3E). No apparent morphologically distinguishable features were found between intimal thickening elicited by AGP or ROSI. Neointima development was accompanied by changes in the media as indicated by the blue staining in the trichrome-stained slides (Figure 2-3D and E) in segments of the common carotid artery not subjected to mechanical injury either by cannulation or clipping. The arteries taken from the contralateral side showed no visible alteration upon microscopic observation (data not shown). The beginning of intimal thickening was clearly observed by the second week and progressed up to the fourth week, the latest time point examined. The neointimal layer developed in response to AGP was not stained with anti-CD31 (Figure 2-4C) but strongly reacted with anti-αSMA antibody (Figure 2-4D). Using double staining, only a few cells in the neointima expressed the CD68 marker (Figure 2-4E) and CD11b positive cells were scarce (Figure 2-4D). Similar immunocytological findings were noted in the ROSI treated mice (Figure 2-5A-F).

2.3.4 Neointimal Responses in LPA GPCR KO Mice

LPA_1, LPA_2, and DKO mice were subjected to intralumenal application of 2.5 μM AGP or ROSI and the carotids were isolated 3 weeks later and neointima formation was quantified. Intima-to-media ratio measurements in LPA_1, LPA_2, and DKO mice showed that AGP (Figure 2-6A, Figure 2-7A) and ROSI (Figure 2-6B) elicited neointima development that was indistinguishable from that seen in WT mice. The cells comprising the neointima were not stained with anti-CD31 (Figure 2-7B) but showed strong immunoreactivity with the anti-αSMA antibody (Figure 2-7C). The neointima contained scattered CD68 positive cells (Figure 2-7D), whereas CD11b positive cells were scarce (Figure 2-7E). Double staining with anti-αSMA and CD68 (not shown) or CD11b (Figure 2-7F) antibodies showed distinct populations of cells expressing the two markers that was similar to the staining patterns seen in WT animals (Figure 2-4E and F, Figure 2-5D-F). The immunohistological staining of the single KO mice showed features (not

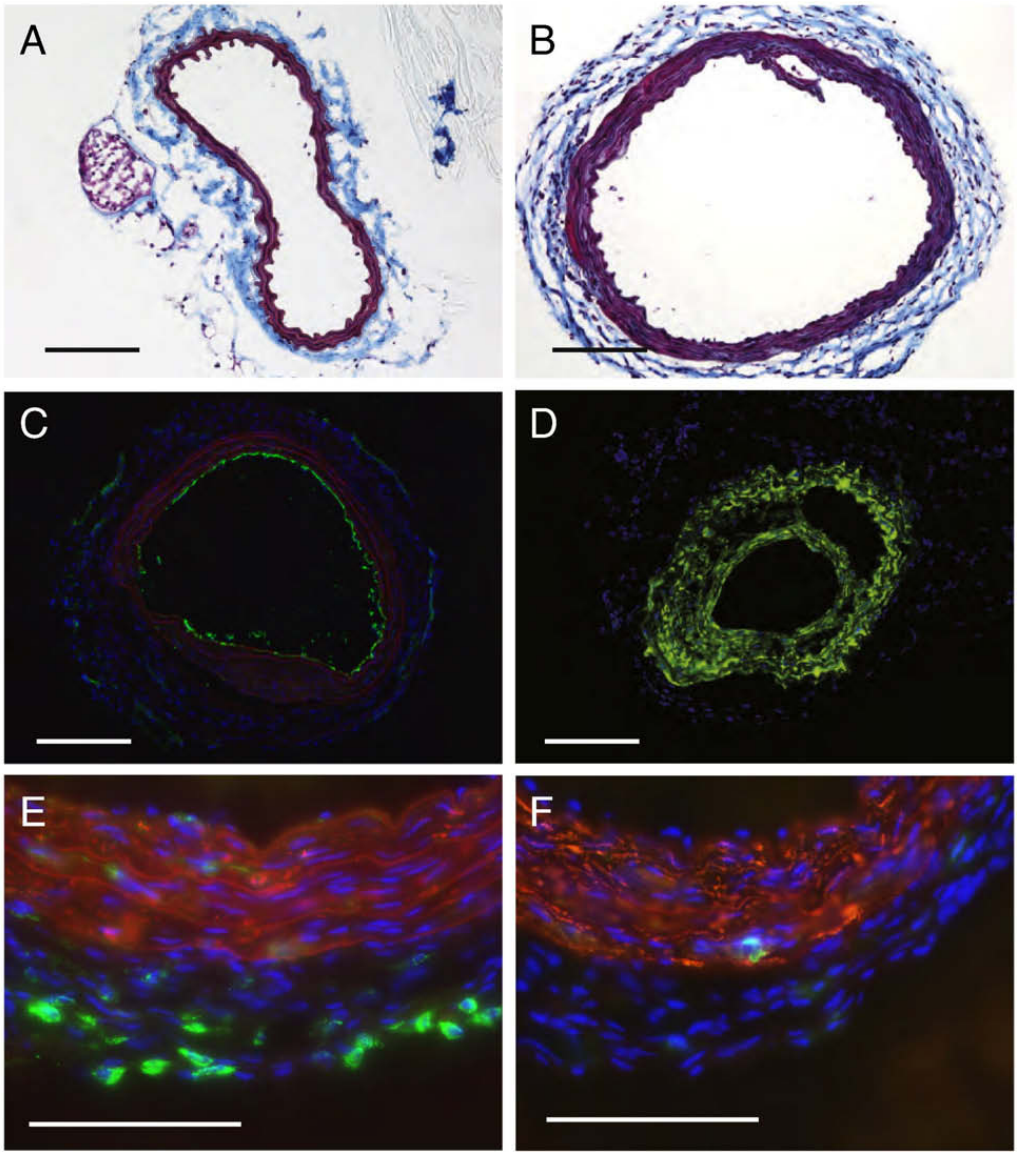

Figure 2-4 Histological and immunohistological staining of neointima in C57/BL6 mouse carotids three weeks after intralumenal application of 2.5 µM AGP

(A) Vehicle injected control carotid artery shows no neointima. (B) AGP-treatment causes concentric neointima with capillary formation within the neointima. (C) Anti-CD31 staining shows single layer of staining and lack of staining in the neointimal layers. (D) Anti-αSMA staining shows intensive immunoreactivity in the neointimal layers. (E) Merged image of anti-CD68 (green) and anti-αSMA (red) staining shows scattered cells bearing this marker in the neointima and no double stained cells in this merged image. (F) Anti-CD11b stained cells are few and anti-αSMA double positive cells are not visible. Calibration bar is 100 µm.

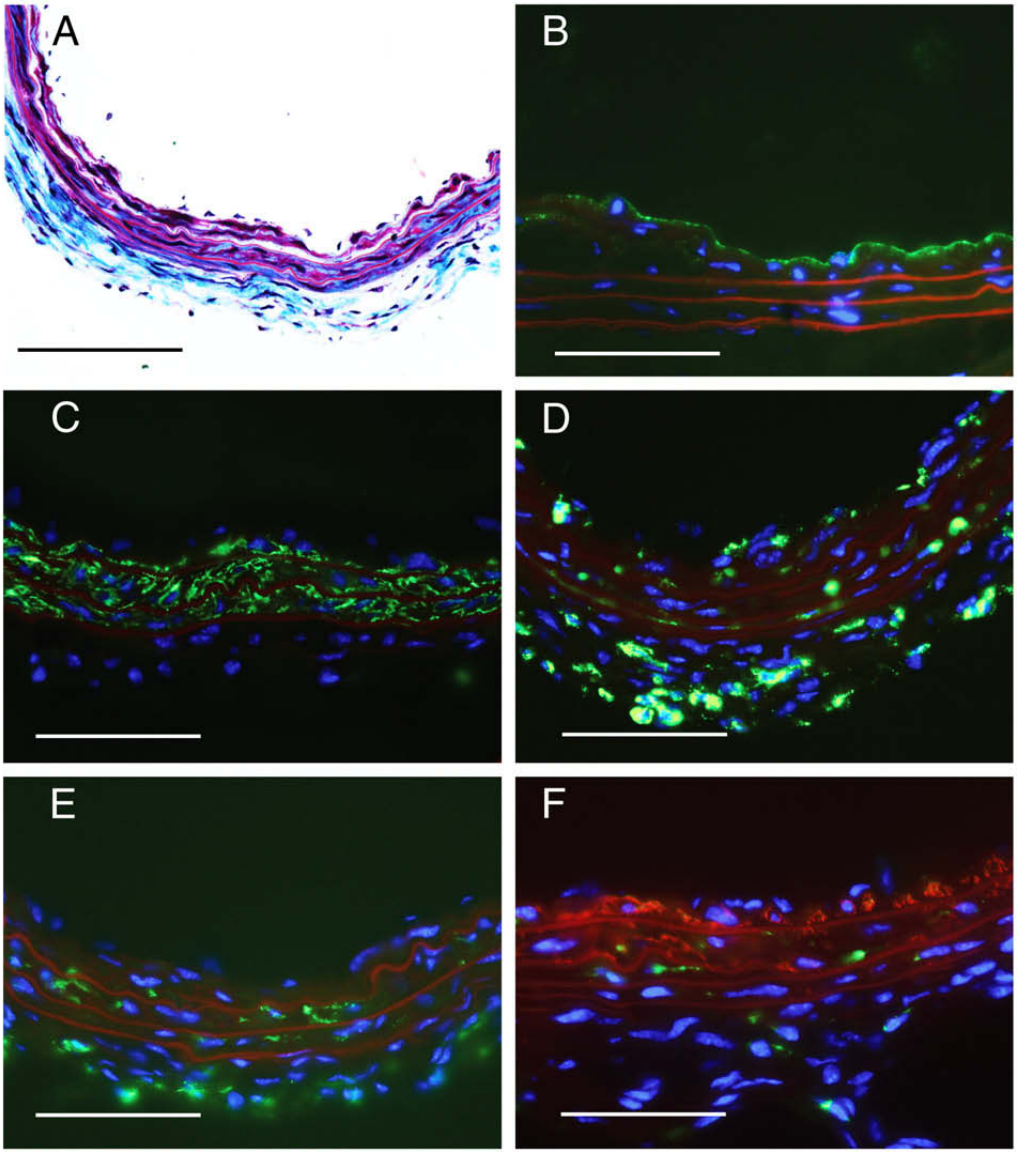

Figure 2-5 Histological and immunohistological staining of neointima three weeks after intralumenal application of 2.5 µM ROSI into the carotid of WT C57BL/6 mice

(A) Masson's trichrome stain shows multi-layered neointima. (B) Anti-CD31 staining shows lack of staining in the neointimal layers. (C) Anti-αSMA staining shows intensive positivity of the neointimal layers. (D) Anti-CD68 stains cells bearing this marker in the neointima and at the media-adventitia boundary. (E) No anti-CD11b stained cells are detected in the neointima. (F) Merged image of double staining with anti-CD11b (green) and anti-αSMA (red) shows distinct populations of cells bearing only one but not both markers. Calibration bar is 100 µm.

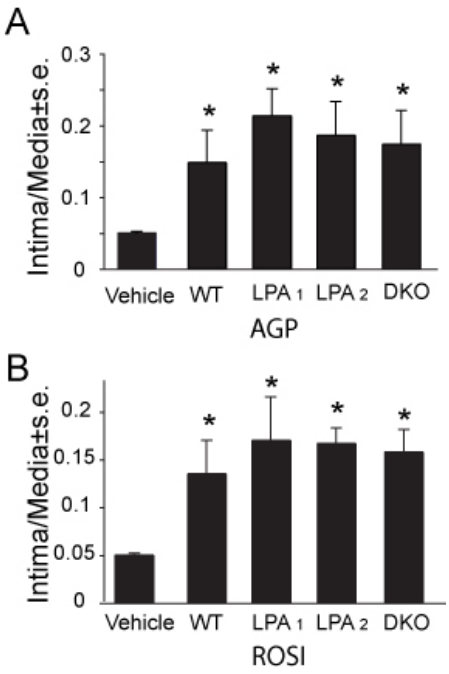

Figure 2-6 Intima-to-media ratios measured in WT and LPA_1, LPA_2, and DKO mice

Effect of 2.5 μM intralumenal application of either AGP (A) or ROSI (B) three weeks after treatment. Note the similar intima-to-media ratios elicited by the treatments regardless of the genotype of the mice. No statistically significant differences were found between the different KOs.

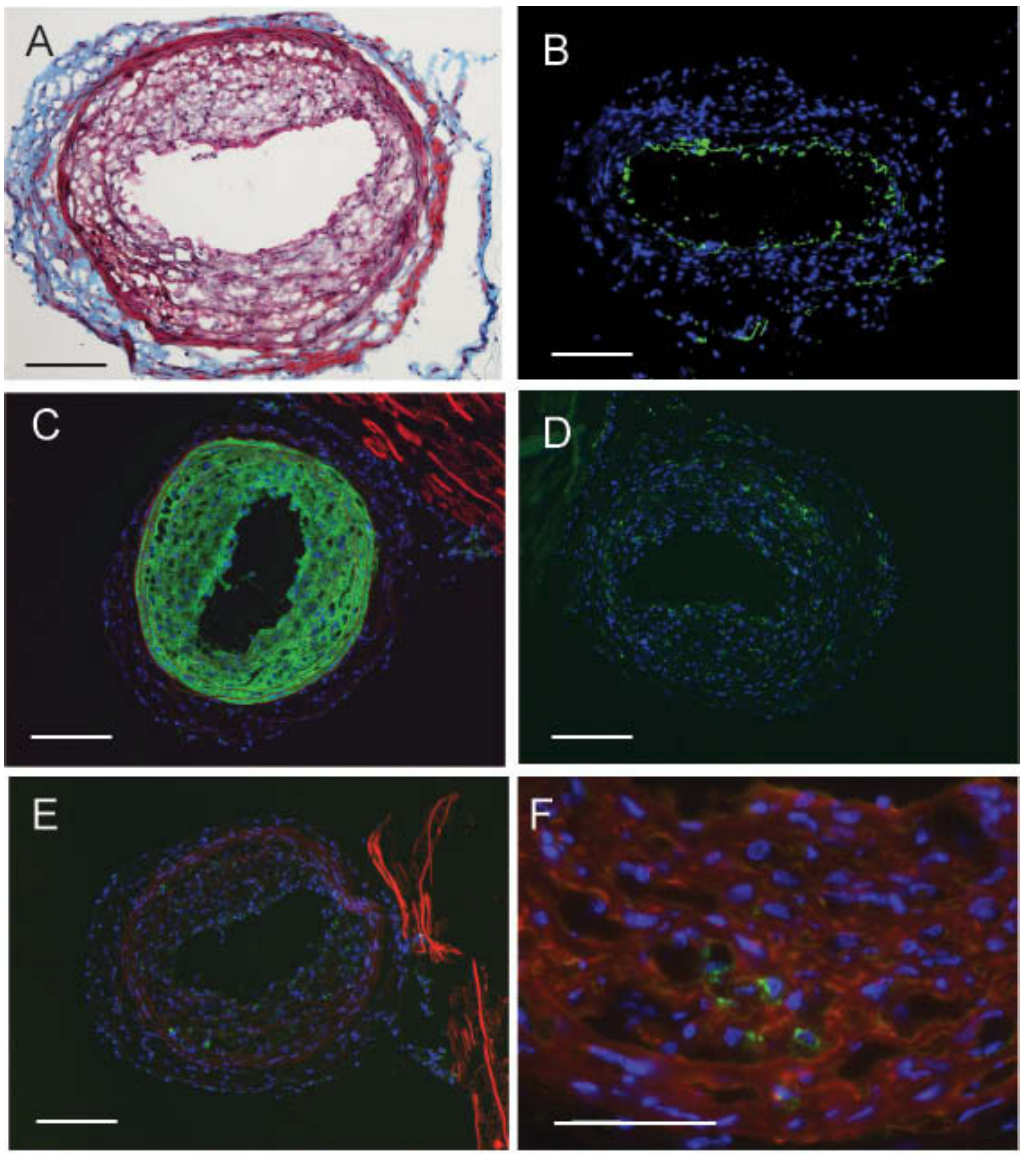

Figure 2-7 Immunohistological phenotyping of neointima three weeks after intralumenal application of 5 µM AGP in DKO mice

(A) Masson trichrome-stained carotid shows multi-layered neointima. (B) Anti-CD31 staining shows lack of staining in the neointimal layers. (C) Anti-αSMA staining shows intensive immunoreactivity in the neointimal layers. (D) Anti-CD68 staining shows positive cells in the neointima. (E) Anti-CD11b stained cells are few and localized at the media-to-adventitia border. (F) Merged double staining for CD11b (green) and anti-αSMA staining shows no double positive cell. Calibration bar is 100 µm.

shown) that were similar to those seen in DKO or WT mice. These observations did not support the requirement for LPA_1 and LPA_2 GPCR in AGP- and ROSI-elicited arterial wall remodeling; thus we focused our investigation to PPARγ.

2.3.5 Neointimal Responses in Conditional PPARγ KO Mice

Knocking out PPARγ causes embryonic lethality, hence we were limited to the availability of conditional KOs that reach adulthood. We chose the Mx1Cre×PPARγ$^{fl/-}$ mouse because in this strain we could experimentally activate Cre-mediated recombination through the Mx1 promoter in the endothelium, VSMC, and macrophages (Akiyama et al., 2002, Schneider et al., 2003). The added benefit of inducible Cre-mediated recombination was that we could compare induced and uninduced littermates. In addition, we examined mice from the parental strains Mx1Cre and PPARγ$^{fl/-}$ for their responses to intracarotid application of AGP and ROSI. In these experiments Mx1Cre mice showed neointima similar to WT mice (Figure 2-8A, Figure 2-9A and B). PPARγ$^{fl/-}$ littermate mice were randomly assigned to two groups, one of which received vehicle, the other was induced with pIpC three weeks prior to carotid surgeries. The uninduced (vehicle injected) group was included to determine whether deletion of one PPARγ allele has any effect on arterial wall remodeling elicited by the two compounds. The pIpC induced control group was designed to assess the effect of pIpC pretreatment on AGP- and ROSI-elicited arterial wall remodeling. Three weeks after these pretreatments the animals were exposed to either vehicle, 2.5 μM AGP, or ROSI for 1 h. After 21 days post carotid surgery the arteries were processed for histology and immunohistology to examine the arterial wall. Determination of the intima-to-media ratio regardless of pretreatment by vehicle or pIpC in the AGP-treated animals showed increases that were identical to those seen in WT animals (Figure 2-8B and G). Similarly, when ROSI was infused into the carotids of pretreated animals the intima-to-media ratio increased (Figure 2-8H, Figure 2-9C and D). These results indicate that neither presence of only a single PPARγ allele nor pretreatment with pIpC abolished arterial remodeling elicited by AGP or ROSI.

Littermates of Mx1Cre×PPARγfl/- animals were randomly assigned to two pretreatment groups to receive either pIpC induction or vehicle. After a 3-week period the carotids of these animals were exposed to either 2.5 μM AGP, 2.5 μM ROSI, or vehicle. Carotid arteries of vehicle pretreated Mx1Cre×PPARγ$^{fl/-}$ animals three weeks after AGP or ROSI treatment showed significant increases in intima-to-media ratio (Figure 2-8C, G, and H, Figure 2-9E and F). The neointima-to-media ratios were similar to that seen in WT animals or PPARγ$^{fl/-}$ animals, establishing that the Mx1Cre×PPARγ$^{fl/-}$ genetic background without pIpC induced Mx1Cre recombination develops arterial wall remodeling in response to AGP or ROSI. In sharp contrast, in the pIpC-induced ΔPPARγ animals AGP or ROSI treatment failed to alter the intima-to-media ratio (Figure 2-8D and F-H, Figure 2-9G and H). These results indicate that conditional KO of PPARγ completely abolished the arterial wall remodeling elicited by AGP or ROSI. Carotid arteries obtained from every group of animals were also stained with anti-CD31, anti-αSMA, anti-CD68, and anti-CD11b antibodies. In those groups of animals that showed

Figure 2-8 Effect of Mx1Cre-mediated conditional knock out of PPARγ on AGP-induced neointima

(A) Trichrome staining of a representative Mx1Cre transgenic mouse carotid three weeks after exposure to 2.5 μM AGP. (B) Representative trichrome-stained carotid of a pIpC-induced PPARγ$^{fl/-}$ mouse three weeks after AGP treatment. (C) Trichrome-stained mouse carotid from a Mx1Cre×PPARγ$^{fl/-}$ mouse without pIpC induction three weeks after exposure to 2.5 μM AGP. (D) Trichrome-stained carotid from a pIpC-induced ΔPPARγ mouse three weeks after AGP treatment. Note the complete lack of neointima development. (E) Anti-αSMA staining of an uninduced Mx1Cre×PPARγ$^{fl/-}$ mouse three weeks after AGP treatment. Note the αSMA positive neointimal cells inside the internal elastic lamina (IEL) that shows red autofluorescence. EEL- external elastic lamina. (F) Anti-αSMA staining of a pIpC-induced ΔPPARγ mouse three weeks after AGP treatment. Note the complete lack of αSMA staining inside the IEL. Calibartion bars are 100 μm. Intima to media ratios in mice with or without pIpC induction three weeks after exposure to 2.5 μm AGP (G) or ROSI (H). Asterisks denote significant differences to uninduced vehicle-treated Mx1Cre×PPARγ$^{fl/-}$ mice ($p< 0.05$, n= 5-10 mouse per group).

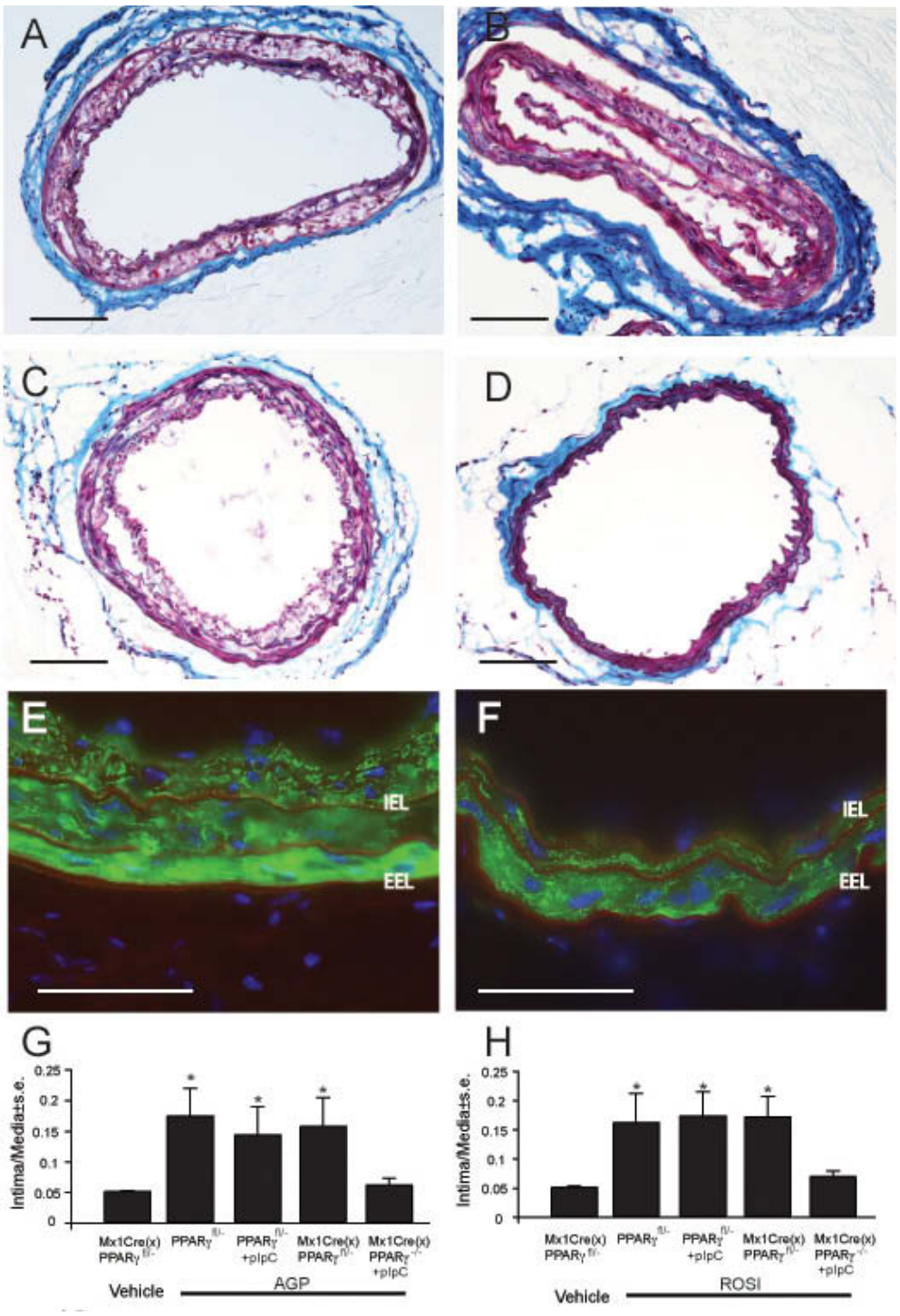
A
B
C
D
E
IEL
EEL
F
IEL
EEL
G
Intima/Media±s.e.
0.25
0.2
0.15
0.1
0.05
0
Mx1Cre(x) PPARγ fl/-
PPARγ fl/-
PPARγ fl/- +plpC
Mx1Cre(x) PPARγ fl/-
Mx1Cre(x) PPARγ -/- +plpC
Vehicle
AGP
H
Intima/Media±s.e.
0.25
0.2
0.15
0.1
0.05
0
Mx1Cre(x) PPARγ fl/-
PPARγ fl/-
PPARγ fl/- +plpC
Mx1Cre(x) PPARγ fl/-
Mx1Cre(x) PPARγ -/- +plpC
Vehicle
ROSI

Figure 2-9 Effect of Mx1Cre-mediated conditional knock out of PPARγ on ROSI-induced neointima

Trichrome (A) and anti-αSMA (B) staining of a pIpC-treated Mx1Cre mouse carotid three weeks after treatment with 2.5 μM ROSI. Trichorme (C) and anti-αSMA (D) staining of a carotid from a pIpC-induced $PPAR\gamma^{fl/-}$ mouse. Trichorme (E) and anti-αSMA (F) staining of a carotid from a non-pIpC-induced Mx1Cre×$PPAR\gamma^{fl/-}$ mouse carotid. Note the anti-αSMA positive neointimal cells inside the IEL. Trichorme (G) and anti-αSMA (H) staining of an pIpC-induced ΔPPARγ mouse three weeks after ROSI treatment. Note the complete lack of αSMA staining inside the IEL. Calibartion bars are 100 μm.

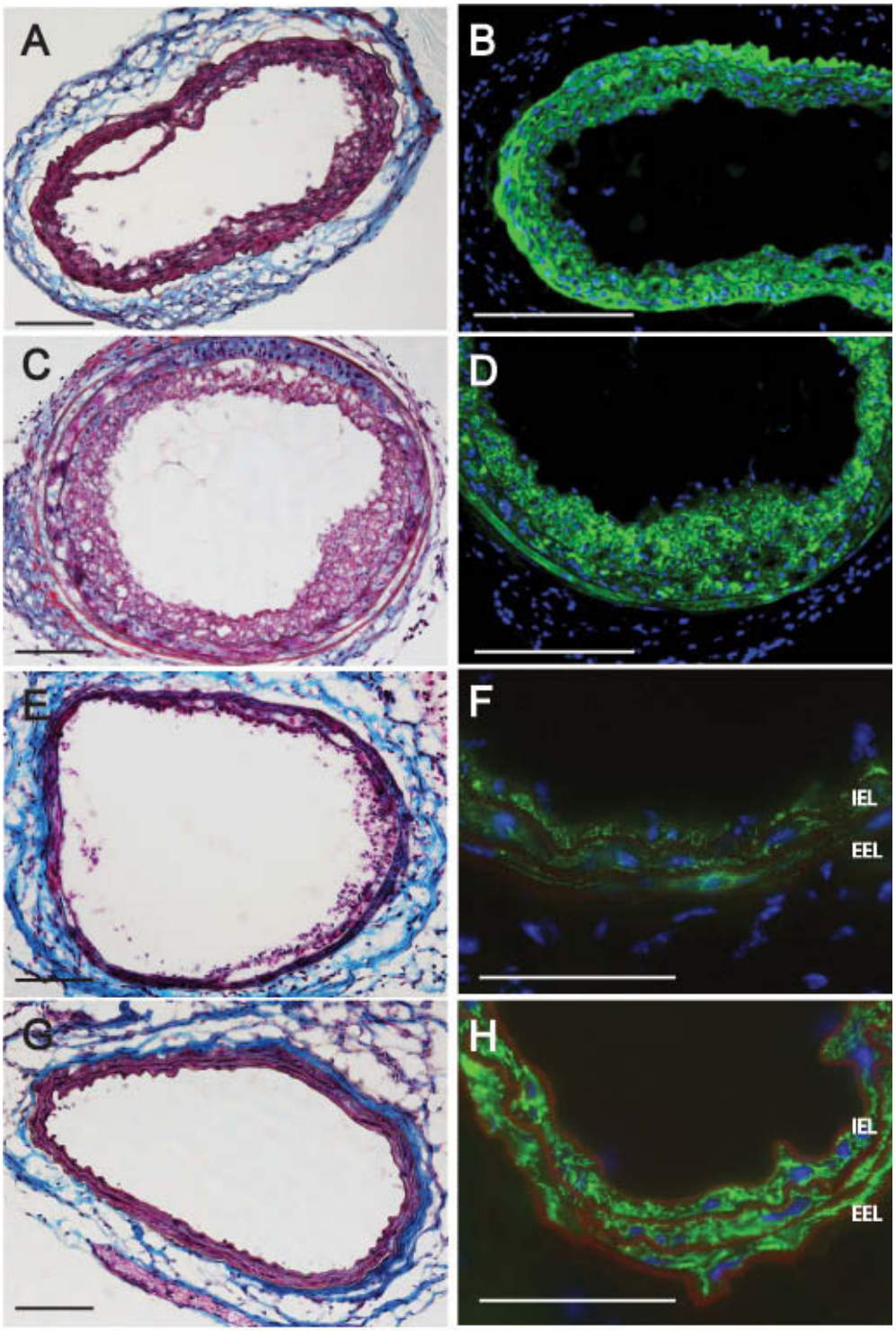
A
B
C
D
E
F
IEL
EEL
G
H
IEL
EEL

increased intima-to-media ratios the immunohistological profile was qualitatively indistinguishable form that of the WT treated with AGP or ROSI. In ΔPPARγ animals that showed no alterations in the intima-to-media ratio we did not observed an increase in SMA positive cells (Figure 2-8F, Figure 2-9H) or alterations in the CD68 or CD11b (not shown) marker-bearing cell populations.

2.4 DISCUSSION

Arterial wall remodeling is considered a prelude to atherosclerotic disease and its pharmacological modulation is of significance in the prevention of several associated pathologies. Injury-induced and post-angioplasty arterial wall remodeling also represent human pathologies that would benefit from pharmacological intervention. The growth factor-like phospholipid mediator LPA has been shown to induce arterial wall remodeling in the absence of injury following only a brief 1-h-long topical application into the lumen of the carotid artery (Yoshida et al., 2003, Zhang et al., 2004). In the present study we sought genetic evidence for the role of LPA_1 and LPA_2 GPCRs and the intracellular LPA receptor PPARγ in this chemically-induced model of arterial wall remodeling.

First, we attempted to resolve the apparent contradiction between chronic ROSI-induced attenuation of injury-elicited neointima (Lim et al., 2006, Lee et al., 2009) and the ROSI-induced neointimal response in the non-injury model by comparing AGP and ROSI effects in the two models. We hypothesized that the mechanisms underlying neointima formation in the chemically-induced and injury-induced models differ leading to the opposite outcome in the response to ROSI application. In the balloon injury model AGP significantly augmented the intima-to-media ratio over that elicited by the injury (Figure 2-2A-C). In contrast, ROSI treatment did not cause either a significant attenuation or augmentation in the intima-to-media ratio relative to the injury control, although the neointima in this treatment group was lesser than in the injury control group (Figure 2-2A and D). This set of experiments clearly indicates that ROSI and AGP application to an injured vessel with disrupted epithelium elicit different outcomes. Future experiments will be conducted using the KO mouse models to evaluate the role of LPA GPCR and PPARγ after vessel wall injury.

Our second objective was to establish and validate a chemically-induced arterial remodeling model in the mouse. We scaled down the treatment from the previously reported rat model (Yoshida et al., 2003, Zhang et al., 2004) and found that in C57BL/6 mice, which represent the genetic background of our knockouts, lumenal application of AGP elicited carotid remodeling at low micromolar concentrations (Figure 2-3C and D). No such changes were found in vehicle treated (Figure 2-3B) or sham operated animals or in the contralateral carotid of AGP-treated mice. Just as in the rat, in mice luminal intracarotid application of ROSI (Figure 2-3E and F) mimicked the effects of AGP when applied at the same concentration and over the same time course. This observation extended the utility of this model from the rat to the mouse, creating the opportunity for inclusion of transgenic and knockout mice in our experiments.

The cellular markers of the treated carotids were examined using antibodies specific to Von Willebrand factor (CD31), αSMA, the pan macrophage marker CD68, and the CD11b marker, which is expressed by tissue macrophages including dendritic cells. Carotid arteries collected from AGP- or ROSI-treated WT mice showed a single layer of CD31 positive cell layer (Figure 2-4C, Figure 2-5B) indicating that the cells in the neointima lack this endothelial cell marker. The neointimal layer showed very strong staining with the αSMA marker (Figure 2-4D, Figure 2-5C) suggesting that the AGP- or ROSI-induced neointima involves the expansion of a cell lineage expressing this smooth muscle cells and myofibroblast marker. Infiltration by cells of the macrophage lineage has been noted in atherosclerotic lesions as well as in the injury-induced neointima (Levy et al., 2007, Papaspyridonos et al., 2008, Seimon et al., 2009). We applied double immunostaining for αSMA cells and CD68 markers in search for double positive cells but failed to detect double positive cells (Figure 2-4E). Immunostaining for the CD11b marker showed few cells localized to the media-adventitia boundary. We did not detect double CD11b and αSMA immunoreactive cells (Figure 2-4F, Figure 2-5F). These observations provide important insight into the mechanism of AGP-induced arterial wall remodeling. It has been reported that LPA blocks the egress of macrophage/dendritic cells from the subendothelium leading to their accumulation (Llodra et al., 2004) and our experiments showed few CD68 and CD11b positive monocytoid cells within multiple layers of αSMA positive cells. Thus in this model the overwhelming majority of neointimal cells expresses αSMA marker which tends to favor a hypothesis that the vascular smooth muscle lineage dominates the cell type responsive to AGP or ROSI stimulation. Whether macrophages are retained initially and cytokines derived from them lead to a secondary immigration and/or proliferation of αSMA positive cells remains to be subject in future studies. Even if this hypothesis will turn out to be correct, the initiating signal that attracts macrophages into the subendothelium would have to originate from the AGP-activation of cells resident to the normal carotid wall. LPA through the LPA_1 and LPA_2 GPCRs has been shown to induce the expression of proinflammatory chemokines including MIP-1beta, IL-8, and MCP-1(Lin and Boyce, 2005, Lin et al., 2006, Kaneyuki et al., 2007). Thus if LPA_1 and/or LPA_2 receptors were required for the accumulation of macrophages leading to neointima, we should have found no macrophage accumulation and neointima in the DKO mice but this was not supported by the experimental findings. Because in rats we found that the effects of LPA or AGP on carotid artery remodeling were indistinguishable from that of ROSI, we tested this compound also. The cellular composition of the ROSI-elicited neointima resembled those in AGP treated carotids (Figure 2-5). These similarities provide added circumstantial support to the hypothesis that these compounds activate a similar mechanism leading to arterial wall remodeling.

LPA_1, LPA_2, and DKO mice have been generated and show no spontaneous vascular pathology (Contos et al., 2002). Because LPA_1 and LPA_2 both are activated by AGP (Fujiwara et al., 2005), we focused initially on their role in LPA-induced arterial wall remodeling. Because of the availability of these single KOs, we also crossed them and established DKO animals. Both AGP and ROSI elicited neointima in the three KO strains that were statistically and immunohistologically indistinguishable from that seen in the WT mice (Figure 2-6, Figure 2-7). LPA GPCR are activated by both saturated and

unsaturated acyl-LPA with a rank order of potency of acyl-LPA > alkyl-GP (Fujiwara et al., 2005, Williams et al., 2009). Only LPA_5 prefers AGP over LPA (Panchatcharam et al., 2008, Williams et al., 2009) but transcripts of this receptor subtype were the least abundant in the mouse carotid (Figure 2-3A). Moreover, LPA GPCRs do not show stereoselectivity to AGP (Yokoyama et al., 2002). The structure-activity relationship for LPA-induced neointima formation is markedly different from that described for LPA GPCR (Zhang et al., 2004): it shows a rank order of alkyl-GP > acyl-LPA, only unsaturated but not saturated fatty acyl species stimulate lesion formation, and the effect shows stereoselectivity for 1-O-AGP over 3-O-AGP. Whereas, LPA-induced cell VSMC proliferation and migration is blocked by pertussis toxin (Tokumura et al., 1994), pretreatment by this toxin only slightly attenuated, but did not abolish neointima formation (Zhang et al., 2004). Diacylglycerol pyrophosphate, a competitive antagonist of the LPA_3 and LPA_1 receptors (Fischer et al., 2001), produced only a partial inhibition of neointima formation. Based on the present results from the LPA GPCR KOs we now expand our previous indirect pharmacological observations and conclude that neither LPA_1 nor LPA_2 receptors are required for AGP- and ROSI-induced arterial wall remodeling.

Because the specific PPARγ antagonist GW9662 fully abolished arterial wall remodeling in rat carotids exposed to AGP, or ROSI, we examined the effect of these agents in conditional PPARγ KO mice. Knocking out PPARγ leads to embryonic lethality and the inducible conditional KO of PPARγ activated by the IFN-regulated Mx1Cre transgene offers an ideal model system in our case because the Mx1Cre is predominantly expressed in endothelial cells, vascular smooth muscle cells and in also in macrophages (Akiyama et al., 2002, Schneider et al., 2003), which represent the three cell types implicated in the literature in neointima formation. The inducible Mx1Cre-regulated recombination of the single floxed PPARγ allele also provided littermate controls that were not exposed to pIpC induction. We also evaluated the effect of pIpC induction in PPARγfl/- animals three weeks prior to AGP or ROSI treatment of the carotid artery to determine whether it would alter the responsiveness of the arterial wall. Quantitative RT-PCR for PPARγ showed that three weeks was sufficient to induce the recombination of the floxed PPARγ allele with high penetration although recombination was not complete (Figure 2-1). Topical intracarotid application of AGP or ROSI in pIpC-induced $PPAR\gamma^{fl/-}$ animals elicited arterial wall remodeling with intima-to-media ratio indistinguishable from that seen in WT animals (Figure 2-8G and H). These findings indicate that pIpC induction does not affect the arterial wall remodeling elicited by AGP and ROSI. Furthermore, these results also establish that deletion of one PPARγ allele does not attenuate AGP- or ROSI-induced neontima. Uninduced Mx1Cre×$PPAR\gamma^{fl/-}$ developed neointima in response to the treatments indicating that spontaneous recombination and the ensuing deletion of this nuclear hormone receptor, if present, is not sufficient to abolish arterial wall remodeling. The immunohistological observations of the arterial wall of these AGP or ROSI treated mice showed qualitative features that resembled those seen in WT animals (Figure 2-8, Figure 2-9). In sharp contrast, in ΔPPARγ mice AGP or ROSI failed to cause a significant change in intima-to-media ratio (Figure 2-8G and H).

Immunohistological examination of carotid arteries taken from these mice showed no αSMA positive cells between the endothelium and the internal elastic lamina (Figure 2-8F, Figure 2-9H). These observations taken together provide genetic evidence for the requirement of PPARγ in the arterial remodeling elicited by AGP and ROSI. The present findings combined with our previous report showing that the PPARγ antagonist GW9662 fully blocked AGP- and ROSI-induced arterial wall remodeling in rats, now provide two independent lines of evidence for the requirement of PPARγ in neointima development in the non-injury model.

LPA and AGP activate platelets, stimulate the formation of platelet-monocyte aggregates (Fueller et al., 2003), and accumulate in the lipid rich core of human atherosclerotic plaques. LPA production in blood is linked to platelet activation (Sano et al., 2002). LPA activates the expression of V-CAM and E-selectin adhesion molecules in endothelial cells which promote cell adherence and invasion of the vessel wall by blood cells (Rizza et al., 1999). LPA also stimulates proinflammatory cytokine production (Kaneyuki et al., 2007, Lin et al., 2007) and inhibits the egress of macrophages from the subendothelium (Llodra et al., 2004). This abundance of evidence combined with our present observations support the role of LPA in vascular wall remodeling and the present study underlines the importance of PPARγ as an important molecular target in this pathology.

CHAPTER 3. PHOSPHOLIPASE D2-DEPENDENT INHIBITION OF THE NUCLEAR HORMONE RECEPTOR PPARγ BY CYCLIC PHOSPHATIDIC ACID*

3.1 INTRODUCTION

PPARγ plays an essential role in regulating lipid and glucose homeostasis, cell proliferation, apoptosis, and inflammation (Ricote and Glass, 2007, Tontonoz and Spiegelman, 2008). These pathways have a direct impact on human diseases, in particular in diabetes(Lehmann et al., 1995), atherosclerosis(Li et al., 2000), and cancer (Sarraf et al., 1998). Synthetic agonists of PPARγ include the thiazolidinedione (TZD) class of drugs, which are widely used to improve insulin sensitivity in type 2 diabetes. Physiological agonists of PPARγ include 15d-PGJ_2 (Forman et al., 1995), modified fatty acids (Nagy et al., 1998, Li et al., 2008), select species of lysophosphatidic acid (1-acyl-2-hydroxy-*sn*-glycero-3-phosphate, LPA; Figure 3-1A) (McIntyre et al., 2003), and oxidized phospholipids (Tontonoz et al., 1998). Another phospholipid, 1-palmitoyl-2-oleoyl-sn-glycerol-3-phosphocholine has recently been recognized as a physiologically relevant agonist of PPARα (Chakravarthy et al., 2009). Despite the beneficial effects of PPARγ on glucose and lipid homeostasis, excess PPARγ activity can be deleterious. PPARγ agonists promote adipocytic differentiation of 3T3-L1 cells and also stimulate the uptake of low-density lipoprotein (LDL) by macrophages, leading to foam cell formation in the arterial wall (Tontonoz et al., 1998, Moore et al., 2001). When applied topically to the carotid arterial wall in rodents, select molecular species of LPA and the TZD drug rosiglitazone (ROSI) induce PPARγ-mediated intimal thickening (Zhang et al., 2004, Cheng et al., 2009). Alkyl-ether analogs of LPA accumulate in the atherogenic oxidized-LDL (Zhang et al., 2004) and human atherosclerotic plaques (Rother et al., 2003), and are potent agonists of PPARγ (Tsukahara et al., 2006). This led us to hypothesize that select LPA analogs could be endogenous regulators of PPARγ; hence, we investigated the structure-activity relationship of activation by naturally occurring lysophospholipids (Figure 3-1A).

* Adapted with permission. Tsukahara T, Tsukahara R, Fujiwara Y, Yue J, Cheng Y, Guo H, Bolen A, Zhang C, Balazs L, Re F, Du G, Frohman MA, Baker DL, Parrill AL, Uchiyama A, Kobayashi T, Murakami-Murofushi K, Tigyi G (2010) Phospholipase D2 dependent inhibition of the nuclear hormone receptor PPARgamma by cyclic phosphatidic acid. Mol Cell 39:421-432.

Figure 3-1 CPA is an antagonist of PPARγ

(A) Structures of the lysophospholipids and ROSI. (B) CPA does not activate PPARγ-dependent PPRE-ACox-Luc expression. CV-1 cells were transfected with ACox-luc plus pcDNA3.1-PPARγ and treated for 20 h with 5 mM each of ROSI, LPA 18:1, AGP 18:1, CPA 18:1, MG, AG, or OA. Luciferase activities are presented as relative light units (RLU, mean ± SEM, n = 4, *p < 0.05, **p < 0.01). (C) Different molecular species of CPA and CGP dose-dependently suppress ROSI-induced PPARγ-dependent PPRE-TK-Luc reporter gene activation in B103 cells. B103 cells (3.0×10^4) were transfected with pMH100-PPRE-TK-Luc, pCMX-PPARγ-Gal4, and pSV-β-gal. After transfection, the cells were exposed to CPA or CGP (0.1, 1 and 10 μM) with or without ROSI (10 μM) for 20h, and reporter gene expression measured (mean ± SEM, n=4). (D and E) Competitive displacement of 5 nM [^{3}H]-ROSI or [^{32}P]-AGP from PPARγ-LBD was determined using 2.5 mM cold ROSI, AGP, or CPA. (F) CPA 18:1 and CGP 18:1 displace [^{3}H]-ROSI from purified LBD of PPARγ. Competition binding was performed using 5 nM [^{3}H]-ROSI and increasing concentrations of CPA or CGP. (G) BODIPY-CPA competitively displaces [^{3}H]-ROSI from PPARγ LBD. Competition biding assay was performed using purified 3 μg PPARγ-LBD with 5 nM [^{3}H]-ROSI and increasing concentrations of either ROSI or BODIPY-CPA competitor. (H and I) Uptake of BODIPY-CPA (3 nmoles) into RAW264.7 macrophages. The rate of accumulation and the metabolic fate of labeled CPA were monitored in the medium (M or circles) and macrophages (C or squares) using TLC. The major fluorescent metabolite observed co-migrated with a standard for BODIPY-FA (fatty acid), indicating phospholipase/acyl transferase action. BODIPY-LPA was not detected. (J) BODIPY-CPA rapidly accumulated in the cell-associated pool and was present in the cytoplasm. Representative fluorescent microscopy image of 3 nmole BODIPY-CPA-treated RAW264.7 macrophages after 0.5 min and 30 min exposure (bar, 50 mm).

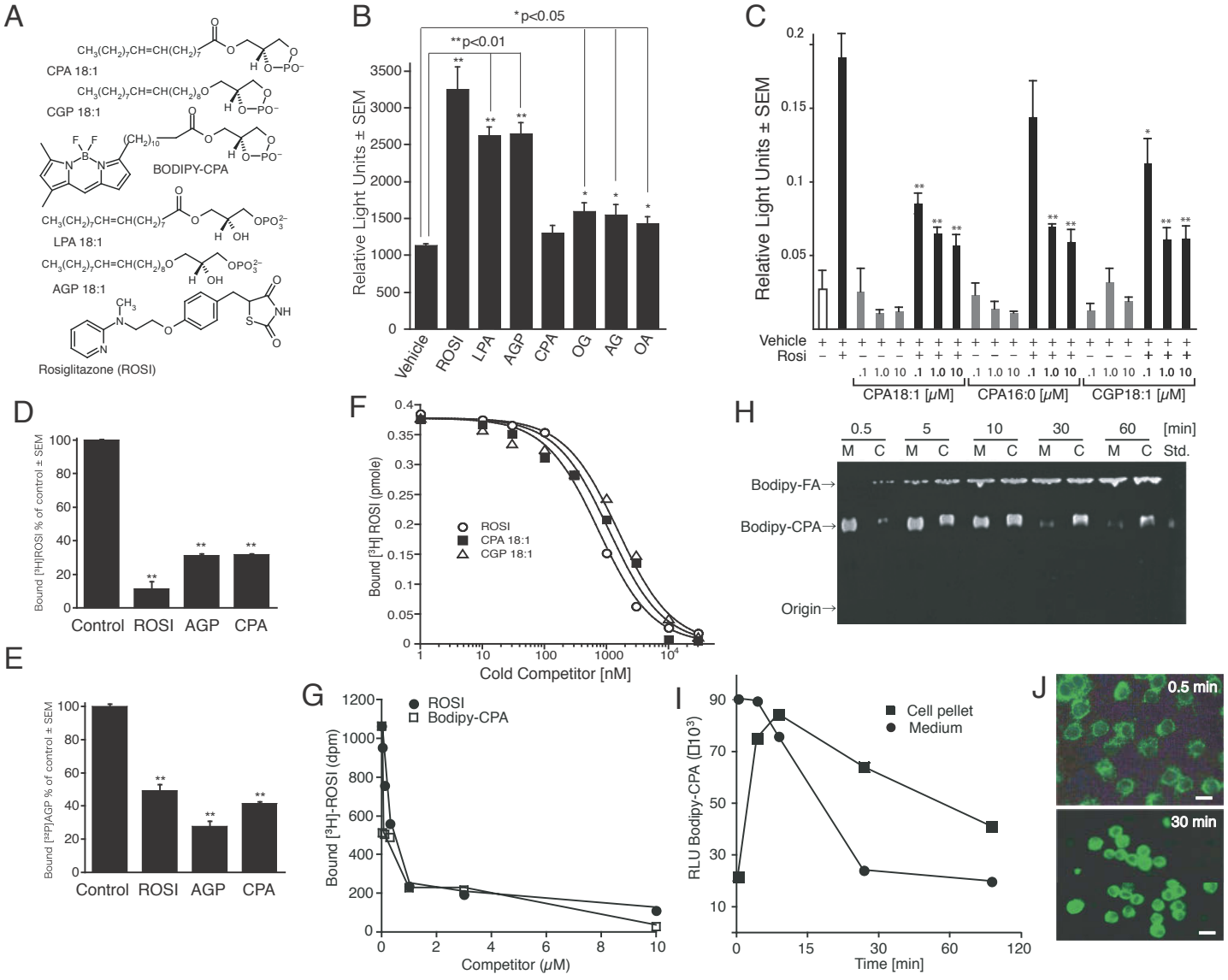
A
CPA 18:1
CGP 18:1
BODIPY-CPA
LPA 18:1
AGP 18:1
Rosiglitazone (ROSI)
B
*p<0.05
**p<0.01
Relative Light Units ± SEM
Vehicle
ROSI
LPA
AGP
CPA
OG
AG
OA
C
Relative Light Units ± SEM
Vehicle
Rosi
CPA18:1 [μM]
CPA16:0 [μM]
CGP18:1 [μM]
D
Bound [3H]ROSI % of control ± SEM
Control
ROSI
AGP
CPA
E
Bound [33P]AGP % of control ± SEM
Control
ROSI
AGP
CPA
F
Bound [3H] ROSI (pmole)
ROSI
CPA 18:1
CGP 18:1
Cold Competitor [nM]
G
ROSI
Bodipy-CPA
Bound [3H]-ROSI (dpm)
Competitor (μM)
H
0.5
5
10
30
60
[min]
M
C
Std.
Bodipy-FA→
Bodipy-CPA→
Origin→
I
Cell pellet
Medium
RLU Bodipy-CPA (□10³)
Time [min]
J
0.5 min
30 min

3.2 EXPERIMENTAL PROCEDURES

3.2.1 Cells

All cell lines were from ATCC unless stated otherwise. MDA-MB-231 cells were grown in Leibovitz's L-15 medium (Gibco) containing 10% (v/v) FBS, 100 U/ml penicillin, and 10 μg/ml streptomycin. CV-1, B103 (rat neuroblastoma cells, from Dr. Jerold Chun, Scripps Institute, La Jolla, CA), RAW 264.7 mouse macrophage cells and 3T3-L1 mouse fibroblast cells were grown in Dulbecco's modified Eagle's medium containing 10% FBS, penicillin, streptomycin, and 1 mM sodium pyruvate. Tetracycline operator-regulated PLD1 and PLD2 transfected CHO have been characterized elsewhere (Du et al., 2004) and were grown in Ham's F12 medium with 5% FBS. Induction of PLD expression was done by 1.5 μg/ml doxycycline (Sigma) for 24 h. Sf-9 insect cells (Invitrogen) were grown in serum-free medium Sf-900 II (Life Sciences).

3.2.2 Ligand-Binding Assays

Ligand binding assays were preformed as described in detail previously (Tsukahara et al., 2006).

3.2.3 PPAR Reporter Gene Assays

Determination of PPARα, β/δ, and γ activation was done in CV-1 cells (endogenously express $LPA_{1/2/3}$) or B103 cells (lack endogenous $LPA_{1/2/3}$ receptors and PPARγ) transfected with 125 ng of the appropriate reporter gene (pGL3-PPRE-acyl-CoA oxidase luciferase or in some experiments with MH100-PPRE-TK-luciferase) and 62.5 ng of pcDNA3.1-PPARγ or pCMX-PPARγ-Gal4 and 12.5 ng of pSV–β-galactosidase (Promega) construct as previously reported (Tsukahara et al., 2006). To monitor activation of PPARα, 62.5 ng of pG4M-PPARα-ligand binding domain and 12.5 ng of pSV-β-galactosidase or 125 ng of 17 m5×-βGLOB-luc plasmids were transfected into B103 cells using Lipofectamine 2000. For PPAR β/δ, we used 62.5 ng of pG4M-PPARβ/δ-LBD plasmid DNA and 12.5 ng of pSV-β-galactosidase or 125 ng of 17m5×-βGLOB-luc plasmids. Twenty-four hours after transfection, cells were treated with Opti-MEM containing 10 μM test compound dissolved in DMSO and cultured for an additional 20 h. Luciferase activity was measured with the Steady-Glo Luciferase Assay System (Promega) using a Fusion Alpha plate reader (Perkin-Elmer).

3.2.4 Co-Repressor Two-Hybrid Assays

The effect of CPA on SMRT co-repressor binding to PPARγ was done as described by Yu et al. (Yu et al., 2005). Briefly, CV-1 cells were plated onto 96-well

plate at the density of 1.0×10^4 cells per well in DMEM containing 10% FBS. The next day, the cells were transiently transfected with 71 ng of UAS-Luc, 14.3 ng of Gal4-SMRT, 14.3 ng of pVP16-PPARγ2, and 10 ng of pSV–β-galactosidase (Promega) using Lipofectamine LTX (Invitrogen). Twenty hours after transfection, the cells were pretreated with various concentrations of CPA or CGP 18:1 in Opti-MEM (Invitrogen) for 30 min, followed by treated with Opti-MEM containing 1nM ROSI for 6 h. Luciferase and β-galactosidase activities were measured as above. Samples were run in quintuples, and the mean ± SEM were calculated. Data are representative of at least three independent transfections. Student's *t* test was used to test for statistical analysis and $p<0.05$ was considered significant.

3.2.5 Biosynthetic Labeling of Cells and Measurement of CPA Synthesis

MDA-MB-231 cells (3.5×10^6) or CV-1 cells (1.0×10^6) were serum-starved for 12 h and washed with phosphate-free medium and incubated in balanced salt solution (135 mM NaCl, 4.5 mM KCl, 1.5 mM $CaCl_2$, 0.5 mM $MgCl_2$, 5.6 mM glucose, 10 mM HEPES-NaOH, pH7.2) containing 1 mCi/ml [^{32}P]-orthophosphoric acid. After 3 h, the labeling medium was removed, and the cells were washed 3×with Ca^{2+}/Mg^{2+} free phosphate-buffered saline (PBS) and preincubated at 37 ^{o}C in serum-free medium for 15 min. After treatment with 100 nM PMA (Fluka) for 30 min, the cells were washed once with ice-cold PBS and collected by centrifugation. The phospholipids were extracted (Bligh and Dyer, 1959), spotted on indicator-free high-performance silica gel TLC plates (Whatman) and separated by two-dimensional TLC using chloroform-methanol-acetic acid-1% sodium disulfite (100:40:12:5) solvent in the first dimension and chloroform-methanol-ammonium hydroxide (3:6:1) in the second dimension. Unlabeled LPA and CPA standards were mixed into the samples and visualized by 0.01% primulin (Sigma) staining, whereas radioactivity was detected by a Cyclone phosphorimager (Perkin-Elmer).

3.2.6 Statistical Methods

Significant differences were based on student's t-test relative to the appropriate control. Equilibrium binding constants (K_D) were calculated from the binding data using the Kaleida-Graph Software version 4.0 (Synergy Software).

3.3 RESULT

3.3.1 CPA Is a Specific and a High-Affinity Antagonist of PPARγ

When testing lysophospholipids using a PPARγ reporter gene assay, we observed that CPA at concentrations as high as 5 μM failed to activate transcription (Figure 3-1B). In contrast, lower concentrations of LPA 18:1 and its ether analog alkyl glycerophosphate

(AGP 18:1) strongly activated PPARγ. Smaller chemical components of CPA namely oleoyl glycerol (OG), alkyl glycerol (AG), and oleic acid (OA) showed weak activation. To establish a direct interaction between CPA and the PPARγ ligand-binding domain (LBD), recombinant LBD was purified to examine the displacement of agonists [^{3}H]-ROSI (Figure 3-1C) and [^{32}P]-AGP (Figure 3-1D) by CPA. CPA and its ether analog 1-O-octadecyl-2,3-cyclic-glycerophosphate (CGP 18:1, Figure 3-1A) displaced both labeled agonists, and Scatchard analysis revealed single high-affinity binding constants at 124 ± 19 nM and 172 ± 27 nM, respectively (Figure 3-1E), which was comparable to that of ROSI (84 ± 6 nM).

To monitor the metabolic fate and distribution of exogenously applied CPA, we synthesized a fluorescent analog BODIPY-CPA (Figure 3-1A), which also displaced [^{3}H]-ROSI from the PPARγ-LBD (Figure 3-1F). BODIPY-CPA was applied to RAW 267.4 macrophages and uptake of the fluorescent lipid was determined as a function of time (Figure 3-1G and H). BODIPY-CPA uptake peaked at 15 min before beginning to undergo metabolism by deacylation into BODIPY-fatty acid, whereas no BODIPY-LPA or any other metabolic product was detectable, indicating the stability of the cyclic-phosphate ring. The cellular half-life of BODIPY-CPA in this experiment was approximately 60 min and the label was present in both the cytoplasm and nuclei of the cells after 30 min (Figure 3-1I). Exogenously applied CPA species inhibited PPARγ-dependent gene expression elicited by TZDs ROSI (Figure 3-1J), pioglitazone and troglitazone (Figure A-1A and B) in a cell-based PPARγ reporter gene assay. The highly homologous PPARα and PPARβ/δ receptors were neither inhibited nor activated by CPA (Figure A-1C-F).

3.3.2 Differential Interactions between Agonists and the Antagonist CPA with the PPARγ-LBD

The crystal structures of the PPARγ-LBD and the ROSI-bound complex have previously been solved (Nolte et al., 1998). Currently no reported studies on antagonist-bound structures of the PPARγ-LBD are currently available in the public domain. Using a crystal structure of the highly homologous PPARα bound to antagonist GW6471, we generated a homology model of the inactive PPARγ-LBD complex. The active-LBD and inactive-LBD served as targets in computational docking studies with ROSI, AGP 18:1, and CPA 18:1 (Figure 3-2A and B). CPA 18:1 forms ion-pairing interactions with residue R288 was previously shown for the interaction of AGP 18:1 with PPARγ-LBD (Tsukahara et al., 2006). This interaction is required for binding of the phosphate-containing agonists. However, only the alkyl chain of AGP 18:1 showed favorable interactions with a hydrophobic residue of the AF-12 helix, L469, in the active-LBD (Figure 3-2B). In contrast, CPA 18:1 bound with higher affinity to the inactive-LBD, failing to stabilize the active conformation of the AF-12 helix (Figure 3-2A). The docked positions of ROSI and AGP overlap and differ from the docked position of CPA. This is consistent with the agonist activity of ROSI and AGP, and corresponding lack of such activity for CPA. Although CPA does not overlap with the docked position of AGP and ROSI, interactions with common residues occur from a

Figure 3-2 CPA inhibits PPARγ activation and is generated by PLD

(A) Comparison of ROSI crystallized in PPARγ (1FM6) and CPA 18:1 docked into the inactive homology model of PPARγ. Blue ribbons show the backbone structure of the inactive PPARγ homology model. The inactive homology model differs from the active crystallographic structures only in the position of the AF-12 segment, which is shown as a green and a red ribbon in the inactive homology model and the crystallographic structure, respectively. Ligands are shown as ball and stick models. (B) Comparison of AGP 18:1 docked into the activated crystallographic structure of PPARγ (1FM9) and overlay of CPA 18:1 docked into the inactive homology model of PPARγ. Note that agonists ROSI and AGP occupy the same location and interact with residue R288, while CPA prevents the AF-12 domain from acquiring its activated conformation (red) by stabilizing the inactivated conformation (green). (C and D) Arginine 288 is required for inhibition of PPARγ by CPA. Purified WT and R288A mutant PPARγ (1 μg) were incubated with 5 nM [^{3}H]-ROSI or [^{32}P]-AGP 18:1 under equilibrium binding conditions with 2.5 μM cold ROSI, AGP, and CPA, and the bound ligand quantified using a filtration assay (mean ± SEM, n = 4). (E) ROSI-induced SMRT release from PPARγ is dose-dependently inhibited by both CPA 18:1 and CGP 18:1. CV-1 cells were transfected with UAS-Luc, pECE-Gal4-SMRT (containing full length SMRT), pVP16-PPARγ2, and pSV-β-gal. After transfection, the cells were treated with CPA 18:1 or CGP 18:1 for 30 min, followed by 1nM ROSI for 6 h. Luciferase activities are presented as fold increase (mean ± SEM, n=4, representative of 3 transfections). (F) Stimulation of biosynthetically [^{32}P]-orthophosphate-labeled MDA-MB-231 cells with PMA (100 nM, 30 min) leads to CPA generation. PMA stimulation (100 nM) was also performed in the presence of either 1.5% 1-BuOH or t-BuOH. Phospholipids were separated using 2D-TLC and visualized using phosphorimaging. Arrows point to the position of the authentic CPA standard and asterisks indicate the position of the LPA standard. (G) CPA production in PMA-stimulated cells is inhibited by 1-BuOH but not by t-BuOH. Phosphorimaging-based quantification of labeled CPA after stimulation of MDA-MB-231 cells by 100 nM PMA in the presence or not of 1.5% v/v 1-BuOH and t-BuOH (mean cpm ± SEM, n = 4).

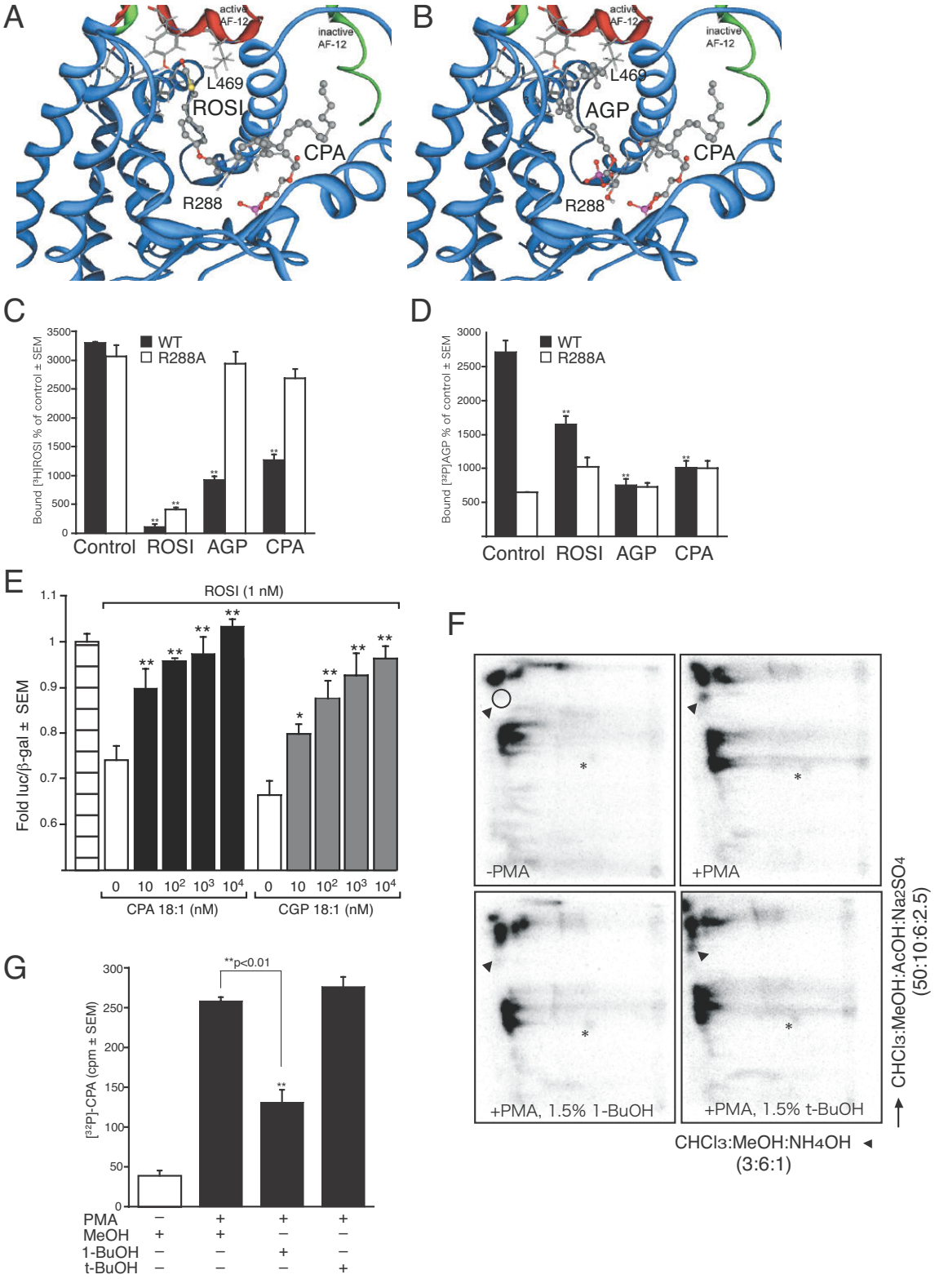
A
active AF-12
inactive AF-12
L469
ROSI
CPA
R288
B
active AF-12
inactive AF-12
L469
AGP
CPA
R288
C
WT
R288A
Bound [3H]ROSI % of control ± SEM
Control
ROSI
AGP
CPA
D
WT
R288A
Bound [32P]AGP % of control ± SEM
Control
ROSI
AGP
CPA
E
ROSI (1 nM)
Fold luc/β-gal ± SEM
CPA 18:1 (nM)
CGP 18:1 (nM)
F
-PMA
+PMA
+PMA, 1.5% 1-BuOH
+PMA, 1.5% t-BuOH
CHCl3:MeOH:NH4OH
(3:6:1)
CHCl3:MeOH:AcOH:Na2SO4
(50:10:6:2.5)
G
**p<0.01
[32P]-CPA (cpm ± SEM)
PMA
MeOH
1-BuOH
t-BuOH

different pocket. These common interactions preclude binding of CPA at the same time as either ROSI or AGP, which explains the competitive antagonistic effect of CPA.

The phosphate group common to LPA and AGP has been previously validated to form a salt bridge with R288 in the LBD (Tsukahara et al., 2006). The R288A mutant loses AGP binding and activation; nevertheless, binding to and activation by ROSI remains unchanged (Tsukahara et al., 2006). To evaluate the computationally predicted role of R288 in CPA binding, we expressed its alanine mutant LBD recombinant protein, and examined it for binding to [^{3}H]-ROSI and to [^{32}P]-AGP 18:1 (Figure 3-2C and D). The R288A mutant bound [^{3}H]-ROSI but did not bind [^{32}P]-AGP 18:1. Although an excess of unlabeled ROSI, AGP 18:1, or CPA 18:1 competed with [^{3}H]-ROSI binding at the WT PPARγ LBD, only ROSI displaced the labeled ligand in the R288A mutant. These results confirm the critical role of the predicted salt bridge between residue R288 and CPA 18:1 and support the hypothesis that CPA functions as a high-affinity antagonist of PPARγ.

The inactive conformation of PPARγ promotes binding of corepressor proteins. Antagonists should prevent the agonist-induced dissociation of this complex. Using a two-hybrid assay (Yu et al., 2005) in CV-1 cells that allows detection of the complex formed between PPARγ and its corepressor SMRT, we tested the effect of CPA on ROSI-induced dissociation of this molecular complex. CPA and CGP dose-dependently stabilized the SMRT-PPARγ and antagonized ROSI-induced dissociation of the complex (Figure 3-2E).

3.3.3 Activation of PLD2 Generates CPA

CPA has been detected in mammalian tissues (Murakami-Murofushi et al., 2000). To establish a physiological role for CPA in the regulation of PPARγ, we determined whether cellular activation of phospholipase D (PLD) can generate it because prior work showed that the catalytic mechanism of PLD from *Streptomyces chromofuscus* includes CPA as a reaction intermediate (Friedman et al., 1996). MDA-MB-231 breast cancer cells, which express both PLD PLD1 and PLD2 isoenzymes (Eisen and Brown, 2002), were biosynthetically labeled with [^{32}P]-orthophosphate and stimulated with 100 nM phorbol myristate acetate (PMA), a strong nonselective activator of both PLD isoforms. After 30 min of stimulation the phospholipids were extracted, separated and compared to phospholipids from vehicle-stimulated cells using two-dimensional thin layer chromatography (2DTLC). No label was detected at the position of an authentic CPA standard spiked into the sample in the vehicle-treated cells (Figure 3-2F). In contrast, a spot co-migrating with the CPA standard became detectable in PMA-stimulated cells. The hydrolysis of lysophosphatidyl choline (LPC) by PLD includes a transphosphatidylation step that can be inhibited by the primary alcohol 1-butanol (1-BuOH), but not by secondary alcohol 2-methyl-2-propanol (t-BuOH). When the PMA-stimulated cells were treated with 1-BuOH, the intensity of the [^{32}P]-CPA spot on 2DTLC was significantly reduced, whereas t-BuOH had no effect (Figure 3-2F and G).

To determine which of the two PLD isozymes was responsible for CPA production, we used CHO cell lines stably expressing tetracycline-inducible alleles of wild-type (WT) or catalytically-inactive (CI) forms of PLD1 or PLD2 (Du et al., 2004). PMA stimulation of cells with doxycycline (DOX)-induced expression of PLD1 caused a two-fold increase in CPA production, which was similar to that observed for WT cells. In contrast, PMA-stimulation of cells with DOX-induced PLD2 expression caused a ten-fold increase in CPA production compared to unstimulated WT cells (Figure 3-3A) and elevated the basal levels of CPA. However, expression of the catalytically-inactive PLD2 (CI-PLD2) failed to amplify the PMA-induced CPA production. In the absence of DOX induction, all four cell lines contained very low amounts of CPA, and PMA stimulation yielded similar increases in CPA (Figure A-2A). These findings suggest that PLD2 activation underlies the stimulus-coupled CPA production.

To obtain direct proof that PLD2 generates CPA, recombinant WT and CI-PLD2 were purified and reacted with [^{14}C]-LPC *in vitro*, and the reaction products were separated by TLC (Figure 3-3B). WT-PLD2, but not the CI-PLD2, generated [^{14}C]-CPA (V_{max} = 190 pmol/min/mg; K_m = 8 μM; Figure A-2B). Addition of 1-BuOH to this reaction generated lysophosphatidylbutanol, whereas inclusion of t-BuOH yielded no such product (Figure 3-3C and D). These data indicate that mammalian PLD2 is capable of producing CPA from LPC *in vitro* and *in vivo*.

3.3.4 Physiological Stimulation of PLD2 Generates CPA

CPA levels were then quantified in unstimulated control and PMA-stimulated MDA-MB-231 cells by liquid chromatography mass spectrometry (LC-MS). CPA was below the detection limit in control cell extracts (Figure A-2C). Treatment with 100nM PMA for 30 min resulted in the generation of CPA 16:0 and 18:1 (595 ± 1.5 pmol and 293 ± 25.6 pmol / 3×10^7 cells, respectively; Figure A-2D). Insulin is a physiological activator of PLD2 (Slaaby et al., 2000). LC-MS quantification of CPA in insulin-stimulated cells showed peak production with 967 ± 111.2 pmol CPA 16:0 and 573 ± 33.5 pmol CPA 18:1 per 3×10^7 cells, respectively (Figure A-2E). Insulin generated higher levels of CPA compared to PMA (Figure 3-3E) that peaked at 30 min (Figure 3-3F). Insulin stimulation of CV-1 cells did not increase the biosynthetically labeled pool of LPA (Figure 3-4A, Figure A-3A-C), indicating that the major lysophospholipid product of PLD2 is CPA.

We extended our studies to human peripheral blood monocytes and found that insulin, lipopolysaccharide, H_2O_2, or PMA stimulation of PLD2 of within 30 minutes caused production of CPA 18:1 and 16:0 (Figure 3-4B, Figure A-2F-I). In resting monocytes the level of CPA 16:0 and 18:0 was 0.14 and 1.5 pmole/10^7 cells, respectively. After stimulation with 100 nM PMA CPA 16:0 rose ~ 1,300-fold and CPA 18:1 rose ~ 390-fold (Figure 3-4B). After stimulation with 100 nM insulin CPA 16:0 rose 8.5-fold and CPA 18:1 rose 67-fold. Addition of the PLD2 inhibitor 5-fluoro-2-indolyl des-chlorohalopemide (FIPI 750nM) inhibited production of both CPA species (Figure 3-4B, Figure A-2G and H). Thus, physiological stimuli of PLD2 in

Figure 3-3 *In vitro* and *in vivo* generation of CPA by PLD2

(A) PLD2 is the major source of CPA *in vivo*. CHO cells expressing *tet*-regulated WT or CI-PLD1 or PLD2 constructs were induced by DOX and subsequently stimulated with 100 nM PMA for 30 min. Cellular phospholipids were biosynthetically labeled with 0.1 mCi [^{32}P]-Pi for 12 h, and CPA generation quantified using phosphorimaging after 2D-TLC separation (mean ± SEM, n = 3). (B) PLD2 generates CPA *in vitro*. Affinity-purified WT or CI-PLD2 (10 mg/reaction) was incubated with [^{14}C]-LPC 16:0 at 40 ºC for 1 h. The reaction mixtures were spotted on a TLC plate and separated. Authentic cold CPA and LPA standards were used to determine the product Rfs. (C) 1-BuOH but not t-BuOH diverts recombinant PLD2 formation of CPA to lysophosphatidyl butanol (lyso-PtBuOH). TLC analysis of [^{14}C]-phospholipids generated by purified PLD2 from Sf-9 insect cells after treatment with 0.5% 1-BuOH or t-BuOH. (D) Quantification of CPA and [^{14}C]-lyso-PtBuOH formation by PLD2 in the presence of 0.5% 1-BuOH and t-BuOH (n = 3). N.D., not detectable. (E) LC-MS quantification of CPA 16:0 and 18:0 after stimulation of MDA-MB-231 cells by 100 nM insulin or PMA for 30 min (pmol mean ± SEM, n = 3). (F) Time course of insulin-stimulated CPA production in MDA-MB-231 cells. Cells (3×10^6) biosynthetically labeled with [^{32}P]-orthophosphate were exposed to 100 nM insulin for different times and the CPA purified using 2DTLC and quantified using liquid scintillation counting (n=3).

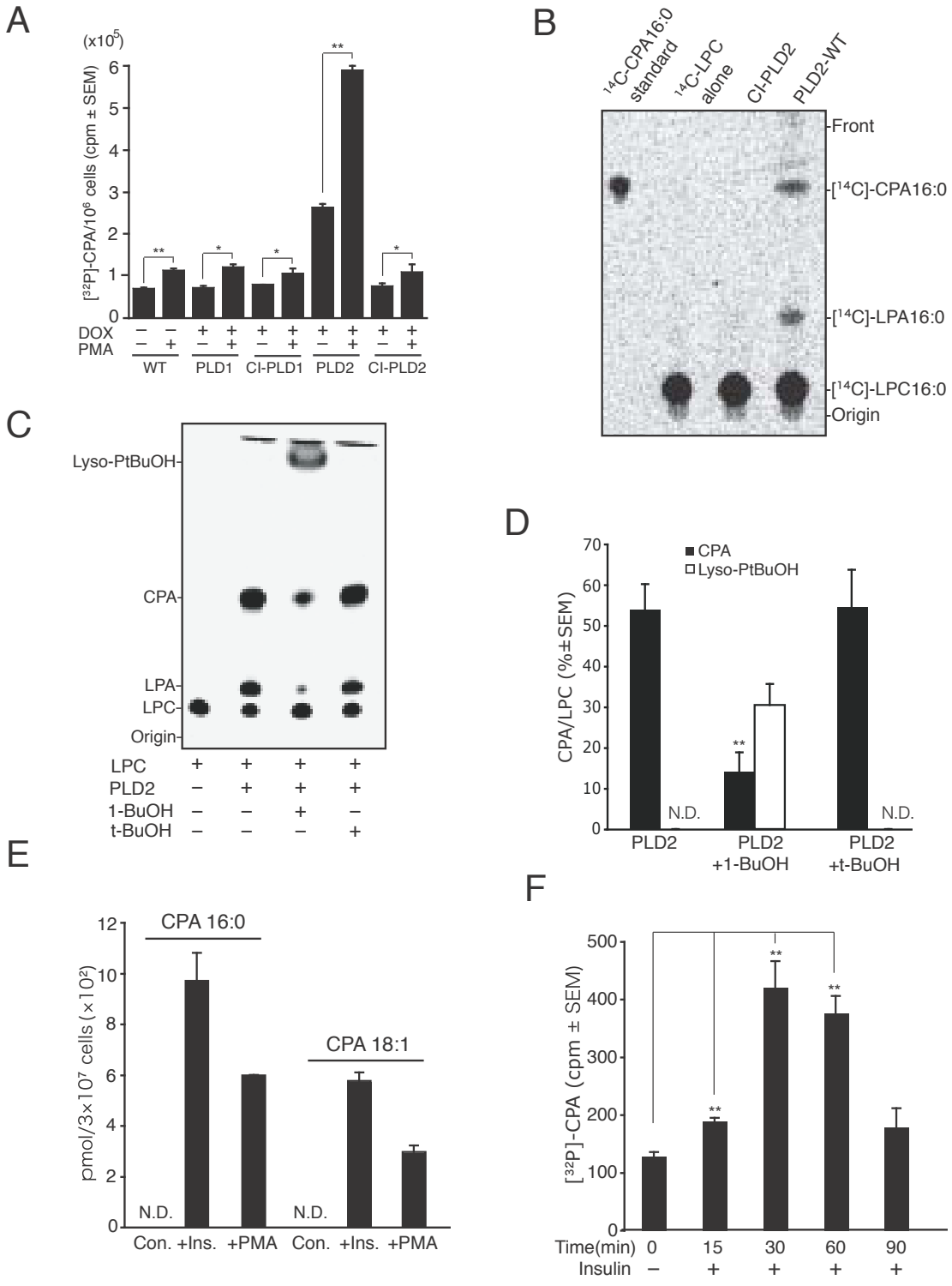
A
(x10^5)
[32P]-CPA/10^6 cells (cpm ± SEM)
DOX
PMA
WT
PLD1
CI-PLD1
PLD2
CI-PLD2
B
14C-CPA16:0 standard
14C-LPC alone
CI-PLD2
PLD2-WT
Front
[14C]-CPA16:0
[14C]-LPA16:0
[14C]-LPC16:0
Origin
C
Lyso-PtBuOH
CPA
LPA
LPC
Origin
LPC
PLD2
1-BuOH
t-BuOH
D
CPA
Lyso-PtBuOH
CPA/LPC (%±SEM)
N.D.
PLD2
PLD2 +1-BuOH
PLD2 +t-BuOH
E
CPA 16:0
CPA 18:1
pmol/3×10^7 cells (×10^2)
N.D.
Con.
+Ins.
+PMA
F
[32P]-CPA (cpm ± SEM)
Time(min)
Insulin

Figure 3-4 PLD2 activation inhibits PPARγ

(A) Insulin stimulation elevates CPA but not LPA levels. CV-1 cells (3×10^6) were labeled with [^{32}P]-orthophosphate for 6 h and stimulated with 100 nM insulin or the DMSO solvent for 30 min at 37 ^{o}C. Lipids were extracted, separated by 2DTLC and quantified by phosphorimaging (n = 3). (B) CPA is generated in human peripheral blood mononuclear cells in response to PLD2 stimulation. The cells were pretreated with the PLD2 inhibitor FIPI (750 nM) or solvent control for 30 min prior to stimulation by 100 nM insulin, PMA 100 nM, 1 μg/ml LPS, or 1 mM H_2O_2. Data are representative of three other experiments with different donors. (C) Stimulation of PLD2 with insulin or mastoparan inhibits ROSI-induced PPARγ-reporter gene expression in a PLD-dependent manner. CV-1 cells were transfected with ACox–luc together with pcDNA3.1-PPARγ plasmid and treated for 20 h with 10 μM ROSI, 100 nM insulin, 20 μM mastoparan, and/or 1.5% 1-BuOH. Luciferase activities are presented as RLU (mean ± SEM, n = 4). (D) Insulin attenuates PPARγ activation. The ACox-luc reporter alone or in combination with the PPARγ plasmid was transfected into B103 cells and exposed to ROSI (5 mM) alone or with insulin. Reporter gene expression was measured 20h later (n = 5). (E) CI-PLD2 inhibits insulin-induced CPA production in CV-1 cells. Cells were either transduced with a CI-PLD2 or an empty adenovirus at MOI of 10. Phospholipids were biosynthetically labeled using [^{32}P]-orthophosphate for 24 h post-transduction, and the cells stimulated with 100 nM insulin for 30 min. Phospholipids were separated using 2DTLC and visualized by phosphorimaging. Radioactivity incorporated into the CPA spot was scraped off and quantified by liquid scintillation counting (cpm mean ± SEM, n = 3, **$p < 0.01$). (F) CI-PLD2 acts as a dominant negative and abolishes insulin-induced inhibition of ROSI-induced PPARγ activation. CV-1 cells were either transduced with an adCI-PLD2 or an empty adenovirus. Subsequently, the transduced cells were transfected with the ACox-luc reporter gene and PPARγ plasmids for an additional 24 h. Cells were stimulated with 10 mM ROSI with or without 100 nM insulin for 20 h, and luciferase reporter expression determined (mean ± SEM , n=3, **$p < 0.01$).

A

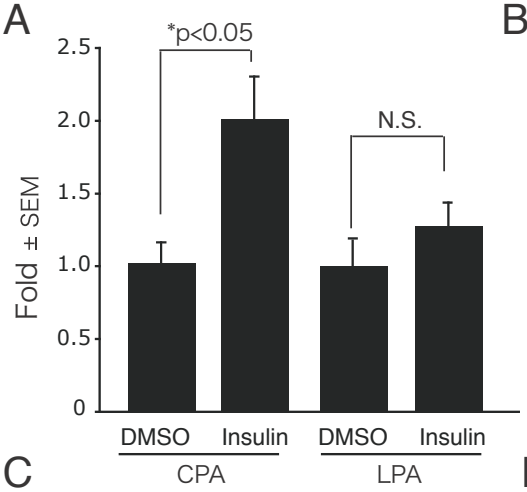

B

Treatment	CPA 16:0 (pmole/10 ^{7}cell)	CPA 18:1 (pmole/10 ^{7}cell)
Vehicle control	0.09	0.57
FIPI alone	0.13	0.47
Insulin	0.46	317.95
Insulin + FIPI	0.40	165.04
PMA	128.18	609.09
PMA + FIPI	96.67	295.10
LPS	130.15	600.27
LPS + FIPI	101.36	283.67
H_2O_2	0.87	399.43
H_2O_2 + FIPI	0.48	271.74

C

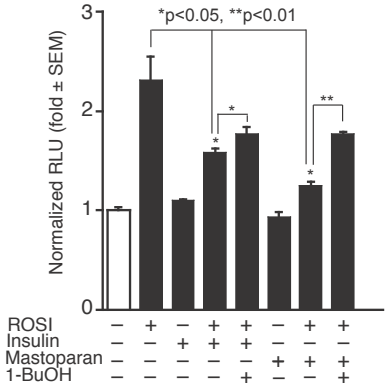

D

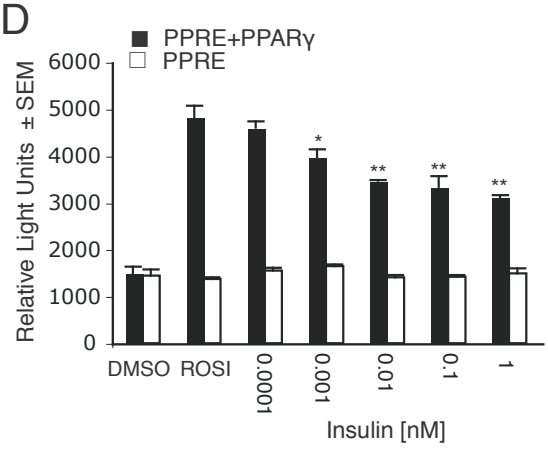

E

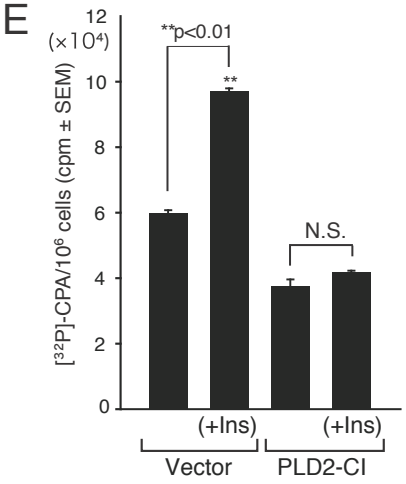

F

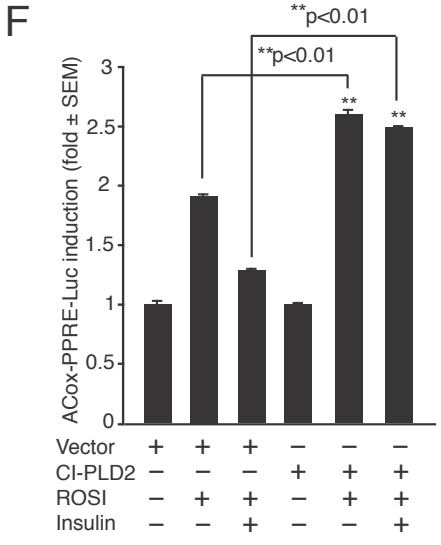

primary human monocytic cells and also in cultured bone marrow-derived mouse and human peripheral blood mononuclear cells (data not shown) elicited a rapid and substantial rise CPA level. These results are consistent with the second messenger properties of CPA; low levels in unstimulated cells, a substantial rise rapidly following PLD2 stimulation, and deacylation-mediated breakdown (Figure 3-1G).

Another stimulator of PLD2 is mastoparan. Stimulation of PLD2 with mastoparan or insulin increases CPA production, which in turn should inhibit the transcriptional activity of PPARγ. To test this hypothesis, CV-1 cells were transfected with PPARγ reporter plasmids, and exposed to ROSI with and without stimulation with 20 μM mastoparan or 100 nM insulin (Figure 3-4C). Neither PLD-stimulating agent alone caused a significant activation in acetyl CoA-oxidase-luciferase (ACox-luc) reporter gene expression. Rather, mastoparan and insulin both attenuated the ROSI-induced transcriptional activity of PPARγ. When 1-BuOH was added to the cells to quench PLD2-mediated CPA production, the inhibitory effect was attenuated, most strongly for mastoparan (Figure 3-4C). Attenuation of ROSI-induced ACox-luc reporter expression positively correlated with the concentration of insulin applied (Figure 3-4D).

Insulin stimulates a complex signaling network of which PLD2 activation represents only one component. To obtain evidence that the PLD2 branch of insulin signaling is necessary for CPA production, we treated cells with adenoviral (ad) CI-PLD2, which should abrogate CPA production and the attenuate of PPARγ activation. Insulin elicited an increase in the biosynthetically-labeled pool of [^{32}P]-CPA in CV-1 cells; and adCI-PLD2 reduced the insulin-induced generation of [^{32}P]-CPA (Figure 3-4E). We also probed the requirement of PLD2 for insulin-induced inhibition of PPARγ by using ad CI-PLD2 to attenuate of CPA production in the reporter gene assay. adCI-PLD2 completely abrogated the inhibitory effect of insulin on PPARγ (Figure 3-4F). In addition, we knocked down PLD2 expression using a lentivirally-delivered shRNA against PLD2 in RAW264.7 and NIH3T3-L1 cells (Figure A-3D-F). PLD2 knockdown caused a more than 75% reduction in PMA- and insulin-stimulated CPA 18:1 production in RAW264.7 and 3T3L1 cells (Figure 3-5A and B).

CPA and LPA share similar structure. One concern when treating cells with CPA is that CPA may activate LPA GPCR receptors directly before it enters cells. B103 neuroblastoma cells, which express barely detectable levels of PPARγ$_{1\&2}$ (Figure 3-5C inset) and also lack the LPA$_{1/2/3}$ GPCR (Tsukahara et al., 2006). Hence, B103 cells represent an ideal cell model for add-back expression of the PPARγ and PPRE-Acox-luc reporter. In wild type B103 cells transfected only with the PPRE-Acox-luc reporter ROSI caused a marginal activation. However, in B103 cells transfected with PPARγ and the reporter, ROSI- or AGP-induced ACox-luc expression that was inhibited by CPA (5 μM) and insulin (1 nM) (Figure 3-5C). These observations are consistent with the hypothesis that CPA is a physiological product of PLD2 and that PLD2-dependent inhibition of PPARγ activity is mediated by CPA independently of the LPA$_{1/2/3}$ GPCR.

Figure 3-5 CPA production by PLD2 inhibits PPARγ-mediated cellular responses

(A and B) PLD2 knockdown inhibits insulin- and PMA-induced CPA production in RAW264.7 and 3T3-L1 cells. 3×10^6 RAW264.7 or NIH3T3 cells expressing scrambled shRNA or PLD2 shRNA were stimulated with 30 nM insulin or 100 nM PMA for 30 min prior to extraction of phospholipids for MS analysis (n=3). (C) B103 cells were transfected with the ACox-luc reporter gene alone or together with the PPARγ plasmid and exposed to ROSI (5 mM) with or without CPA (5 mM), AGP (5 mM) and insulin (1 nM) for 20 h, and reporter gene expression measured (mean ± SEM, n = 3). The inset shows PPARγ expression in WT B103 cells or cells transfected with the pcDNA3.1-PPARγ construct as determined by western blotting. (D) CPA inhibits foam cell formation and AC-LDL accumulation in the RAW264.7 mouse macrophage cell line. Cells were stimulated with combinations of 5 mM CPA and ROSI in the presence of 25 mg/ml AC-LDL for 24 h. Lipid accumulation was determined by ORO staining (bar = 50 mm). (E) CPA and the PPARγ antagonist GW9662 (5 mM each) inhibited ROSI- and AGP-induced (5 mM each) lipid accumulation in RAW264.7 macrophages. ORO accumulation was quantifed spectrophotometrically (mean ± SEM, n = 3). The inset shows PPARγ expression as assessed by western blotting and the lower panel shows β-actin as a loading control. (F) CPA inhibition of PPARγ target gene *cd36* activation requires a PPRE element. CV-1 cells were transfected with PPARγ together with a *cd36* reporter gene containing PPRE at position -273 in the promoter, or a truncated version at position -261 lacking the PPRE, and were treated for 20 h with 10 mM ROSI, AGP, or CPA. Luciferase activity was determined, and data are presented as RLU (mean ± SEM, n = 4).

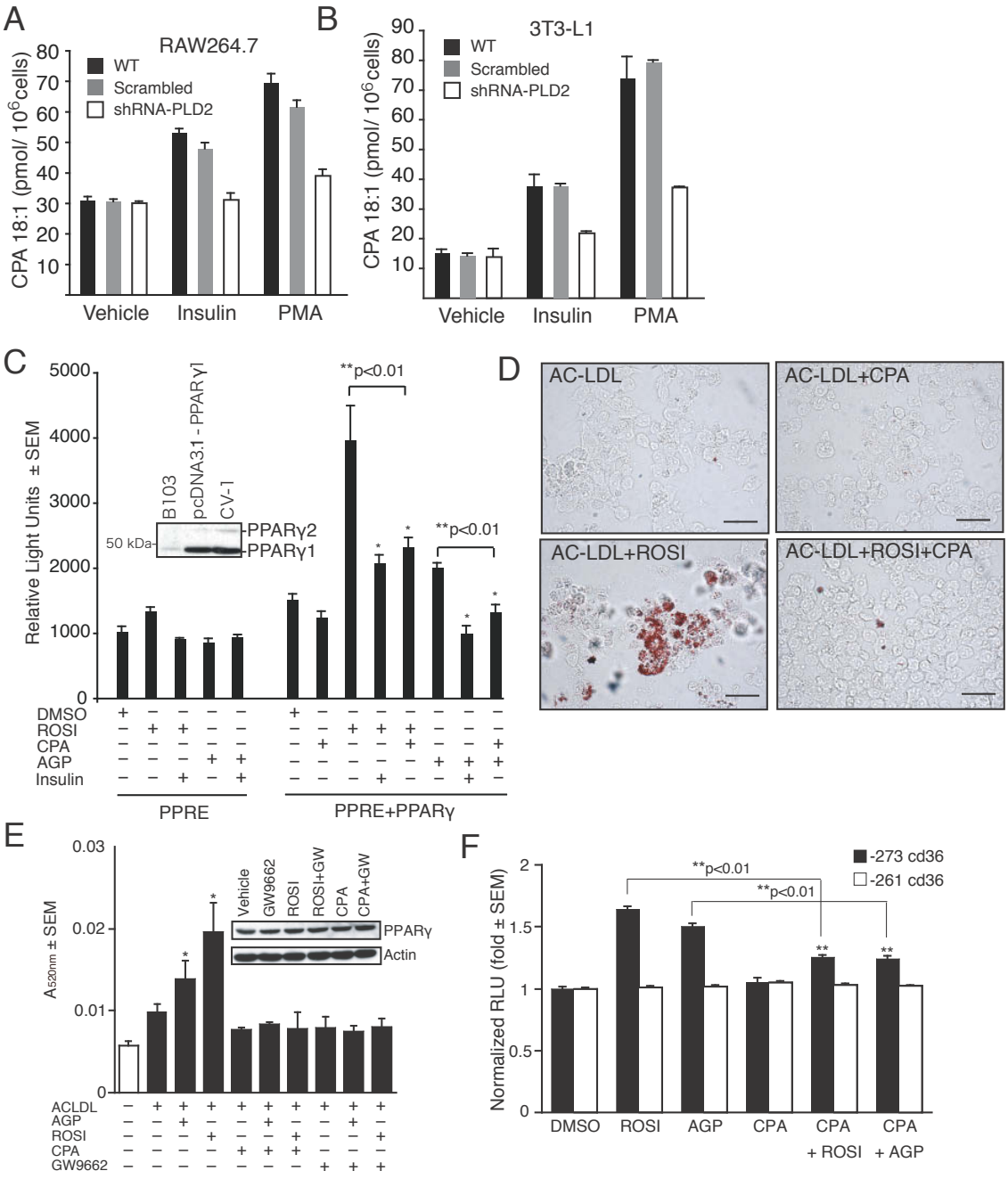
A
RAW264.7
WT
Scrambled
shRNA-PLD2
CPA 18:1 (pmol/ 10^6cells)
Vehicle
Insulin
PMA
B
3T3-L1
C
Relative Light Units ± SEM
**p<0.01
B103
pcDNA3.1 - PPARγ1
CV-1
50 kDa
PPARγ2
PPARγ1
DMSO
ROSI
CPA
AGP
Insulin
PPRE
PPRE+PPARγ
D
AC-LDL
AC-LDL+CPA
AC-LDL+ROSI
AC-LDL+ROSI+CPA
E
A520nm ± SEM
Vehicle
GW9662
ROSI
ROSI+GW
CPA
CPA+GW
PPARγ
Actin
ACLDL
AGP
ROSI
CPA
GW9662
F
Normalized RLU (fold ± SEM)
-273 cd36
-261 cd36
DMSO
ROSI
AGP
CPA
CPA + ROSI
CPA + AGP

3.3.5 CPA Inhibits PPARγ-Dependent Physiological Responses

We also examined the effect of CPA on PPARγ-regulated lipid accumulation in RAW 264.7 macrophages after exposure to acetylated low-density lipoprotein (AC-LDL). Uptake of AC-LDL by unstimulated RAW 264.7 cells was below the detection limit of the Oil Red O (ORO)-staining (Figure 3-5D). When the AC-LDL was coapplied with 5 μM ROSI, many ORO-positive macrophages were visible. CPA (5M) addition to ROSI-stimulated macrophages completely abolished ORO-stained cells, supporting the hypothesis that CPA inhibits PPARγ-regulated AC-LDL uptake. The inhibitory effect of CPA on AC-LDL uptake was compared with that of the synthetic PPARγ antagonist GW9662 (Figure 3-5E). Both CPA and GW9662 at 5 μM completely abolished ORO accumulation elicited by either ROSI or AGP in these cells, while causing no change in the expression of PPARγ (Figure 3-5E inset). The scavenger receptor CD36, under direct transcriptional regulation of PPARγ, plays an important role in the uptake of oxidized phospholipids into macrophages (Boullier et al., 2000). In CV-1 cells, CPA inhibited ROSI- or AGP-activated *cd36* reporter gene activation only when the reporter construct contained an intact PPARγ response element (PPRE) between nucleotides -273 to -261 in the promoter (Figure 3-5F). When the *cd36* promoter was a truncated at position -261, neither ligand showed significant modulation of the expression, which is consistent with the hypothesis that CPA exerts its inhibitory effect on lipid accumulation via the inhibition of PPARγ transcriptional targets. PPARγ is required for adipocytic differentiation of 3T3-L1 cells (Tzameli et al., 2004). In 3T3-L1 cells, 100 nM ROSI treatment elicits the expression of the adipocytic marker FABP4, which is a direct target of PPARγ (Figure 3-6A). CPA treatment caused an anti-adipogenic effect evident by the reduced expression of FABP4 mRNA, protein, and by reduced lipid accumulation using ORO staining (Figure 3-6B).

Stimulation with low nanomolar insulin leads to PLD2-dependent CPA formation that inhibited PPARγ-dependent reporter gene expression (Figure 3-4A-F). To examine the effects of low-dose insulin on adipocytic differentiation, at concentrations similar to that found in plasma under fasting conditions (~ 1 nM), 3T3-L1 cells were induced to differentiate with ROSI for 14 days in the absence or presence of insulin and lipid accumulation quantified using ORO staining (Figure 3-6C). Continuous low-dose insulin treatment resulted in the inhibition of adipogenesis as indicated by reduced lipid accumulation, consistent with the dose-response relationship of insulin-induced inhibition of PPARγ-reporter gene activation we found in B103 cells (Figure 3-4D). We reasoned that because PLD2 knockdown in 3T3-L1 cells attenuated insulin-activated CPA production (Figure 3-5B), it should also reverse the inhibition of PPARγ target genes *fabp4* and *cd36*. PLD2 knockdown reversed insulin or mastoparan inhibition of *fabp4* and *cd36* expression compared to 3T3-L1 cells transduced with scrambled shRNA (Figure 3-6D and E).

Stimulation of macrophages with ROSI elicits direct activation of PPARγ-regulated genes (Hodgkinson and Ye, 2003). We selected five PPARγ target genes and monitored their transcriptional regulation in mouse peritoneal macrophages treated with ROSI in combination with CPA or GW9662 for 12h. ROSI stimulation

Figure 3-6 CPA inhibits PPARγ-dependent transcriptional responses

(A) 3T3-L1 cells, which express both PPARγ_1 and PPARγ_2 protein (western blotting inset), were pretreated with 1 mM CPA, AGP or vehicle for 24 h and exposed to 100 nM ROSI. Quantitative RT-PCR (QT-PCR) for the adipocyte marker *fabp4* was performed 5 days later. (B) CPA inhibited ROSI-induced lipid accumulation. 3T3-L1 cells pretreated with 1 mM CPA or vehicle for 24 h were induced to differentiate with ROSI (100 nM every other day) and stained with ORO after 10 days. Quantification of lipid accumulation was done spectrophotometrically (n=3). (C) Insulin or CPA inhibited lipid accumulation in 3T3-L1 cells. Cells were pretreated with 1 mM CPA or vehicle for 24 h and induced with 100 nM ROSI with or without 1 mM CPA or insulin and stained with ORO after 2 weeks. Quantification of lipid accumulation was done spectrophotometrically (n=3, **p=0.0002 for DMSO *vs.* ROSI, *p=0.0126 for ROSI *vs.* ROSI+0.03 nM insulin, **p=0.0010 for ROSI *vs.* ROSI + 0.3 nM insulin, *p=0.0494 for ROSI *vs.* ROSI+1 nM Insulin, and **p=0.0041 for ROSI *vs.* ROSI+CPA). (D and E) ROSI-induced gene expression of PPARγ target genes fabp4 and cd36 is inhibited by PLD2 in 3T3-L1 cells. 3T3-L1 cells expressing scrambled shRNA or PLD2 shRNA were pretreated with 30nM insulin or 10mM mastoparan for 30 min and cultured in ROSI (10 μM) or vehicle for 24 h. Total RNA was isolated and mRNA levels determined by QT-PCR (n=4). (F) Inhibition of ROSI-induced expression of PPARγ regulated genes by CPA in mouse peritoneal macrophages. Macrophages isolated from C57BL/6 mice were exposed to a 5 μM ROSI with or without 5 μM CPA or 1 μM GW9662 (positive control) for 12 h, and RNA was isolated. mRNA levels for the PPARγ upregulated (*cd36*, *cyp27a1*, *hadh*, *capn3)* and downregulated *(csf1)* gene targets were determined by QT-PCR) (n=3, representative experiment shown).

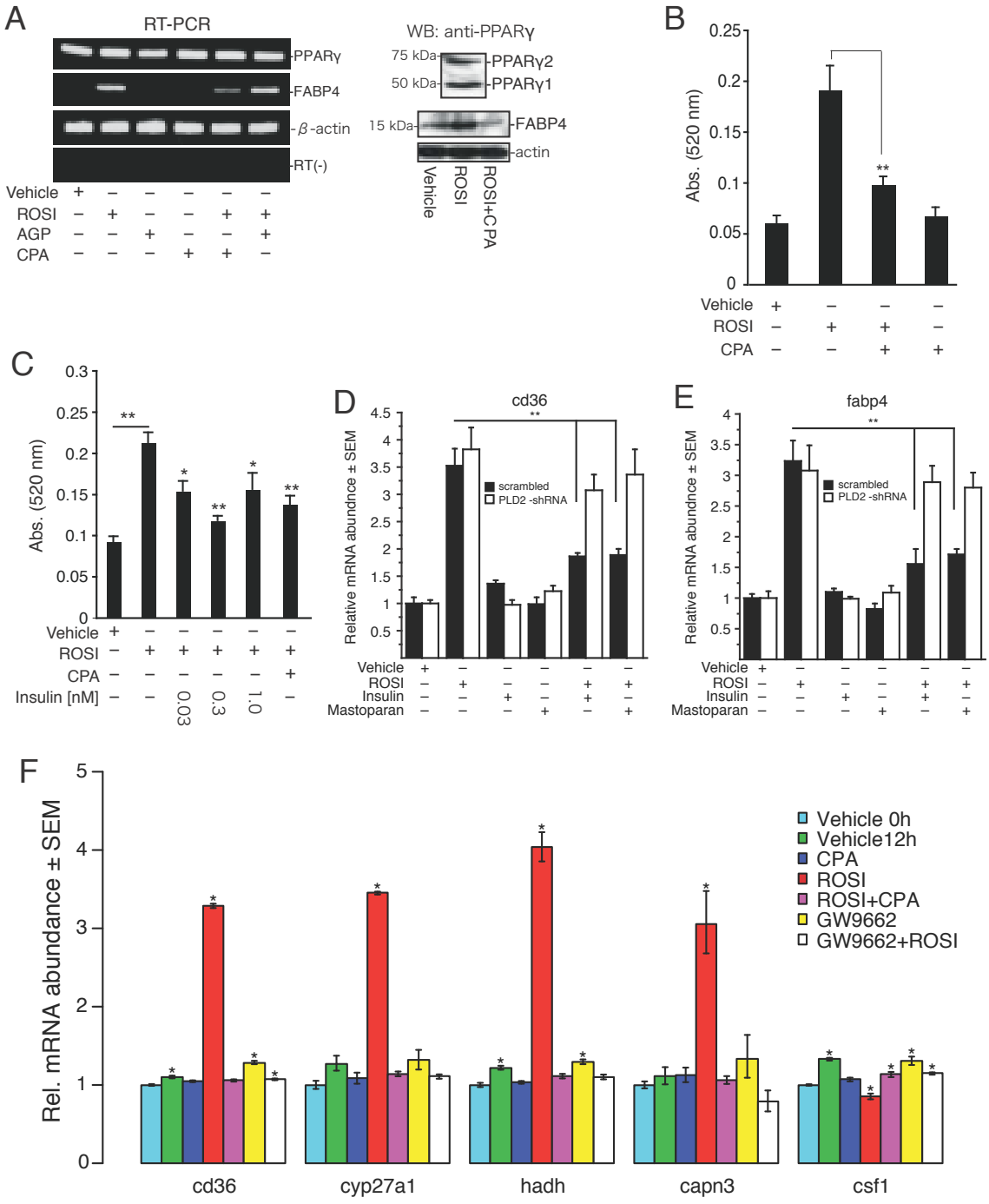
A
RT-PCR
PPARγ
FABP4
β-actin
RT(-)
Vehicle + – – – – –
ROSI – + – – + +
AGP – – + – – +
CPA – – – + + –
WB: anti-PPARγ
75 kDa
50 kDa
15 kDa
PPARγ2
PPARγ1
FABP4
actin
Vehicle
ROSI
ROSI+CPA
B
Abs. (520 nm)
0.25
0.2
0.15
0.1
0.05
0
**
Vehicle + – – –
ROSI – + + –
CPA – – + +
C
Abs. (520 nm)
0.3
0.25
0.2
0.15
0.1
0.05
0
**
*
**
*
**
Vehicle + – – – – –
ROSI – + + + + +
CPA – – – – – +
Insulin [nM] – – 0.03 0.3 1.0 –
D
cd36
**
Relative mRNA abundnce ± SEM
4.5
4
3.5
3
2.5
2
1.5
1
0.5
scrambled
PLD2 -shRNA
Vehicle + – – – – –
ROSI – + – – + +
Insulin – – + – + –
Mastoparan – – – + – +
E
fabp4
**
Relative mRNA abundnce ± SEM
4
3.5
3
2.5
2
1.5
1
0.5
scrambled
PLD2 -shRNA
Vehicle + – – – – –
ROSI – + – – + +
Insulin – – + – + –
Mastoparan – – – + – +
F
Rel. mRNA abundance ± SEM
5
4
3
2
1
0
Vehicle 0h
Vehicle12h
CPA
ROSI
ROSI+CPA
GW9662
GW9662+ROSI
cd36
cyp27a1
hadh
capn3
csf1

activated the expression of *cd36, cyp27a1, hadh* and *capn3* by 3- to 4-fold, whereas inhibited the expression of *csf1*. CPA as well as GW9662 completely abolished the transcriptional regulation of these genes by ROSI (Figure 3-6F).

To examine the regulatory role of CPA on a PPARγ-dependent pathophysiological response we utilized a rodent model of vascular remodeling. ROSI and AGP induce neointima when applied topically within the carotid artery (Zhang et al., 2004). Neointima formation requires PPARγ because it is abolished by the antagonist GW9662 and is absent in mice with conditional knockout of PPARγ targeted to cells of the vessel wall (Cheng et al., 2009). We hypothesized that co-application of CPA with the PPARγ agonists AGP or ROSI should mitigate neointimal thickening. AGP or ROSI with or without CPA was injected lumenally into the common carotid artery of rats, which had been transiently ligated proximally and distally from the carotid glomus. After a 1 h treatment, the cannula was withdrawn and blood flow through the common carotid artery restored. Histological evaluation of the dissected common carotid arteries 3 weeks later revealed multilayered neointimal thickening in the rats treated with 5 μM AGP (Figure 3-7A) or ROSI (Figure A-4B) whereas, no neointima was found in the solvent-treated carotids (Figure A-4A). The neointimal thickening was abolished in those animals that received 5 μM CPA in addition to AGP or ROSI (Figure 3-7B and C, Figure A-4C and D). Our experiments identified insulin as a physiologically relevant stimulator of CPA production. Therefore, endogenous production of CPA activated by low concentrations of insulin should prevent neointima formation in this model. To test this possibility, we co-applied 3 nM insulin with 10 μM AGP or ROSI lumenally for 1 h using the same experimental paradigm described for the application of CPA. Examination of the intima-to-media ratio three weeks later showed that low-dose insulin treatment alone induced no vascular remodeling, but insulin co-treatment significantly reduced the neointima formation elicited by AGP or ROSI (Figure 3-4E-G, Figure 3-7D-F). These results are consistent with the hypothesis that exogenously applied or endogenously generated CPA is effective in negatively modulating PPARγ-dependent vascular wall responses *in vivo*.

3.4 DISCUSSION

The present findings provide evidence that CPA is a *bona fide* second messenger and a negative physiological regulator of PPARγ. CPA is a high-affinity ligand of PPARγ with an apparent Kd in the hundred-nanomolar range, comparable to that of TZDs. CPA binds to a site within the LBD that prevents activation by three different TZD compounds and the endogenous phospholipid agonist AGP, and it stabilizes binding of the corepressor SMRT. CPA lacks the ability to activate PPARγ due to its cyclic phosphate moiety. In contrast, AGP and LPA both possess a free phosphate and are agonists of PPARγ (Tsukahara et al., 2006). CPA is barely detectable in resting cells but is generated intracellularly in a stimulus-coupled manner by PLD2 and is then degraded by phospholipase(s) or acyltransferase(s) via deacylation. PLD2 is the target and convergence point of several receptor-coupled signal transduction pathways (Huang and Frohman, 2007) suggesting that PPARγ is modulated by stimuli of this enzyme. The

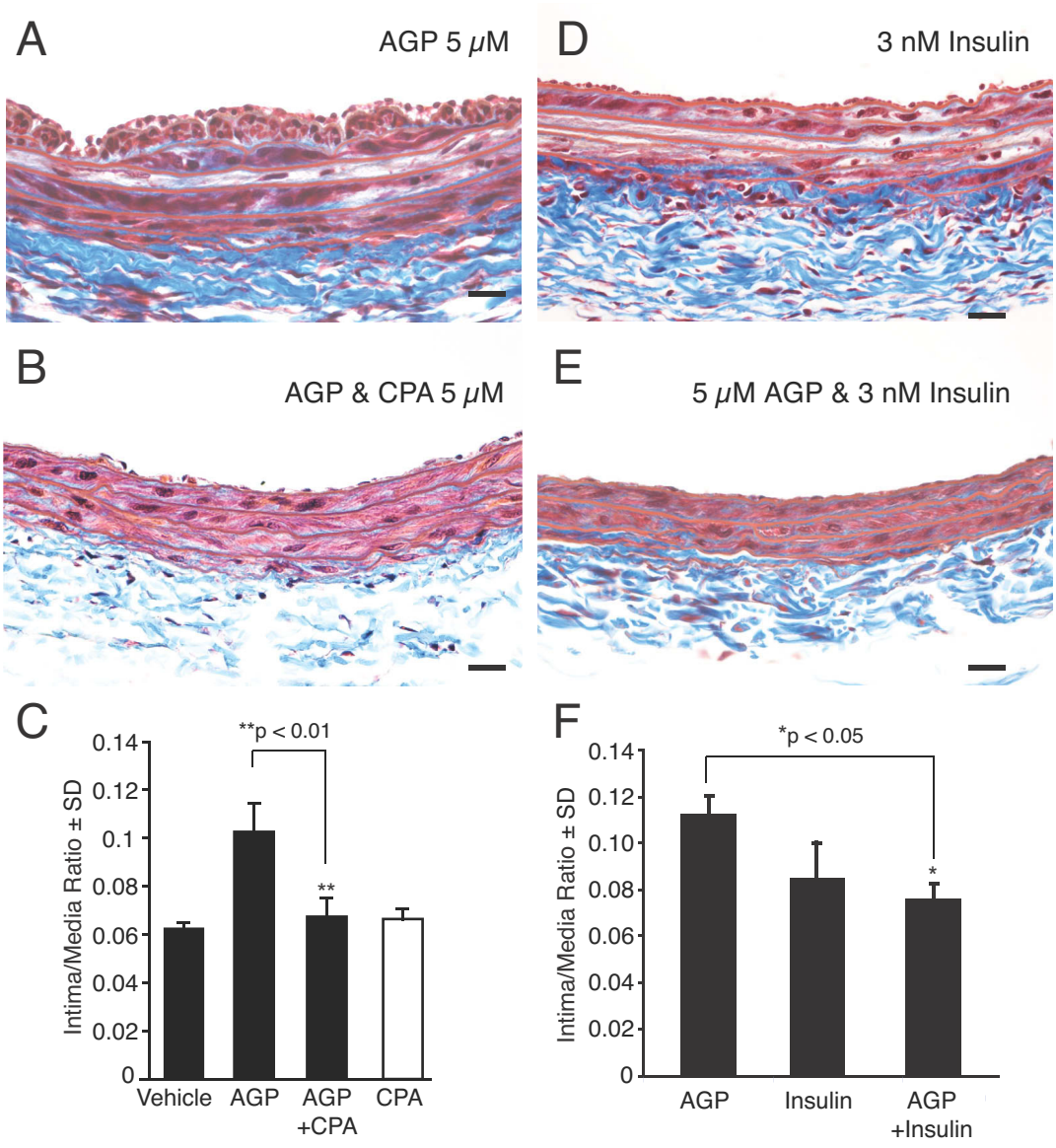

Figure 3-7 CPA and insulin prevent carotid wall remodeling

(A-C) Carotid arteries of anesthetized adult rats (5 per group) were exposed to 5 μM AGP alone (A) or with 5 μM CPA (B) for 1 h. (Masson trichrome staining, bar 200 μm). (C) CPA treatment blocks increase in intima-to-media ratios AGP-induced rat carotid arteries (n=5 per group). (D-F) Insulin (3 nM) was applied alone (D) or with 5 μM AGP (E) intralumenally for 1 h and neointima formation assessed three weeks alters. Bar represents 200 μm. (F) Quantification of intima/media ratios (n=5).

present findings establish that PLD2 can produce at least two second messengers, PA from the hydrolysis of phosphatidylcholine and CPA from LPC, depending on substrate availability. The availability of LPC is likely to be regulated by activation of phospholipases A2, which are concomitantly activated by the same stimuli that activate PLD2 (Kim et al., 1999). Physiological stimuli of PLD2 can generate CPA in biologically effective concentrations, as indicated by our findings using the foam-cell formation and adipocyte differentiation models in cultured cell lines and also using primary monocytes/macrophages, and PPARγ-dependent vascular remodeling *in vivo*. In addition, the present data reinforce the long-standing observation that low concentrations of insulin protect against neointimal growth (Breen et al., 2009).

Current paradigms for PPARγ signaling do not take into consideration the possibility of endogenous negative regulators fine-tuning, and under certain conditions even abrogating the cellular responses mediated through this nuclear hormone receptor. Our findings challenge this view by identifying CPA as an endogenous negative regulator of PPARγ. Individual variations in patients in the activation of the PLD2-CPA axis are likely to modulate therapeutic responses to the widely used class of TZD drugs targeting PPARγ. Hence, the present results provide new grounds for rethinking our current concepts governing the regulation of this nuclear hormone receptor and raise the possibility of utilizing this phospholipid scaffold as a lead for the synthesis of novel medicines acting on PPARγ.

CHAPTER 4. REGULATION OF NUCLEAR HORMONE RECEPTOR PPARγ BY ENDOGENOUS LYSOPHOSPHATIDIC ACIDS*

4.1 INTRODUCTION

4.1.1 Lysophosphatidic Acid (LPA) in the Vasculature

LPA has been identified as a bioactive lipid and is produced in serum after the activation of multiple biochemical pathways linked to platelet activation (Sano et al., 2002, Spector, 2003, Tigyi and Parrill, 2003, Bolen et al., 2011). The concentration of LPA in plasma is in the nanomolar range, whereas it can reach concentrations as high as 10 μM in serum during blood clotting (Baker et al., 2001, Aoki et al., 2002, Baker et al., 2002). LPA production in blood requires autotaxin (ATX), which is a secreted lysophospholipase D that generates LPA from lysophosphatidylcholine (LPC) (Tokumura et al., 2002, Umezu-Goto et al., 2002).

LPA plays an important role in vascular development (van Meeteren et al., 2006). ATX-deficient mice die at approximately embryonic day 9.5 with severe vascular formation defects in the yolk sac and enlarged embryonic blood vessels (Tanaka et al., 2006, van Meeteren et al., 2006). Mice that overexpress ATX have elevated plasma LPA levels and show bleeding diathesis, whereas $ATX^{+/-}$ heterozygous mice have almost half the plasma LPA levels and are prone to thrombosis (Pamuklar et al., 2009).

LPA promotes proliferation and migration of vascular smooth muscle cells (VSMCs) (Hayashi et al., 2001, Siess, 2002, Kim et al., 2006). LPA increases endothelial permeability (Schulze et al., 1997, Alexander et al., 1998, van Nieuw Amerongen et al., 2000) and induces E-selectin, vascular cell adhesion molecule-1 (VCAM-1), and vascular endothelial growth factor-C (VEGF-C) expression in human endothelial cells (Rizza et al., 1999, Lin et al., 2008). Hayashi et al. reported that LPA promotes VSMC dedifferentiation from the contractile phenotype to a secretory phenotype and stimulates VSMC signaling pathways *in vitro* (Hayashi et al., 2001).

Many of the cellular responses elicited by LPA, including platelet activation (Siess et al., 1999, Rother et al., 2003, Haseruck et al., 2004), endothelial cell activation (Siess et al., 1999), proliferation, migration, and phenotypic modulation of VSMCs (Hayashi et al., 2001, Siess, 2002, Kim et al., 2006), are all involved in neointima formation. Oxidative modification of low-density lipoprotein (LDL) is considered to be an early event in arterial wall remodeling leading to atherosclerosis (Stocker and Keaney, 2004, Asmis et al., 2005); and uptake and oxidation of LDL in the arterial wall is an important mechanism in the pathogenesis of atherosclerosis (Meydani, 2001). It has been

* Adapted with permission. Tsukahara R, Tsukahahara T, Tigyi G (2011) Regulation of the nuclear hormone receptor PPARgamma by endogenous lysophosphatidic acids. In: Lysophospholipid receptors: Signaling and biochemistry, in press. NJ: Wiley.

shown that LPA is formed during mild oxidation of LDL (mox-LDL)(Siess et al., 1999, Law et al., 2000). In addition, the lipid-rich core of human atherosclerotic plaques, which accumulates oxidized lipids including mox-LDL, contains several species of acyl-LPA and AGP (Siess et al., 1999). Acyl-LPA and AGP accumulated in human atherosclerotic plaques are likely to activate platelets and initiate thrombus formation upon plaque rupture (Rother et al., 2003, Spector, 2003). Following plaque rupture, LPA becomes available to circulating platelets, initiating activation, which in turn may contribute to the induction of thrombosis, leading to myocardial infarction and stroke. A clinical study has shown that the serum LPA level is significantly elevated in patients with acute myocardial infarction (Chen et al., 2003).

4.1.2 Neointima Formation Induced by LPA

Atherosclerosis is the leading cause of death and serious morbidity in developed countries. Neointimal lesions are characterized by accumulation of cells within the arterial wall and are an initial step in the pathogenesis of atherosclerosis, which leads to the ischemic syndromes of heart and stroke (Ross, 1999, Baim et al., 2002).

Yoshida et al. first reported that LPA species containing unsaturated fatty acyl groups 16:1, 18:1, and 18:2 induced neointima formation when injected intralumenally into the rat carotid artery, whereas saturated acyl-LPA species such as 16:0 and 18:0 were inactive (Yoshida et al., 2003). This model comes close to the pathophysiological response seen in humans when mechanical injury is not the cause of the arterial wall remodeling leading to neointimal lesions. In Yoshida's model, LPA was injected through the external carotid artery into a ligated section of the common carotid artery (CCA) that was rinsed free of blood and maintained close to the mean arterial perfusion pressure. There was no mechanical injury or removal of endothelial cells in the CCA. A brief one-hour exposure to unsaturated but not to saturated species of LPA caused neointima development. Our group found that the LPA-elicited neointima was not mediated by the LPA G protein-coupled receptors (GPCRs) LPA_1 and LPA_2, which are the major LPA receptor subtypes expressed in the vessel wall (Cheng et al., 2009). A peroxisome proliferator-activating receptor γ (PPARγ)-specific inhibitor, GW9662, abolished the LPA-induced neointima formation, suggesting that arterial wall remodeling elicited by LPA is a PPARγ-mediated response (Zhang et al., 2004). Conversely, the PPARγ-specific agonist rosiglitazone (ROSI; Figure 4-1) also elicited neointima formation in the same model. Genetic evidence also supports the role of PPARγ in arterial wall remodeling. When conditional knockout $PPAR\gamma^{-/-}$ mice with this receptor knocked out in the endothelial cells, VSMCs, and cells of the macrophage/monocyte lineage were exposed to AGP (Figure 4-1) or ROSI, neither agent elicited neointima formation or vascular wall remodeling (Cheng et al., 2009). It is important to note that in a carotid injury model, ROSI diminished the size of the neointima. The opposite effect of ROSI and LPA in these two different models indicates differences in the mechanism underlying vascular wall remodeling in the two models (Cheng et al., 2009). These results, combined with the observation that GW9662 abolished neointima in response to ROSI or AGP (Zhang et al., 2004), suggest that PPARγ is required for LPA-induced

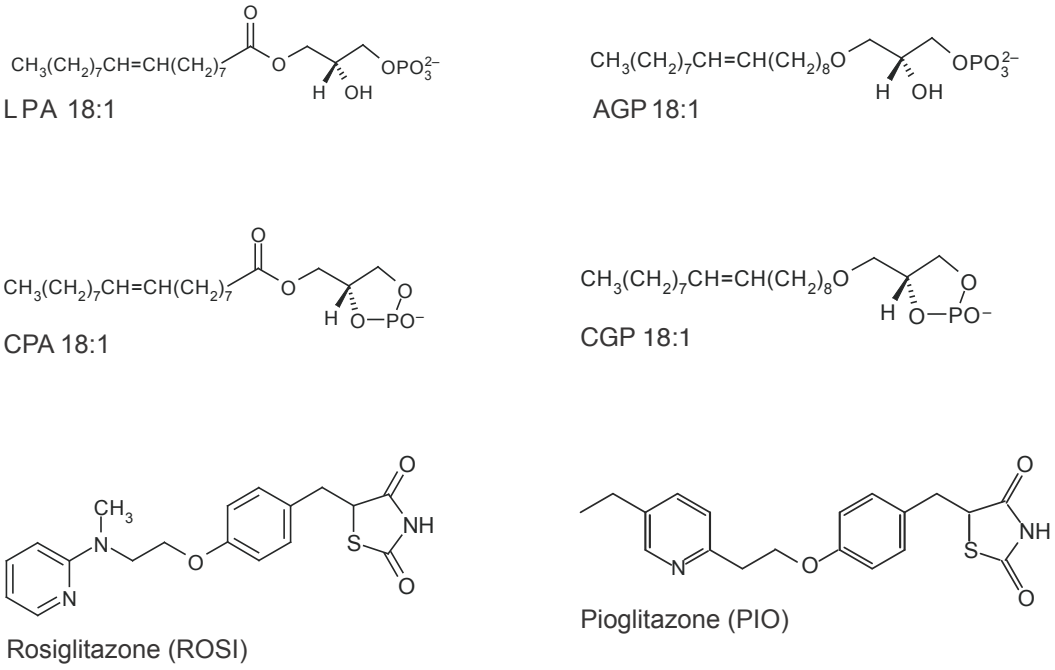

Figure 4-1 Structures of the lysophosphatidic acids, ROSI, and PIO

neointima formation in the absence of vascular wall injury.

Subramanian et al. reported that LPA_1 and LPA_3 GPCRs play an important role in neointima formation (Subramanian et al., 2010). Using a wire-injury model, these authors showed that neointima formation was inhibited by the LPA_1 and LPA_3 inhibitor Ki16425 and that vascular wall remodeling induced by LPA was inhibited by short-term knockdown of either LPA_1 or LPA_3 with siRNA (Subramanian et al., 2010). In sharp contrast with the findings of Subramanian et al., $LPA_1^{-/-}$ mice in our non-injury model develop neointimal in response to AGP stimulation. Moreover, although LPA_1 and LPA_3 GPCRs are respectively 12 and 100 times less sensitive to AGP than LPA (Fujiwara et al., 2005), AGP is more potent than LPA in inducing neointima formation (Zhang et al., 2004). They also observed that Mac-2 positive cells were accumulated in the neointimal area after vascular injury (Subramanian et al., 2010); in contrast, our non-injury model showed few macrophages in the neointimal region induced by AGP or ROSI (Cheng et al., 2009), suggesting that the cellular elements leading to neointima formation are different between the two models.

Although some clinical studies in diabetic patients have shown a reduction in carotid artery wall thickness after treatment with thiazolidinediones (TZDs) (Minamikawa et al., 1998, Haffner et al., 2002), other studies suggested that ROSI increases the risk of myocardial infarction and death from cardiovascular causes (Goldberg et al., 2005, Nissen and Wolski, 2007, 2010), indicating that TZD therapy may actually increase the risk of cardiovascular events. Moreover, in 2010, the U.S. Food and Drug Administration restricted use of ROSI to patients with type 2 diabetes due to the potential for cardiovascular ischemic risks, including heart attack.

4.1.3 PPARγ – an Intracellular LPA Receptor

Only unsaturated acyl-LPA species induce neointima formation; saturated acyl-LPA species are inactive (Yoshida et al., 2003, Zhang et al., 2004) indicating the need for an unsaturated fatty acid in the activation of the mechanism that underlies the formation of neointima. The structure-activity relationship of neointima induction by LPA does not match that of the known LPA GPCRs because saturated LPA species activate the LPA GPCRs (Zhang et al., 2004, Fujiwara et al., 2005). However, the structure-activity relationship of PPARγ activation by LPA species matches that of the neointima response *in vivo* (Zhang et al., 2004). ROSI and the unsaturated acyl-LPA species all activate the peroxisome activator response element-contianing acyl-coenzyme A oxidase-luciferase (PPRE-Acox-Luc) reporter construct, whereas all saturated species, 2,3-cyclic phosphatidic acid (CPA) (Figure 4-1), and the related lipid mediator sphingosine-1-phosphate were inactive (Tsukahara et al., 2006).

PPARs are members of the nuclear hormone receptor superfamily, many of which function as lipid-activated transcription factors (Tontonoz and Spiegelman, 2008). There are three types of PPAR; PPARα, β/δ, and γ. PPARγ, the most extensively studied among the three PPAR subtypes, plays an important role in regulating lipid metabolism, glucose

homeostasis, cell differentiation, and motility (Duval et al., 2002, Evans, 2005, Kiec-Wilk et al., 2005). PPARγ has two isoforms, PPARγ$_1$ and γ$_2$. PPARγ$_2$ differs from PPARγ$_1$ only by 30 additional amino acids at the N-terminus, caused by differential promoter usage and alternative splicing (Fajas et al., 1997). PPARγ$_1$ is expressed ubiquitously in almost all tissues, whereas PPARγ$_2$ is highly expressed in only in the adipose tissue (Lehrke and Lazar, 2005). Genetic deletion of PPARγ$_1$ causes embryonic mortality (Asami-Miyagishi et al., 2004). In contrast, deletion of PPARγ$_2$ causes minimal alterations in lipid metabolism (Medina-Gomez et al., 2005). PPARγ heterodimerizes with the retinoid X receptor α (RXRα), and it is the ligand binding domain (LBD) of PPARγ that interacts with its agonists, including LPA (Weatherman et al., 1999). The PPARγ-RXRα heterodimer binds the peroxisome proliferator response element (PPRE) in the promoter region of the target genes. In the absence of ligands, the corepressors NCoR and SMRT (Chen and Evans, 1995, Dowell et al., 1999, Yu et al., 2005) bind to the heterodimer to suppress the target gene activation. Upon ligand binding, PPARγ undergoes a conformational change that facilitates the dissociation of the corepressors and recruits the p300 coactivator and the PGC-1α coactivator (Nolte et al., 1998, Yu and Reddy, 2007), resulting in target gene transcription (Lala et al., 1996).

A number of putative physiological agonists of PPARγ have been identified, including 15d-PGJ2 (Forman et al., 1995), oxidatively modified fatty acids (Nagy et al., 1998, Baker et al., 2005, Li et al., 2008), select species of LPA and AGP (McIntyre et al., 2003, Zhang et al., 2004, Tsukahara et al., 2006), oxidized phospholipids (Davies et al., 2001), and nitrated fatty acids (Li et al., 2008). Among these ligands, AGP stands out with an equilibrium binding constant of 60 nM (Tsukahara et al., 2006) that is similar to that of the TZD class of synthetic agonists. The TZD class of antidiabetics, including ROSI, pioglitazone, and troglitazone, are full agonists of PPARγ and have been clinically used to improve insulin sensitivity and lipid metabolism in type 2 diabetics (Froberg and Andersen, 2005, Lautamaki et al., 2005, Negro et al., 2005, Sarafidis et al., 2005).

However, despite the beneficial effects of PPARγ on glucose and lipid homeostasis, excessive PPARγ activity can be deleterious. PPARγ agonists promote adipocytic differentiation of 3T3-L1 cells and also stimulate the uptake of LDL by macrophages, leading to foam cell formation in the arterial wall (Moore et al., 2001). Our results suggest that LPA-mediated activation of PPARγ can also contribute to vascular wall pathologies.

PPARγ plays an important role in the cardiovascular system. PPARγ is expressed in all cell types of the vessel wall (Marx et al., 1998, Delerive et al., 1999, Rangwala and Lazar, 2004), as well as in monocytes and macrophages (Tontonoz et al., 1998). PPARγ expression is upregulated in VSMCs (Law et al., 2000), endothelial cells (Delerive et al., 1999), and macrophages (Tontonoz et al., 1998) in human atherosclerotic plaques and neointimal lesions. PPARγ expression is also elevated in neointimal lesions after mechanical injury to the endothelium (Law et al., 2000). ROSI suppresses neointima formation after endothelial injury in rats (Lim et al., 2006). On the other hand, in our non-injury model, ROSI induces neointima formation when intraluminally applied into

carotid arteries (Zhang et al., 2004, Cheng et al., 2009). Thus, the mechanisms underlying neointima formation in the chemically induced neointima model are likely to be different from those in the non-injury induced neointima models.

4.1.4 2,3-Cyclic Phosphatidic Acid (CPA) – an Endogenous Antagonist of PPARγ

CPA, an analog of LPA with a five-atom ring linking the phosphate to two of the glycerol carbons (Figure 4-1), is found in diverse organisms from slime mold to humans (Murakami-Murofushi et al., 2000); its functions are largely unknown. The concentration of CPA in human serum is estimated to be ~0.01 μM, 10-fold lower than that of LPA (Eichholtz et al., 1993, Kobayashi et al., 1999). Although CPA is structurally similar to LPA, CPA shows several unique actions compared to LPA. CPA inhibits cell proliferation (Fischer et al., 1998), induces actin stress fiber formation (Fischer et al., 1998), promotes differentiation and survival of cultured embryonic hippocampal neurons (Fujiwara et al., 2003), inhibits LPA-induced platelet aggregation (Gueguen et al., 1999), and suppresses cancer cell invasion and metastasis *in vitro* and *in vivo* (Mukai et al., 1999, Ishihara et al., 2004, Uchiyama et al., 2007). Our group showed that CPA negatively regulates PPARγ functions by stabilizing the SMRT-PPARγ complex (Tsukahara et al., 2010). Furthermore, we showed that CPA is generated intracellularly by phospholipase D2 (PLD2) (Tsukahara et al., 2010).
5-Fluoro-2-indolyl des-chlorohalopemide (FIPI) is an inhibitor of both PLD1 and PLD2 isozymes (Su et al., 2009). FIPI inhibits PLD2-mediated CPA production in human peripheral mononuclear cells stimulated with LPS (Tsukahara et al., 2010). We also demonstrated that activation of PLD2-mediated CPA production or topical application of CPA together with PPARγ agonists prevents neointima formation, adipocytic differentiation, lipid accumulation, and the upregulation of PPARγ target gene transcription in mouse macrophages (Tsukahara et al., 2010). These findings support our hypothesis that CPA is an endogenous antagonist of PPARγ.

In the following material, we describe some of the fundamental methodologies that we and others have used in probing the actions of LPA and CPA on PPARγ *in vitro* and *in vivo*.

4.2 METHODS PROBING PPARγ FUNCTION WITH LPA

4.2.1 Reporter Gene Assay for Ligand Activation of PPARγ

The reporter gene assay is a sensitive method of monitoring ligand-induced gene expression. The determination of PPARγ activation in cells transiently transfected with the PPRE-ACox-Luc or TK-MH100-Luc reporter gene construct has been reported previously (Tsukahara et al., 2006, Tsukahara et al., 2010) (Figure 4-2A and B). We used the B103 rat neuroblastoma cell line because this cell line lacks LPA GPCRs LPA_1, LPA_2 and LPA_3 and expresses very low levels of endogenous PPARγ, making it an ideal

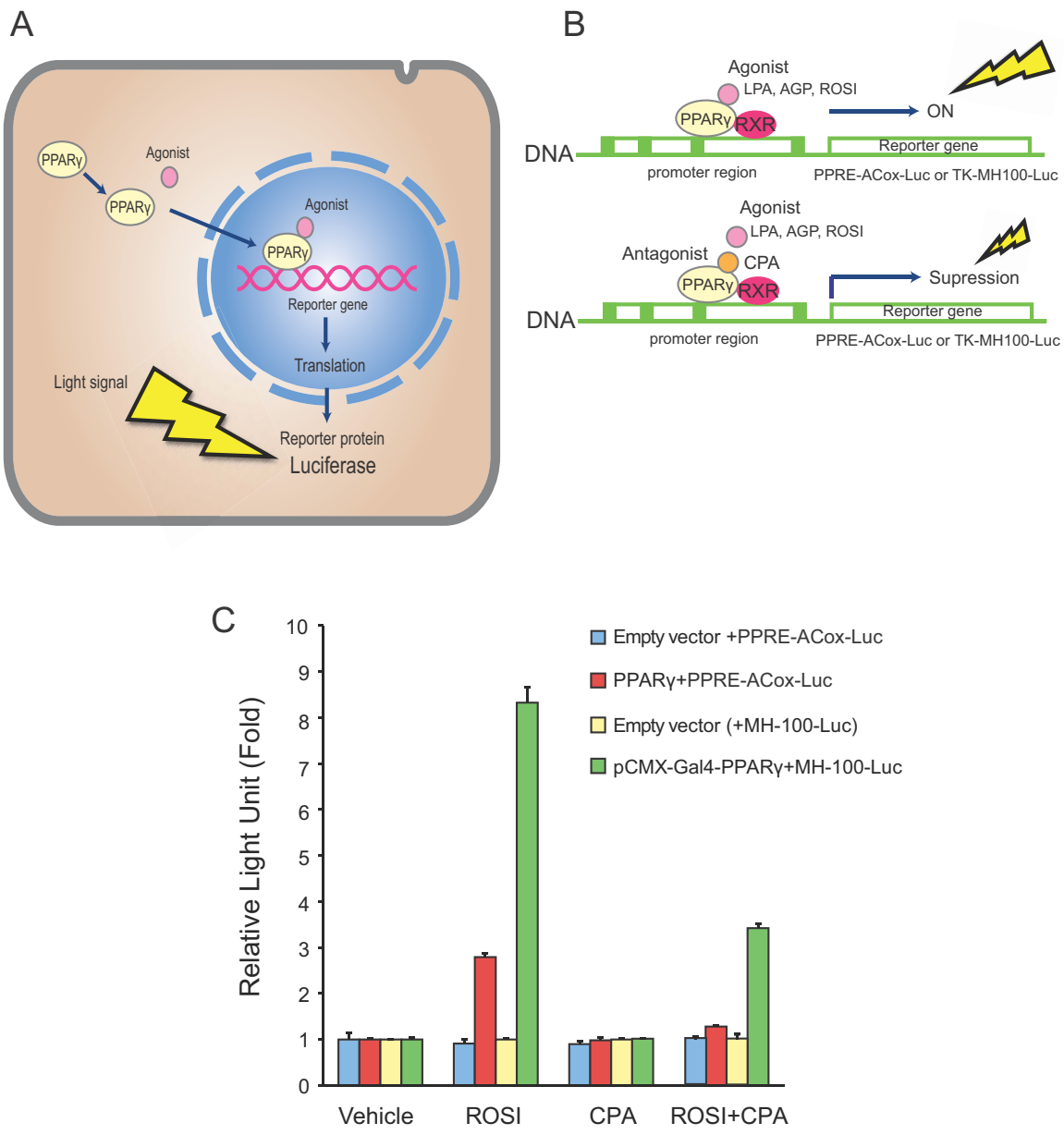

Figure 4-2 CPA inhibits PPARγ-dependent gene expression

(A and B) Schematic diagram of reporter gene assay using PPARγ and its reporter plasmid. PPARγ agonists induce luciferase transcription, whereas PPARγ antagonist inhibits PPARγ agonist-induced reporter gene transcription. (C) CPA suppresses ROSI-induced PPARγ-dependent reporter gene activation in B103 cells. B103 cells (3×10^4) were transfected with reporter plasmid (PPRE-ACox-Luc or TK-MH100-Luc), pcDNA3.1-PPARγ or pCMX-Gal4-PPARγ, and SV40-β-galactosidase. After transfection, the cells were exposed to 10μM CPA with or without ROSI (10 μM) for 20 h, and luciferase activities were measured. Data represent mean ± SEM; n = 4.

low-background cell type for transfection studies. B103 cells, 3.0×10^4 per well, were plated to 96-well plates the day before transfection. Using LipofectAMINE 2000, the cells were transfected with 125 ng of the reporter plasmid (PPRE-ACox-Luc or TK-MH100-Luc), 62.5 ng of pcDNA3.1-PPARγ or pCMX-Gal4-PPARγ, and 12.5 ng of SV40-β-galactosidase (Promega), the latter to monitor transfection efficiency. Twenty hours posttransfection, 10 μM ROSI (Figure 4-1) (ALEXIS Biochemicals), 10 μM AGP 18:1, or 10 μM CPA 18:1 (Avanti Polar Lipids) dissolved in 1% Me_2SO and mixed with Opti-MEM I (Invitrogen) and 1% fetal bovine serum (HyClone) were applied for 20 h at 37°C in the presence of 5% CO_2. Luciferase and β-galactosidase activities were measured with the Steady-Glo luciferase assay system (Promega) and the Galacto-Light Plus system (Applied Biosystems), respectively. Samples were run in quadruplicate, and the means ± S.E. were calculated. Representative data are shown in Figure 4-2C.

4.2.2 Competition Ligand Binding of PPARγ Using ROSI/AGP against LPA/AGP/CPA

PPARγ consists of a ligand binding domain (LBD) and a DNA binding domain (DBD) (Figure 4-3). To test whether LPA/AGP/CPA interacts with the PPARγ LBD, competition ligand binding assays were performed (Figure 4-4A). Hexahistidine (His_6) epitope-tagged PPARγ LBD fusion proteins or empty vector controls containing the His_6 and thrombin recognition site can be expressed in BL-21 (DE3) E. coli cells (Invitrogen). Transformed BL-21 cells were induced using 0.3 mM isopropyl 1-β-D-galactopyranoside (Fisher Scientific) for 12 h at 25°C and collected by centrifugation. The PPARγ LBD was extracted with lysis buffer (50 mM HEPES-KOH, pH 6.8, 200 mM NaCl, 5 mM DTT, 1 mM phenylmethanesulfonyl fluoride, 0.5% Triton X-100, and 15% glycerol) and centrifuged at 12,000 × g for 20 min. Supernatant (1 ml) was incubated with 50 μl of TALON metal affinity resin (BD Biosciences) at 4°C for 1 h in the lysis buffer. The resin was washed five times with wash buffer (50 mM HEPES-KOH, pH 6.8, 200 mM NaCl, 5 mM DTT, 15% glycerol, and 5 mM imidazole) and eluted with 150 mM imidazole in wash buffer. The purity of the PPARγ LBD was determined using sodium dodecyl sulfate-polyacrylamide gel electrophoresis followed by Coomassie Blue staining and western blot analysis using a PPARγ antibody (sc-7196; Santa Cruz Biotechnology). For the equilibrium binding assay, 1 μg of His_6-PPARγ LBD fusion protein (Figure 4-4A) was incubated in binding buffer (50 mM HEPES, pH 6.8, 100 mM NaCl, 5 mM EDTA, and 5 mM DTT) in the presence of 5 nM [^{3}H]ROSI (American Radiolabeled Chemicals) or [^{32}P]AGP at 18°C for 1 h. [^{32}P]AGP 18:1 was synthesized from 1-O-octadecenyl-sn-glycerol 18:1 using recombinant 1,2-diacylglycerol kinase (Calbiochem). 1-O-octadecenyl-sn-glycerol 18:1 was solubilized in 20 μl of an octyl-β-glucoside/cardiolipin solution (7.5% octyl-β-glucoside and 5 mM cardiolipin in 0.5% Triton X-100) by sonication in a bath sonicator (Branson) for 30 s. To the solubilized 1-O-octadecenyl-sn-glycerol 18:1/octyl-β-glucoside/cardiolipin solution was added 50 μl of reaction buffer (100 mM imidazole HCl, pH 6.6, 100 mM NaCl, 25 mM $MgCl_2$, and 2 mM EGTA), 2 μl of 100 mM DTT (freshly prepared), 10 μl of diluted 1,2-diacylglycerol kinase, and water to a total volume of 90 μl. The reaction was started by the addition of 10 μl of [γ-^{32}P]ATP (PerkinElmer; 10 mCi/ml; specific activity,

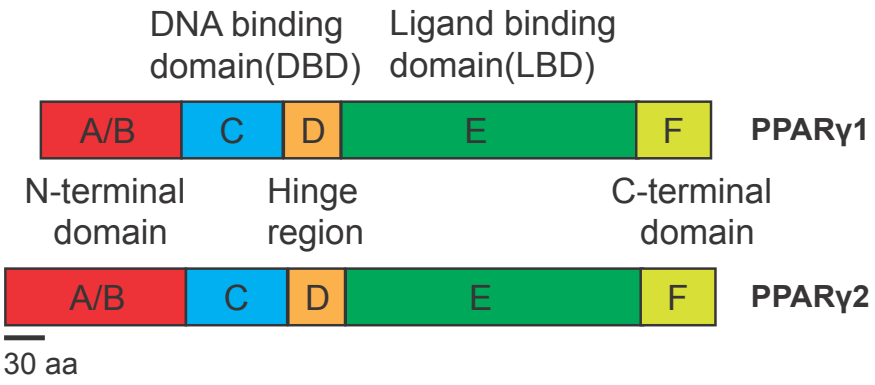

Figure 4-3 The structures of PPARγ$_1$ and PPAR γ$_2$

Human PPARγ$_1$ and PPAR γ$_2$ proteins are 53 and 57 kDa, respectively. The two PPARγ isoforms differ only 30 amino acids at the N-terminal end. Domain C and E represent DNA binding domain (DBD) and ligand binding domain (LBD), respectively.

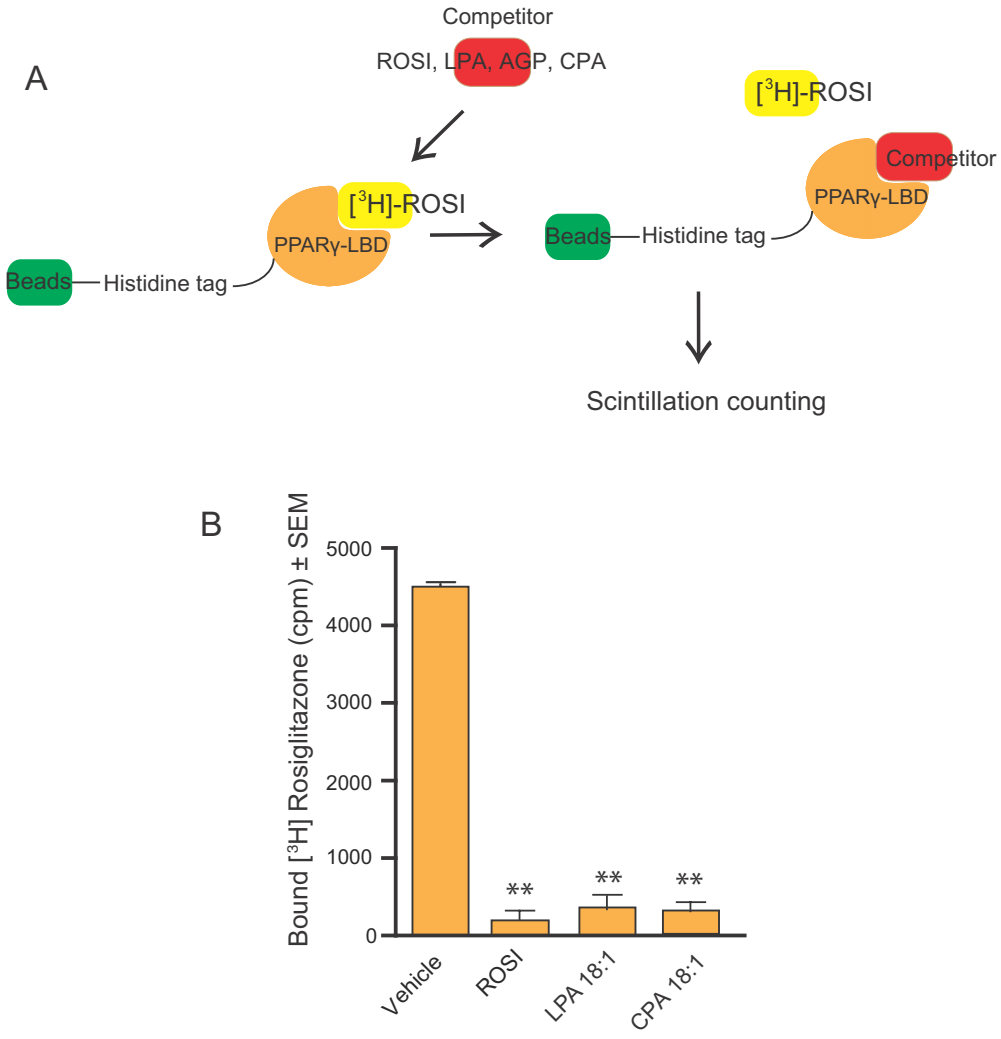

Figure 4-4 CPA is a high affinity ligand of PPARγ

(A) Schematic diagram of competitive ligand binding assay using LPA, AGP, ROSI, and CPA. (B) Competitive displacement of 5 nM [^{3}H]-ROSI from PPARγ-LBD was determined using 2.5 μM cold ROSI, LPA18:1, or CPA. Data are mean ± SEM; **p < 0.01.

111TBq/nmol) and incubated at 25°C for 1 h.

Lipids were extracted by a modification of the method of Bligh and Dyer (Bligh and Dyer, 1959). NaCl (1 M) was added to bring the aqueous volume to 0.8 ml. Total lipid was extracted with 3 ml of chloroform/methanol (1:2, v/v). Then, 1 ml of chloroform and 1 ml of 1 M NaCl were added and phase separated by centrifugation (3,000 × g, 5 min). The lower phase was collected and dried under nitrogen. This was dissolved in 50 µl of chloroform/methanol (1:2, v/v) and was spotted on a Silica Gel 60 (Merck) thin layer chromatography plate. Plates were developed with chloroform/methanol/acetic acid (65:15:5, v/v) and subjected to radioautography. The radioactive spot corresponding to AGP 18:1 was scraped into a scintillation vial. Counting was carried out in an LS-6500 Beckman scintillation counter. The radioligand bound to the PPARγ LBD fusion protein was precipitated using 36% (w/v) polyethylene glycol 8000 (Fisher Scientific) in the presence of 3.3% (w/v) γ-globulin (Sigma-Aldrich), collected on DEAE-81 filter disks (Whatman), and quantified by liquid scintillation counting. Nonspecific binding was determined in the presence of nonradioactive 10 µM AGP. For competition binding assays, 1 µg of His_6-PPARγ LBD protein was incubated at 18°C for 1 h in 200 µl of binding buffer in the presence of 5 nM [^{3}H]ROSI or 5 nM [^{32}P]AGP with or without 2.5 µM cold compounds. The radioactive ligand-bound His_6-PPARγ LBD was collected on DEAE-81 filter disks. The disks were washed three times with wash buffer (50 mM HEPES, pH 6.8, 100 mM NaCl, 5 mM DTT), and bound radioactivity was quantified by scintillation counting. An example of LPA and CPA competition with [^{3}H]ROSI binding is shown in Figure 4-4B.

4.2.3 Corepressor Mammalian Cell Two-Hybrid Assay

This assay was performed to test the effect of CPA on SMRT corepressor binding to PPARγ (Figure 4-5A). CV-1 cells (African green monkey kidney cell line) were grown in Dulbecco's modified Eagle's medium (DMEM) containing 10% fetal bovine serum (FBS) supplemented with 100 IU/ml penicillin G and 100 µg/ml streptomycin at 37°C in a humidified 5% CO_2 atmosphere. The cells were plated onto 96-well plate at the density of 1.0×10^4 cells per well in DMEM containing 10% FBS. The next day, the cells were transiently transfected with 71 ng UAS-Luc, 14.3 ng Gal4-SMRT, 14.3 ng pVP16-PPARγ$_2$, and 10 ng pSV-β-galactosidase (Promega) using Lipofectamine LTX (Invitrogen) and Opti-MEM (Invitrogen) for 20 h. After 20 h transfection, the cells were pretreated with 10 nM, 100 nM, 1 µM, and 10 µM of CPA 18:1 or cyclic glycerophosphate (CGP, Figure 4-1; Avanti Polar Lipids), which is the alkyl ether analog of CPA 18:1, for 30 min, followed by treatment with 1 nM ROSI for 6 h. Luciferase and β-galactosidase activities were measured with the Steady-Glo luciferase assay system (Promega) and the Galacto-Light Plus system (Applied Biosystems), respectively. Samples were run in quintuplicate, and the mean ± SEM were calculated. The data shown in Figure 4-5B are representative of at least three independent transfections. As shown in Figure 4-5B, CPA 18:1 and its ether analog CGP 18:1 dose dependently stabilized the PPARγ-SMRT complex and prevented ROSI-induced dissociation of the complex (*$p < 0.05$; **$p < 0.01$).

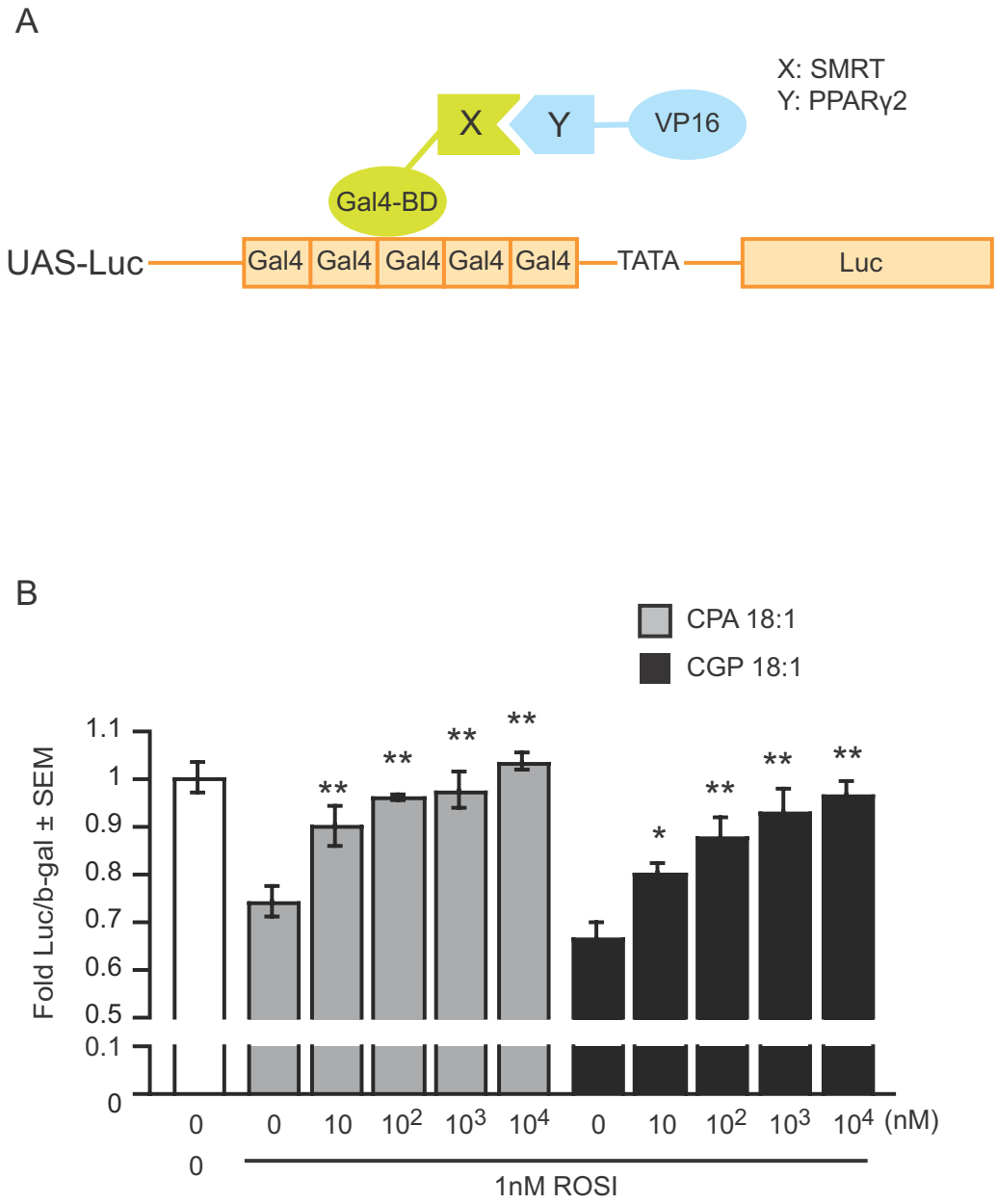

Figure 4-5 CPA inhibits PPARγ activation and recruits PPARγ corepressor

(A) Schematic diagram of two-hybrid assay using full length of SMRT and PPARγ_2. (B) CPA 18:1 and CGP 18:1 dose-dependently inhibited SMRT release from PPARγ induced by ROSI. CV-1 cells were transfected with UAS-Luc, pECE-Gal4-SMRT, pVP16-PPARγ_2, and pSV-β-gal. After transfection, the cells were treated with CPA 18:1 or CGP 18:1 for 30 min, followed by 1 nM ROSI for 6 h, and luciferase activities were measured. Data are mean ± SEM; n = 4; *$p < 0.05$, **$p < 0.01$; representative of three transfections.

4.2.4 Non-Injury Infusion Model Using Rat Carotid Arteries to Elicit Neointima Formation

To examine the regulatory role of CPA in PPARγ-dependent pathophysiological responses, a rat non-injury infusion model was used. The animal procedures were approved by the Institutional Animal Care and Use Committee of the University of Tennessee Health Science Center. Adult male Sprague-Dawley rats weighing 250-300 g were anesthetized with ketamine (80 mg/kg) and xylazine (5 mg/kg). After anesthesia, the forelimbs and incisors were fixed to the surgical board with tape. The hair around the neck was shaved, and the skin was disinfected with povidone-iodine and 70% isopropyl alcohol. The surgery was carried out under a dissecting microscope. The right side of the carotid artery was surgically exposed through a midline incision. The proximal sides of the common carotid artery (CCA) and internal carotid artery (ICA) were ligated using vessel clips (85 gr. pressure, BRI). The distal end of the external carotid artery (ECA) was tied with 5.0 surgical suture (Harvard); subsequently, another 5.0 surgical suture was passed through the proximal end of the ECA and a loose loop was made. A PE-10 catheter (Becton Dickinson) was connected to a servo-controlled peristaltic pump (Model PS-200; Living Systems Instrumentation (ST.Albans, VT)) to maintain the intraarterial pressure at 100 mm Hg. The other end of the PE-10 catheter was inserted into the ECA through arteriotomy without mechanical injury to the CCA. The loose loop was tightened on the ECA to keep the catheter in place. The clip occluding the CCA was temporarily released, and the vessel was rinsed with a retrograde injection of 50 µl of phosphate-buffered saline (PBS) to remove residual blood. The CCA was clipped again, and a treatment solution either 0.1% DMSO (vehicle), 10 µM AGP, 10 µM ROSI, 10 µM PIO, 10 nM insulin, 750 nM FIPI, or the combination of these compounds was applied. The delivery pressure of the solutions was maintained at 100 mm Hg using the peristaltic pump.

In some experiments, ROSI was applied outside the carotid artery in a pluronic gel. Pluronic F-127 (Sigma-Aldrich) was dissolved in PBS (25% w/v) and maintained at 4°C until use. At the time of compound administration via the PE-10 catheter, 100 µl of the pluronic gel containing 100 µM ROSI and 0.1% DMSO was topically applied around the adventitia of the CCA for 1 h. The control group received the pluronic gel without ROSI.

For cotreatment with FIPI, the inhibitor was applied for 30 min as a pretreatment and also included during the application of the PPARγ agonists. After a 60-min incubation, the ligation was loosened to withdraw the catheter and the loop was tied up again to ligate the ECA. The vessel clips on the CCA and ICA were released to restore blood flow. The wound was closed with 4.0 surgical suture. After the surgery, the rats were kept on a warming pad to avoid hypothermia during recovery and were administered Buprenex (0.05 mg/kg). Three weeks after the surgery, transcardial perfusion was performed with 4% buffered paraformaldehyde (pH 7.4), and the CCAs were dissected and postfixed in 4% buffered paraformaldehyde (pH 7.4). The dissected CCAs were embedded in paraffin; and 5-µm thick sections were cut, deparaffinized, and stained with Masson's trichrome stain (Allan Scientific). Neointima formation was

observed under a light microscope. To evaluate neointima progression, the intima-to-media ratio was used. The intima (area between the endothelium and the internal elastic lamina) and media (area between the external and internal elastic lamina) were measured using ImageJ software (version 1.42), and intima-to-media ratios were calculated.

As shown in Figure 4-6 (unpublished data), neointima formation induced by AGP was attenuated by insulin due to the production of CPA through PLD2 activation by insulin (Figure 4-6B, C, and E) (Tsukahara et al., 2010). This insulin effect was blocked by the PLD inhibitor FIPI because the CPA production was not sufficient due to the inhibition of PLD2 activity (Figure 4-6D and E).

Pioglitazone induced arterial wall remodeling; the magnitude, however, was significantly less than that induced by ROSI (Figure 4-7 B, C, and E) (unpublished data). This might be one of the reasons that ROSI shows higher cardiovascular risks. ROSI applied to the outside of CCAs with pluronic gel also induced neointima formation (Figure 4-7D and E), suggesting that ROSI diffused toward the inside of the vessel and promoted arterial wall thickness.

4.2.5 Immunohistochemical Staining

It has been implicated that bone marrow-derived vascular progenitor cells (VPCs) can contribute to neointima formation (Saiura et al., 2001, Zernecke et al., 2005). To assess whether VPCs are recruited to form neointima in response to AGP or ROSI treatment in the non-injury model, immunohistochemical analysis was performed using antibodies to the VSMC marker αSMA and the VPC marker CD133. Five-μm thick cross sections of the rat CCAs were double-stained for αSMA and CD133 to identify VPCs in the neointimal regions. After deparaffinization and rehydration, heat-mediated antigen retrieval was carried out using citrate-based antigen unmasking solution (Vector Laboratories) for 10 min on formalin-fixed tissue slides. After three washes in PBS (pH 7.4), the slides were blocked with blocking solution containing 5% normal goat serum (Vector Laboratories) and 5% normal horse serum (Vector Laboratories) in PBS for 1 h at room temperature. αSMA antibody (mouse monoclonal [clone 1A4], 1:400 dilution; Abcam) and CD133 (rabbit polyclonal [ab19898], 1:100 dilution; Abcam) diluted in blocking solution were applied to the slides and incubated overnight at 4°C. The slides were incubated with fluorescein-conjugated horse anti-mouse IgG (1:200 dilution; Vector Laboratories) secondary antibody or biotinylated goat anti-rabbit IgG (1:500 dilution; Vector Laboratories) secondary antibody dissolved in blocking solution for 30 min, followed by incubation with rhodamine-avidin D (1:1000; Vector Laboratories) for 30 min at room temperature after washes with PBS. The slides were mounted with VECTASHIELD with DAPI (Vector Laboratories) and visualized with a Nikon Eclipse 80i fluorescence microscope.

DMSO-treated CCA showed no CD133-positive cells (Figure 4-8B); however, anti-CD133 staining showed positive cells in the neointimal region (Figure 4-8E), and

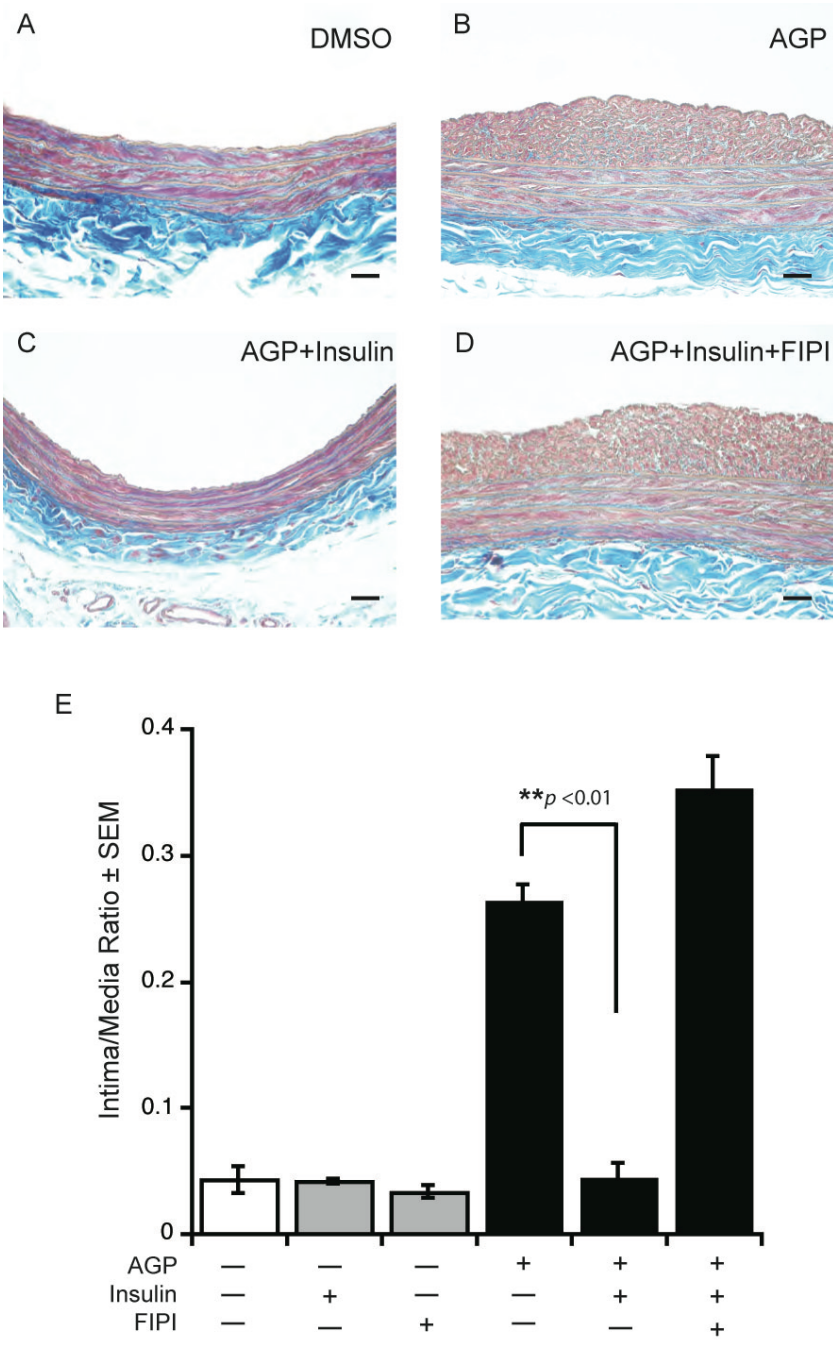

Figure 4-6 PLD inhibitor FIPI inhibits physiological insulin effect on vascular wall remodeling

(A-D) Carotid arteries of anesthetized adult rats were treated with DMSO (vehicle) (A), 10 µM AGP (B), 10 µM AGP and 10 nM insulin (C), or 10 µM AGP, 10 nM insulin, and 750 nM FIPI(D) for 1h. Three weeks after the treatment, the CCAs were dissected and the sections were stained with Masson's trichrome stain. Scale bars represent 200 µm. (E) Quantification of intima/media ratios. Data are mean ± SEM; n=5.

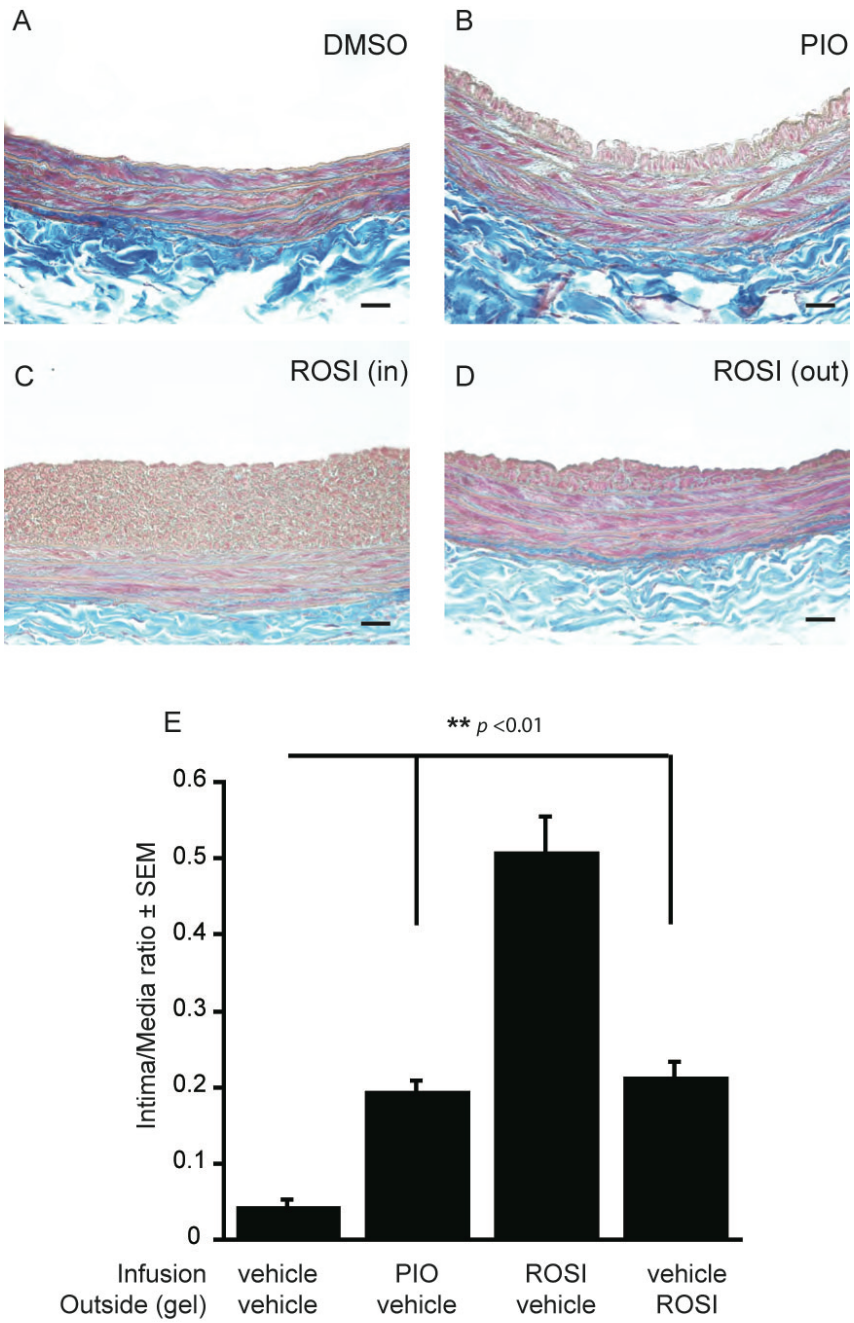

Figure 4-7 PIO induces less neointima and ROSI application from the outside also induces arterial wall thickness

(A-D) Carotid arteries of anesthetized adult rats were transfused with vehicle (A), 10μM PIO (B), or 10 μM ROSI (C) for 1h. 100 μM ROSI was applied to the outside of vessel using 25% pluronic gel for 1h (D). The sections were stained with Masson's trichrome stain. Scale bars represent 200 μm. (E) Quantification of intima/media ratios. Data are mean ± SEM; n=5.

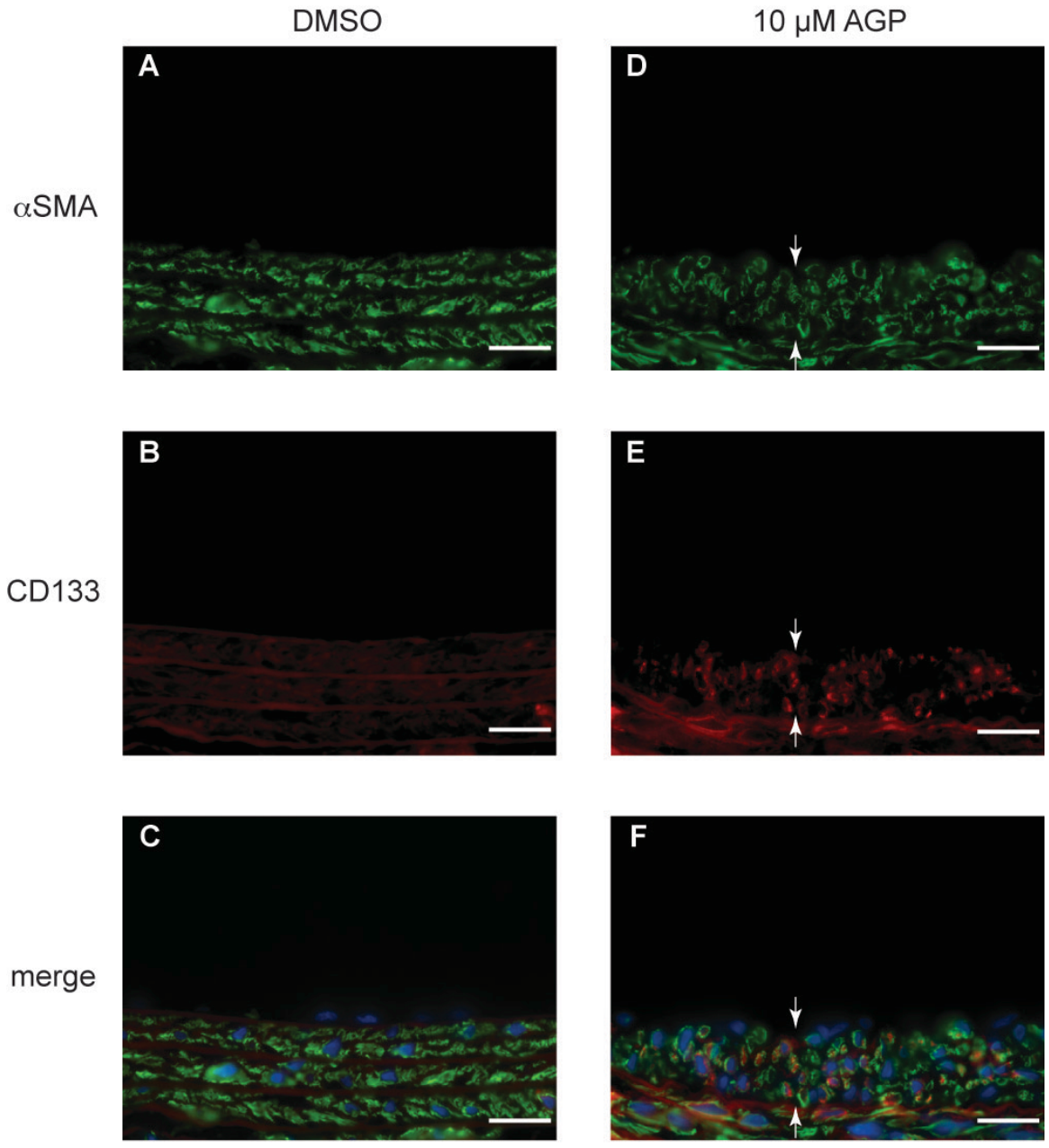

Figure 4-8 Immunohistochemical staining for αSMA and CD133 in the neointima induced by AGP

Rat carotid arteries treated with DMSO (A-C) and 10 μM AGP (D-F) were double-stained for αSMA (green; A and D) and CD133 (red; B and E). The cells were intensively stained with anti-αSMA in the media and neointima layers (A and D). Anti- CD133 stained cells were barely seen (B), however, CD133 positive cells were accumulated in neointima region (E). Double stained cells were seen in the merged image (F). Area between the white arrows is neointima (D-F). Scale bars: 200 μm.

CD133-positive cells were also expressed αSMA (Figure 4-8F).

4.3 SUMMARY

In this chapter, we have focused on the responses mediated by PPARγ modulated by lysophosphatidic acids, especially in the vasculature; and we have introduced some of the fundamental methods for examining the regulation of PPARγ by endogenous lysophosphatidic acids analogs.

CPA is a high-affinity ligand and an endogenous negative regulator of PPARγ, unlike unsaturated acyl species of LPA and AGP, which have agonist properties (Figure 4-9). CPA binds to a site within the LBD, which inhibits PPARγ activation (Figure 4-9). CPA binding to PPARγ facilitates conformational change that leads to recruitment of corepressor SMRT, resulting in stabilization of the SMRT-PPARγ complex. LPA and AGP induce neointima formation through the activation of PPARγ, whereas, CPA inhibits PPARγ-mediated arterial wall remodeling in the non-injury model. In addition, the physiological stimulus of PLD2 is effective in PPARγ-dependent vascular remodeling, and this effect is blocked by the PLD inhibitor FIPI *in vivo*. When vehicle-treated CCAs were stained for CD133, no CD133-positive cells were observed; however, CD133-positive cells were seen in the neointimal region when the artery was treated with AGP. Moreover, the CD133-positive cells in the neointimal region also expressed αSMA, suggesting that VPCs are recruited to form neointima in response to AGP. There are some controversies about the contribution of VPCs (Daniel et al., 2010, Iwata et al., 2010); therefore, further studies are needed to elucidate the role of LPA GPCR and PPARγ in the regulation of VPCs.

These observations detailed in this present chapter were intended to point to the intracellular signaling role of LPA and its analogs. Thus, LPAs fulfill dual roles as mediators through the activation of cell surface GPCRs and as second messenger intracellularly through the activation/inhibition of PPARγ. Overall, our findings may provide a novel mechanism for the regulation of PPARγ and they open novel therapeutic opportunities. Further clarification of the PLD2-CPA axis could lead us to the possibility of synthesizing novel medicines acting on PPARγ.

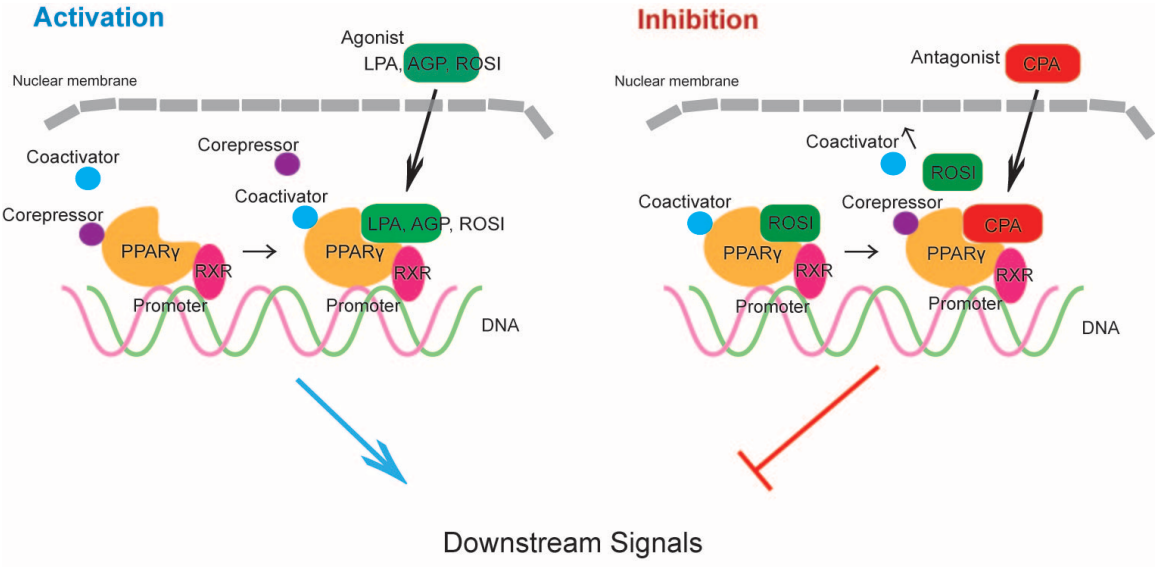

Figure 4-9 Schematic diagram of the PPARγ signaling

LPA, AGP, and ROSI activate PPARγ and promote downstream signals, whereas CPA negatively regulates PPARγ. CPA stabilizes PPARγ-SMRT corepressor complex and inhibits PPARγ-mediated post signal transduction.

LIST OF REFERENCES

Akiyama TE, Sakai S, Lambert G, Nicol CJ, Matsusue K, Pimprale S, Lee YH, Ricote M, Glass CK, Brewer HB, Jr., Gonzalez FJ (2002) Conditional disruption of the peroxisome proliferator-activated receptor gamma gene in mice results in lowered expression of ABCA1, ABCG1, and apoE in macrophages and reduced cholesterol efflux. Mol Cell Biol 22:2607-2619.

Alexander JS, Patton WF, Christman BW, Cuiper LL, Haselton FR (1998) Platelet-derived lysophosphatidic acid decreases endothelial permeability *in vitro*. Am J Physiol 274:H115-122.

Angeli V, Llodra J, Rong JX, Satoh K, Ishii S, Shimizu T, Fisher EA, Randolph GJ (2004) Dyslipidemia associated with atherosclerotic disease systemically alters dendritic cell mobilization. Immunity 21:561-574.

Anliker B, Chun J (2004) Cell surface receptors in lysophospholipid signaling. Semin Cell Dev Biol 15:457-465.

Aoki J, Taira A, Takanezawa Y, Kishi Y, Hama K, Kishimoto T, Mizuno K, Saku K, Taguchi R, Arai H (2002) Serum lysophosphatidic acid is produced through diverse phospholipase pathways. J Biol Chem 277:48737-48744.

Asami-Miyagishi R, Iseki S, Usui M, Uchida K, Kubo H, Morita I (2004) Expression and function of PPARgamma in rat placental development. Biochem Biophys Res Commun 315:497-501.

Asmis R, Begley JG, Jelk J, Everson WV (2005) Lipoprotein aggregation protects human monocyte-derived macrophages from oxLDL-induced cytotoxicity. J Lipid Res 46:1124-1132.

Baim D, Brady TJ, Casscells SW, Dunne M, Fayad Z, Fuster V, Gazelle S, Heldman A, Hatsukami T, Kinlay S, Lafont A, Lee R, Libby P, Meier B, Muller JE, Naghavi M, O'Donnell C, Perin E, Rekhter M, Rumberger J, Russell M, Schwartz R, Selwyn A, Strauss HW, Tearney G, Tomaru T, Tuzcu EM, Wasserman B (2002) Thoughts on the role of the healing professions and the events of September 11, 2001. Circulation 105:1509-1510.

Baker DL, Desiderio DM, Miller DD, Tolley B, Tigyi GJ (2001) Direct quantitative analysis of lysophosphatidic acid molecular species by stable isotope dilution electrospray ionization liquid chromatography-mass spectrometry. Anal Biochem 292:287-295.

Baker DL, Fujiwara Y, Pigg KR, Tsukahara R, Kobayashi S, Murofushi H, Uchiyama A, Murakami-Murofushi K, Koh E, Bandle RW, Byun HS, Bittman R, Fan D, Murph M, Mills GB, Tigyi G (2006) Carba analogs of cyclic phosphatidic acid are selective inhibitors of autotaxin and cancer cell invasion and metastasis. J Biol Chem 281:22786-22793.

Baker DL, Morrison P, Miller B, Riely CA, Tolley B, Westermann AM, Bonfrer JM, Bais E, Moolenaar WH, Tigyi G (2002) Plasma lysophosphatidic acid concentration and ovarian cancer. JAMA 287:3081-3082.

Baker PR, Lin Y, Schopfer FJ, Woodcock SR, Groeger AL, Batthyany C, Sweeney S, Long MH, Iles KE, Baker LM, Branchaud BP, Chen YE, Freeman BA (2005) Fatty acid transduction of nitric oxide signaling: multiple nitrated unsaturated fatty acid derivatives exist in human blood and urine and serve as endogenous peroxisome proliferator-activated receptor ligands. J Biol Chem 280:42464-42475.

Bandoh K, Aoki J, Taira A, Tsujimoto M, Arai H, Inoue K (2000) Lysophosphatidic acid (LPA) receptors of the EDG family are differentially activated by LPA species. Structure-activity relationship of cloned LPA receptors. FEBS Lett 478:159-165.

Banno Y, Takuwa Y, Akao Y, Okamoto H, Osawa Y, Naganawa T, Nakashima S, Suh PG, Nozawa Y (2001) Involvement of phospholipase D in sphingosine 1-phosphate-induced activation of phosphatidylinositol 3-kinase and Akt in Chinese hamster ovary cells overexpressing EDG3. J Biol Chem 276:35622-35628.

Bligh EG, Dyer WJ (1959) A rapid method of total lipid extraction and purification. Can J Biochem Physiol 37:911-917.

Bolen AL, Naren AP, Yarlagadda S, Beranova-Giorgianni S, Chen L, Norman D, Baker DL, Rowland MM, Best MD, Sano T, Tsukahara T, Liliom K, Igarashi Y, Tigyi G (2011) The phospholipase A1 activity of lysophospholipase A-I links platelet activation to LPA production during blood coagulation. J Lipid Res 52:958-970.

Boullier A, Gillotte KL, Horkko S, Green SR, Friedman P, Dennis EA, Witztum JL, Steinberg D, Quehenberger O (2000) The binding of oxidized low density lipoprotein to mouse CD36 is mediated in part by oxidized phospholipids that are associated with both the lipid and protein moieties of the lipoprotein. J Biol Chem 275:9163-9169.

Breen DM, Chan KK, Dhaliwall JK, Ward MR, Al Koudsi N, Lam L, De Souza M, Ghanim H, Dandona P, Stewart DJ, Bendeck MP, Giacca A (2009) Insulin increases reendothelialization and inhibits cell migration and neointimal growth after arterial injury. Arterioscler Thromb Vasc Biol 29:1060-1066.

Brown FD, Thompson N, Saqib KM, Clark JM, Powner D, Thompson NT, Solari R, Wakelam MJ (1998) Phospholipase D1 localises to secretory granules and lysosomes and is plasma-membrane translocated on cellular stimulation. Curr Biol 8:835-838.

Camp HS, Ren D, Leff T (2002) Adipogenesis and fat-cell function in obesity and diabetes. Trends Mol Med 8:442-447.

Carrigan SO, Pink DB, Stadnyk AW (2007) Neutrophil transepithelial migration in response to the chemoattractant fMLP but not C5a is phospholipase D-dependent and related to the use of CD11b/CD18. J Leukoc Biol 82:1575-1584.

Chakravarthy MV, Lodhi IJ, Yin L, Malapaka RR, Xu HE, Turk J, Semenkovich CF (2009) Identification of a physiologically relevant endogenous ligand for PPARalpha in liver. Cell 138:476-488.

Chen JD, Evans RM (1995) A transcriptional co-repressor that interacts with nuclear hormone receptors. Nature 377:454-457.

Chen X, Yang XY, Wang ND, Ding C, Yang YJ, You ZJ, Su Q, Chen JH (2003) Serum lysophosphatidic acid concentrations measured by dot immunogold filtration assay in patients with acute myocardial infarction. Scand J Clin Lab Invest 63:497-503.

Cheng Y, Makarova N, Tsukahara R, Guo H, E S, Farrar P, Balazs L, Zhang C, Tigyi G (2009) Lysophosphatidic acid-induced arterial wall remodeling: requirement of PPARgamma but not LPA1 or LPA2 GPCR. Cell Signal 21:1874-1884.

Choi JW, Herr DR, Noguchi K, Yung YC, Lee CW, Mutoh T, Lin ME, Teo ST, Park KE, Mosley AN, Chun J (2010) LPA receptors: subtypes and biological actions. Annu Rev Pharmacol Toxicol 50:157-186.

Chun J, Hla T, Lynch KR, Spiegel S, Moolenaar WH (2010) International union of basic and clinical pharmacology. LXXVIII. Lysophospholipid receptor nomenclature. Pharmacol Rev 62:579-587.

Cockcroft S (1996) ARF-regulated phospholipase D: a potential role in membrane traffic. Chem Phys Lipids 80:59-80.

Colley WC, Sung TC, Roll R, Jenco J, Hammond SM, Altshuller Y, Bar-Sagi D, Morris AJ, Frohman MA (1997) Phospholipase D2, a distinct phospholipase D isoform with novel regulatory properties that provokes cytoskeletal reorganization. Curr Biol 7:191-201.

Contos JJ, Fukushima N, Weiner JA, Kaushal D, Chun J (2000) Requirement for the LPA1 lysophosphatidic acid receptor gene in normal suckling behavior. Proc Natl Acad Sci U S A 97:13384-13389.

Contos JJ, Ishii I, Fukushima N, Kingsbury MA, Ye X, Kawamura S, Brown JH, Chun J (2002) Characterization of lpa(2) (Edg4) and lpa(1)/lpa(2) (Edg2/Edg4) lysophosphatidic acid receptor knockout mice: signaling deficits without obvious phenotypic abnormality attributable to lpa(2). Mol Cell Biol 22:6921-6929.

Cremers B, Flesch M, Kostenis E, Maack C, Niedernberg A, Stoff A, Sudkamp M, Wendler O, Bohm M (2003) Modulation of myocardial contractility by lysophosphatidic acid (LPA). J Mol Cell Cardiol 35:71-80.

Cui MZ, Laag E, Sun L, Tan M, Zhao G, Xu X (2006) Lysophosphatidic acid induces early growth response gene 1 expression in vascular smooth muscle cells: CRE and SRE mediate the transcription. Arterioscler Thromb Vasc Biol 26:1029-1035.

Daniel JM, Bielenberg W, Stieger P, Weinert S, Tillmanns H, Sedding DG (2010) Time-course analysis on the differentiation of bone marrow-derived progenitor cells into smooth muscle cells during neointima formation. Arterioscler Thromb Vasc Biol 30:1890-1896.

Davies SS, Pontsler AV, Marathe GK, Harrison KA, Murphy RC, Hinshaw JC, Prestwich GD, Hilaire AS, Prescott SM, Zimmerman GA, McIntyre TM (2001) Oxidized alkyl phospholipids are specific, high affinity peroxisome proliferator-activated receptor gamma ligands and agonists. J Biol Chem 276:16015-16023.

Delerive P, Martin-Nizard F, Chinetti G, Trottein F, Fruchart JC, Najib J, Duriez P, Staels B (1999) Peroxisome proliferator-activated receptor activators inhibit thrombin-induced endothelin-1 production in human vascular endothelial cells by inhibiting the activator protein-1 signaling pathway. Circ Res 85:394-402.

Deng W, E S, Tsukahara R, Valentine WJ, Durgam G, Gududuru V, Balazs L, Manickam V, Arsura M, VanMiddlesworth L, Johnson LR, Parrill AL, Miller DD, Tigyi G (2007) The lysophosphatidic acid type 2 receptor is required for protection against radiation-induced intestinal injury. Gastroenterology 132:1834-1851.

Diep QN, Schiffrin EL (2001) Increased expression of peroxisome proliferator-activated receptor-alpha and -gamma in blood vessels of spontaneously hypertensive rats. Hypertension 38:249-254.

Dowell P, Ishmael JE, Avram D, Peterson VJ, Nevrivy DJ, Leid M (1999) Identification of nuclear receptor corepressor as a peroxisome proliferator-activated receptor alpha interacting protein. J Biol Chem 274:15901-15907.

Du G, Huang P, Liang BT, Frohman MA (2004) Phospholipase D2 localizes to the plasma membrane and regulates angiotensin II receptor endocytosis. Mol Biol Cell 15:1024-1030.

Duval C, Chinetti G, Trottein F, Fruchart JC, Staels B (2002) The role of PPARs in atherosclerosis. Trends Mol Med 8:422-430.

E S, Lai YJ, Tsukahara R, Chen CS, Fujiwara Y, Yue J, Yu JH, Guo H, Kihara A, Tigyi G, Lin FT (2009) Lysophosphatidic acid 2 receptor-mediated supramolecular complex formation regulates its antiapoptotic effect. J Biol Chem 284:14558-14571.

Eichholtz T, Jalink K, Fahrenfort I, Moolenaar WH (1993) The bioactive phospholipid lysophosphatidic acid is released from activated platelets. Biochem J 291 (Pt 3):677-680.

Eisen SF, Brown HA (2002) Selective estrogen receptor (ER) modulators differentially regulate phospholipase D catalytic activity in ER-negative breast cancer cells. Mol Pharmacol 62:911-920.

Evans RM (2005) The nuclear receptor superfamily: a rosetta stone for physiology. Mol Endocrinol 19:1429-1438.

Exton JH (2002) Regulation of phospholipase D. FEBS Lett 531:58-61.

Fajas L, Auboeuf D, Raspe E, Schoonjans K, Lefebvre AM, Saladin R, Najib J, Laville M, Fruchart JC, Deeb S, Vidal-Puig A, Flier J, Briggs MR, Staels B, Vidal H, Auwerx J (1997) The organization, promoter analysis, and expression of the human PPARgamma gene. J Biol Chem 272:18779-18789.

Fischer DJ, Liliom K, Guo Z, Nusser N, Virag T, Murakami-Murofushi K, Kobayashi S, Erickson JR, Sun G, Miller DD, Tigyi G (1998) Naturally occurring analogs of lysophosphatidic acid elicit different cellular responses through selective activation of multiple receptor subtypes. Mol Pharmacol 54:979-988.

Fischer DJ, Nusser N, Virag T, Yokoyama K, Wang D, Baker DL, Bautista D, Parrill AL, Tigyi G (2001) Short-chain phosphatidates are subtype-selective antagonists of lysophosphatidic acid receptors. Mol Pharmacol 60:776-784.

Forman BM, Tontonoz P, Chen J, Brun RP, Spiegelman BM, Evans RM (1995) 15-Deoxy-delta 12, 14-prostaglandin J2 is a ligand for the adipocyte determination factor PPAR gamma. Cell 83:803-812.

Friedman P, Haimovitz R, Markman O, Roberts MF, Shinitzky M (1996) Conversion of lysophospholipids to cyclic lysophosphatidic acid by phospholipase D. J Biol Chem 271:953-957.

Froberg K, Andersen LB (2005) Mini review: physical activity and fitness and its relations to cardiovascular disease risk factors in children. Int J Obes (Lond) 29 Suppl 2:S34-39.

Frohman MA, Sung TC, Morris AJ (1999) Mammalian phospholipase D structure and regulation. Biochim Biophys Acta 1439:175-186.

Fueller M, Wang DA, Tigyi G, Siess W (2003) Activation of human monocytic cells by lysophosphatidic acid and sphingosine-1-phosphate. Cell Signal 15:367-375.

Fujiwara Y, Sardar V, Tokumura A, Baker D, Murakami-Murofushi K, Parrill A, Tigyi G (2005) Identification of residues responsible for ligand recognition and regioisomeric selectivity of lysophosphatidic acid receptors expressed in mammalian cells. J Biol Chem 280:35038-35050.

Fujiwara Y, Sebok A, Meakin S, Kobayashi T, Murakami-Murofushi K, Tigyi G (2003) Cyclic phosphatidic acid elicits neurotrophin-like actions in embryonic hippocampal neurons. J Neurochem 87:1272-1283.

Fukushima N, Kimura Y, Chun J (1998) A single receptor encoded by vzg-1/lpa1/edg-2 couples to G proteins and mediates multiple cellular responses to lysophosphatidic acid. Proc Natl Acad Sci U S A 95:6151-6156.

Goldberg RB, Kendall DM, Deeg MA, Buse JB, Zagar AJ, Pinaire JA, Tan MH, Khan MA, Perez AT, Jacober SJ (2005) A comparison of lipid and glycemic effects of pioglitazone and rosiglitazone in patients with type 2 diabetes and dyslipidemia. Diabetes Care 28:1547-1554.

Gosset P, Charbonnier AS, Delerive P, Fontaine J, Staels B, Pestel J, Tonnel AB, Trottein F (2001) Peroxisome proliferator-activated receptor gamma activators affect the maturation of human monocyte-derived dendritic cells. Eur J Immunol 31:2857-2865.

Guan Y, Hao C, Cha DR, Rao R, Lu W, Kohan DE, Magnuson MA, Redha R, Zhang Y, Breyer MD (2005) Thiazolidinediones expand body fluid volume through PPARgamma stimulation of ENaC-mediated renal salt absorption. Nat Med 11:861-866.

Gueguen G, Gaige B, Grevy JM, Rogalle P, Bellan J, Wilson M, Klaebe A, Pont F, Simon MF, Chap H (1999) Structure-activity analysis of the effects of lysophosphatidic acid on platelet aggregation. Biochemistry 38:8440-8450.

Gugger M, White R, Song S, Waser B, Cescato R, Riviere P, Reubi JC (2008) GPR87 is an overexpressed G-protein coupled receptor in squamous cell carcinoma of the lung. Dis Markers 24:41-50.

Guo H, Makarova N, Cheng Y, E S, Ji RR, Zhang C, Farrar P, Tigyi G (2008) The early and late stages in phenotypic modulation of vascular smooth muscle cells: differential roles for lysophosphatidic acid. Biochim Biophys Acta 1781:571-581.

Haffner SM, Greenberg AS, Weston WM, Chen H, Williams K, Freed MI (2002) Effect of rosiglitazone treatment on nontraditional markers of cardiovascular disease in patients with type 2 diabetes mellitus. Circulation 106:679-684.

Haseruck N, Erl W, Pandey D, Tigyi G, Ohlmann P, Ravanat C, Gachet C, Siess W (2004) The plaque lipid lysophosphatidic acid stimulates platelet activation and platelet-monocyte aggregate formation in whole blood: involvement of P2Y1 and P2Y12 receptors. Blood 103:2585-2592.

Hausmann J, Kamtekar S, Christodoulou E, Day JE, Wu T, Fulkerson Z, Albers HM, van Meeteren LA, Houben AJ, van Zeijl L, Jansen S, Andries M, Hall T, Pegg LE, Benson TE, Kasiem M, Harlos K, Kooi CW, Smyth SS, Ovaa H, Bollen M, Morris AJ, Moolenaar WH, Perrakis A (2011) Structural basis of substrate discrimination and integrin binding by autotaxin. Nat Struct Mol Biol 18:198-204.

Hayashi K, Takahashi M, Nishida W, Yoshida K, Ohkawa Y, Kitabatake A, Aoki J, Arai H, Sobue K (2001) Phenotypic modulation of vascular smooth muscle cells induced by unsaturated lysophosphatidic acids. Circ Res 89:251-258.

Hodgkinson CP, Ye S (2003) Microarray analysis of peroxisome proliferator-activated receptor-gamma induced changes in gene expression in macrophages. Biochem Biophys Res Commun 308:505-510.

Huang P, Frohman MA (2007) The potential for phospholipase D as a new therapeutic target. Expert Opin Ther Targets 11:707-716.

Ishihara R, Tatsuta M, Iishi H, Baba M, Uedo N, Higashino K, Mukai M, Ishiguro S, Kobayashi S, Murakami-Murofushi K (2004) Attenuation by cyclic phosphatidic acid of peritoneal metastasis of azoxymethane-induced intestinal cancers in Wistar rats. Int J Cancer 110:188-193.

Ishii I, Contos JJ, Fukushima N, Chun J (2000) Functional comparisons of the lysophosphatidic acid receptors, LP(A1)/VZG-1/EDG-2, LP(A2)/EDG-4, and LP(A3)/EDG-7 in neuronal cell lines using a retrovirus expression system. Mol Pharmacol 58:895-902.

Ishii I, Fukushima N, Ye X, Chun J (2004) Lysophospholipid receptors: signaling and biology. Annu Rev Biochem 73:321-354.

Ishii S, Noguchi K, Yanagida K (2009) Non-Edg family lysophosphatidic acid (LPA) receptors. Prostaglandins Other Lipid Mediat 89:57-65.

Iwata H, Manabe I, Fujiu K, Yamamoto T, Takeda N, Eguchi K, Furuya A, Kuro-o M, Sata M, Nagai R (2010) Bone marrow-derived cells contribute to vascular inflammation but do not differentiate into smooth muscle cell lineages. Circulation 122:2048-2057.

Jones JR, Barrick C, Kim KA, Lindner J, Blondeau B, Fujimoto Y, Shiota M, Kesterson RA, Kahn BB, Magnuson MA (2005) Deletion of PPARgamma in adipose tissues of mice protects against high fat diet-induced obesity and insulin resistance. Proc Natl Acad Sci U S A 102:6207-6212.

Jones JR, Shelton KD, Guan Y, Breyer MD, Magnuson MA (2002) Generation and functional confirmation of a conditional null PPARgamma allele in mice. Genesis 32:134-137.

Kaneyuki U, Ueda S, Yamagishi S, Kato S, Fujimura T, Shibata R, Hayashida A, Yoshimura J, Kojiro M, Oshima K, Okuda S (2007) Pitavastatin inhibits lysophosphatidic acid-induced proliferation and monocyte chemoattractant protein-1 expression in aortic smooth muscle cells by suppressing Rac-1-mediated reactive oxygen species generation. Vascul Pharmacol 46:286-292.

Kiec-Wilk B, Dembinska-Kiec A, Olszanecka A, Bodzioch M, Kawecka-Jaszcz K (2005) The selected pathophysiological aspects of PPARs activation. J Physiol Pharmacol 56:149-162.

Kim J, Keys JR, Eckhart AD (2006) Vascular smooth muscle migration and proliferation in response to lysophosphatidic acid (LPA) is mediated by LPA receptors coupling to Gq. Cell Signal 18:1695-1701.

Kim JH, Lee BD, Kim Y, Lee SD, Suh PG, Ryu SH (1999) Cytosolic phospholipase A2-mediated regulation of phospholipase D2 in leukocyte cell lines. J Immunol 163:5462-5470.

Kobayashi T, Tanaka-Ishii R, Taguchi R, Ikezawa H, Murakami-Murofushi K (1999) Existence of a bioactive lipid, cyclic phosphatidic acid, bound to human serum albumin. Life Sci 65:2185-2191.

Kotarsky K, Boketoft A, Bristulf J, Nilsson NE, Norberg A, Hansson S, Owman C, Sillard R, Leeb-Lundberg LM, Olde B (2006) Lysophosphatidic acid binds to and activates GPR92, a G protein-coupled receptor highly expressed in gastrointestinal lymphocytes. J Pharmacol Exp Ther 318:619-628.

Kou R, Igarashi J, Michel T (2002) Lysophosphatidic acid and receptor-mediated activation of endothelial nitric-oxide synthase. Biochemistry 41:4982-4988.

Lala DS, Mukherjee R, Schulman IG, Koch SS, Dardashti LJ, Nadzan AM, Croston GE, Evans RM, Heyman RA (1996) Activation of specific RXR heterodimers by an antagonist of RXR homodimers. Nature 383:450-453.

Lautamaki R, Airaksinen KE, Seppanen M, Toikka J, Luotolahti M, Ball E, Borra R, Harkonen R, Iozzo P, Stewart M, Knuuti J, Nuutila P (2005) Rosiglitazone improves myocardial glucose uptake in patients with type 2 diabetes and coronary artery disease: a 16-week randomized, double-blind, placebo-controlled study. Diabetes 54:2787-2794.

Law RE, Goetze S, Xi XP, Jackson S, Kawano Y, Demer L, Fishbein MC, Meehan WP, Hsueh WA (2000) Expression and function of PPARgamma in rat and human vascular smooth muscle cells. Circulation 101:1311-1318.

Lee CS, Kwon YW, Yang HM, Kim SH, Kim TY, Hur J, Park KW, Cho HJ, Kang HJ, Park YB, Kim HS (2009) New mechanism of rosiglitazone to reduce neointimal hyperplasia: activation of glycogen synthase kinase-3beta followed by inhibition of MMP-9. Arterioscler Thromb Vasc Biol 29:472-479.

Lee CW, Rivera R, Gardell S, Dubin AE, Chun J (2006) GPR92 as a new G12/13- and Gq-coupled lysophosphatidic acid receptor that increases cAMP, LPA5. J Biol Chem 281:23589-23597.

Lee Z, Cheng CT, Zhang H, Subler MA, Wu J, Mukherjee A, Windle JJ, Chen CK, Fang X (2008) Role of LPA4/p2y9/GPR23 in negative regulation of cell motility. Mol Biol Cell 19:5435-5445.

Leesnitzer LM, Parks DJ, Bledsoe RK, Cobb JE, Collins JL, Consler TG, Davis RG, Hull-Ryde EA, Lenhard JM, Patel L, Plunket KD, Shenk JL, Stimmel JB, Therapontos C, Willson TM, Blanchard SG (2002) Functional consequences of cysteine modification in the ligand binding sites of peroxisome proliferator activated receptors by GW9662. Biochemistry 41:6640-6650.

Lehmann JM, Moore LB, Smith-Oliver TA, Wilkison WO, Willson TM, Kliewer SA (1995) An antidiabetic thiazolidinedione is a high affinity ligand for peroxisome proliferator-activated receptor gamma (PPAR gamma). J Biol Chem 270:12953-12956.

Lehrke M, Lazar MA (2005) The many faces of PPARgamma. Cell 123:993-999.

Leslie DS, Dascher CC, Cembrola K, Townes MA, Hava DL, Hugendubler LC, Mueller E, Fox L, Roura-Mir C, Moody DB, Vincent MS, Gumperz JE, Illarionov PA, Besra GS, Reynolds CG, Brenner MB (2008) Serum lipids regulate dendritic cell CD1 expression and function. Immunology 125:289-301.

Levy AP, Levy JE, Kalet-Litman S, Miller-Lotan R, Levy NS, Asaf R, Guetta J, Yang C, Purushothaman KR, Fuster V, Moreno PR (2007) Haptoglobin genotype is a determinant of iron, lipid peroxidation, and macrophage accumulation in the atherosclerotic plaque. Arterioscler Thromb Vasc Biol 27:134-140.

Li AC, Brown KK, Silvestre MJ, Willson TM, Palinski W, Glass CK (2000) Peroxisome proliferator-activated receptor gamma ligands inhibit development of atherosclerosis in LDL receptor-deficient mice. J Clin Invest 106:523-531.

Li AC, Glass CK (2002) The macrophage foam cell as a target for therapeutic intervention. Nat Med 8:1235-1242.

Li Y, Zhang J, Schopfer FJ, Martynowski D, Garcia-Barrio MT, Kovach A, Suino-Powell K, Baker PR, Freeman BA, Chen YE, Xu HE (2008) Molecular recognition of nitrated fatty acids by PPAR gamma. Nat Struct Mol Biol 15:865-867.

Lim S, Jin CJ, Kim M, Chung SS, Park HS, Lee IK, Lee CT, Cho YM, Lee HK, Park KS (2006) PPARgamma gene transfer sustains apoptosis, inhibits vascular smooth muscle cell proliferation, and reduces neointima formation after balloon injury in rats. Arterioscler Thromb Vasc Biol 26:808-813.

Lin CI, Chen CN, Chen JH, Lee H (2006) Lysophospholipids increase IL-8 and MCP-1 expressions in human umbilical cord vein endothelial cells through an IL-1-dependent mechanism. J Cell Biochem 99:1216-1232.

Lin CI, Chen CN, Huang MT, Lee SJ, Lin CH, Chang CC, Lee H (2008) Lysophosphatidic acid upregulates vascular endothelial growth factor-C and tube formation in human endothelial cells through LPA(1/3), COX-2, and NF-kappaB activation- and EGFR transactivation-dependent mechanisms. Cell Signal 20:1804-1814.

Lin CI, Chen CN, Lin PW, Chang KJ, Hsieh FJ, Lee H (2007) Lysophosphatidic acid regulates inflammation-related genes in human endothelial cells through LPA1 and LPA3. Biochem Biophys Res Commun 363:1001-1008.

Lin DA, Boyce JA (2005) IL-4 regulates MEK expression required for lysophosphatidic acid-mediated chemokine generation by human mast cells. J Immunol 175:5430-5438.

Liscovitch M (1996) Phospholipase D: role in signal transduction and membrane traffic. J Lipid Mediat Cell Signal 14:215-221.

Liscovitch M, Czarny M, Fiucci G, Tang X (2000) Phospholipase D: molecular and cell biology of a novel gene family. Biochem J 345 (Pt 3):401-415.

Llodra J, Angeli V, Liu J, Trogan E, Fisher EA, Randolph GJ (2004) Emigration of monocyte-derived cells from atherosclerotic lesions characterizes regressive, but not progressive, plaques. Proc Natl Acad Sci U S A 101:11779-11784.

Marx N, Schonbeck U, Lazar MA, Libby P, Plutzky J (1998) Peroxisome proliferator-activated receptor gamma activators inhibit gene expression and migration in human vascular smooth muscle cells. Circ Res 83:1097-1103.

McIntyre TM, Pontsler AV, Silva AR, St Hilaire A, Xu Y, Hinshaw JC, Zimmerman GA, Hama K, Aoki J, Arai H, Prestwich GD (2003) Identification of an intracellular receptor for lysophosphatidic acid (LPA): LPA is a transcellular PPARgamma agonist. Proc Natl Acad Sci U S A 100:131-136.

Medina-Gomez G, Virtue S, Lelliott C, Boiani R, Campbell M, Christodoulides C, Perrin C, Jimenez-Linan M, Blount M, Dixon J, Zahn D, Thresher RR, Aparicio S, Carlton M, Colledge WH, Kettunen MI, Seppanen-Laakso T, Sethi JK, O'Rahilly S, Brindle K, Cinti S, Oresic M, Burcelin R, Vidal-Puig A (2005) The link between nutritional status and insulin sensitivity is dependent on the adipocyte-specific peroxisome proliferator-activated receptor-gamma2 isoform. Diabetes 54:1706-1716.

Meredith D, Panchatcharam M, Miriyala S, Tsai YS, Morris AJ, Maeda N, Stouffer GA, Smyth SS (2009) Dominant-negative loss of PPARgamma function enhances smooth muscle cell proliferation, migration, and vascular remodeling. Arterioscler Thromb Vasc Biol 29:465-471.

Meydani M (2001) Vitamin E and atherosclerosis: beyond prevention of LDL oxidation. J Nutr 131:366S-368S.

Minamikawa J, Tanaka S, Yamauchi M, Inoue D, Koshiyama H (1998) Potent inhibitory effect of troglitazone on carotid arterial wall thickness in type 2 diabetes. J Clin Endocrinol Metab 83:1818-1820.

Monovich L, Mugrage B, Quadros E, Toscano K, Tommasi R, LaVoie S, Liu E, Du Z, LaSala D, Boyar W, Steed P (2007) Optimization of halopemide for phospholipase D2 inhibition. Bioorg Med Chem Lett 17:2310-2311.

Moore KJ, Rosen ED, Fitzgerald ML, Randow F, Andersson LP, Altshuler D, Milstone DS, Mortensen RM, Spiegelman BM, Freeman MW (2001) The role of PPAR-gamma in macrophage differentiation and cholesterol uptake. Nat Med 7:41-47.

Muehlich S, Schneider N, Hinkmann F, Garlichs CD, Goppelt-Struebe M (2004) Induction of connective tissue growth factor (CTGF) in human endothelial cells by lysophosphatidic acid, sphingosine-1-phosphate, and platelets. Atherosclerosis 175:261-268.

Mukai M, Imamura F, Ayaki M, Shinkai K, Iwasaki T, Murakami-Murofushi K, Murofushi H, Kobayashi S, Yamamoto T, Nakamura H, Akedo H (1999) Inhibition of tumor invasion and metastasis by a novel lysophosphatidic acid (cyclic LPA). Int J Cancer 81:918-922.

Munnik T, Arisz SA, De Vrije T, Musgrave A (1995) G protein activation stimulates phospholipase D signaling in plants. The Plant Cell 7:2197-2210.

Murakami M, Shiraishi A, Tabata K, Fujita N (2008) Identification of the orphan GPCR, P2Y(10) receptor as the sphingosine-1-phosphate and lysophosphatidic acid receptor. Biochem Biophys Res Commun 371:707-712.

Murakami-Murofushi K, Mukai M, Kobayashi S, Kobayashi T, Tigyi G, Murofushi H (2000) A novel lipid mediator, cyclic phosphatidic acid (cPA), and its biological functions. Ann N Y Acad Sci 905:319-321.

Murakami-Murofushi K, Uchiyama A, Fujiwara Y, Kobayashi T, Kobayashi S, Mukai M, Murofushi H, Tigyi G (2002) Biological functions of a novel lipid mediator, cyclic phosphatidic acid. Biochim Biophys Acta 1582:1-7.

Nagy L, Tontonoz P, Alvarez JG, Chen H, Evans RM (1998) Oxidized LDL regulates macrophage gene expression through ligand activation of PPARgamma. Cell 93:229-240.

Nakane S, Tokumura A, Waku K, Sugiura T (2001) Hen egg yolk and white contain high amounts of lysophosphatidic acids, growth factor-like lipids: distinct molecular species compositions. Lipids 36:413-419.

Negro R, Mangieri T, Dazzi D, Pezzarossa A, Hassan H (2005) Rosiglitazone effects on blood pressure and metabolic parameters in nondipper diabetic patients. Diabetes Res Clin Pract 70:20-25.

Nissen SE, Wolski K (2007) Effect of rosiglitazone on the risk of myocardial infarction and death from cardiovascular causes. N Engl J Med 356:2457-2471.

Nissen SE, Wolski K (2010) Rosiglitazone revisited: an updated meta-analysis of risk for myocardial infarction and cardiovascular mortality. Arch Intern Med 170:1191-1201.

Nolte RT, Wisely GB, Westin S, Cobb JE, Lambert MH, Kurokawa R, Rosenfeld MG, Willson TM, Glass CK, Milburn MV (1998) Ligand binding and co-activator assembly of the peroxisome proliferator-activated receptor-gamma. Nature 395:137-143.

Pamuklar Z, Federico L, Liu S, Umezu-Goto M, Dong A, Panchatcharam M, Fulkerson Z, Berdyshev E, Natarajan V, Fang X, van Meeteren LA, Moolenaar WH, Mills GB, Morris AJ, Smyth SS (2009) Autotaxin/lysopholipase D and lysophosphatidic acid regulate murine hemostasis and thrombosis. J Biol Chem 284:7385-7394.

Panchatcharam M, Miriyala S, Yang F, Rojas M, End C, Vallant C, Dong A, Lynch K, Chun J, Morris AJ, Smyth SS (2008) Lysophosphatidic acid receptors 1 and 2 play roles in regulation of vascular injury responses but not blood pressure. Circ Res 103:662-670.

Papaspyridonos M, McNeill E, de Bono JP, Smith A, Burnand KG, Channon KM, Greaves DR (2008) Galectin-3 is an amplifier of inflammation in atherosclerotic plaque progression through macrophage activation and monocyte chemoattraction. Arterioscler Thromb Vasc Biol 28:433-440.

Pasternack SM, von Kugelgen I, Aboud KA, Lee YA, Ruschendorf F, Voss K, Hillmer AM, Molderings GJ, Franz T, Ramirez A, Nurnberg P, Nothen MM, Betz RC (2008) G protein-coupled receptor P2Y5 and its ligand LPA are involved in maintenance of human hair growth. Nat Genet 40:329-334.

Plevin R, Cook SJ, Palmer S, Wakelam MJ (1991) Multiple sources of sn-1,2-diacylglycerol in platelet-derived-growth-factor-stimulated Swiss 3T3 fibroblasts. Evidence for activation of phosphoinositidase C and phosphatidylcholine-specific phospholipase D. Biochem J 279 (Pt 2):559-565.

Rangwala SM, Lazar MA (2004) Peroxisome proliferator-activated receptor gamma in diabetes and metabolism. Trends Pharmacol Sci 25:331-336.

Ricote M, Glass CK (2007) PPARs and molecular mechanisms of transrepression. Biochim Biophys Acta 1771:926-935.

Ricote M, Huang J, Fajas L, Li A, Welch J, Najib J, Witztum JL, Auwerx J, Palinski W, Glass CK (1998) Expression of the peroxisome proliferator-activated receptor gamma (PPARgamma) in human atherosclerosis and regulation in macrophages by colony stimulating factors and oxidized low density lipoprotein. Proc Natl Acad Sci U S A 95:7614-7619.

Riebeling C, Morris AJ, Shields D (2009) Phospholipase D in the Golgi apparatus. Biochim Biophys Acta 1791:876-880.

Rizza C, Leitinger N, Yue J, Fischer DJ, Wang DA, Shih PT, Lee H, Tigyi G, Berliner JA (1999) Lysophosphatidic acid as a regulator of endothelial/leukocyte interaction. Lab Invest 79:1227-1235.

Rosen ED, MacDougald OA (2006) Adipocyte differentiation from the inside out. Nat Rev Mol Cell Biol 7:885-896.

Ross R (1999) Atherosclerosis is an inflammatory disease. Am Heart J 138:S419-420.

Rother E, Brandl R, Baker DL, Goyal P, Gebhard H, Tigyi G, Siess W (2003) Subtype-selective antagonists of lysophosphatidic acid receptors inhibit platelet activation triggered by the lipid core of atherosclerotic plaques. Circulation 108:741-747.

Saiura A, Sata M, Hirata Y, Nagai R, Makuuchi M (2001) Circulating smooth muscle progenitor cells contribute to atherosclerosis. Nat Med 7:382-383.

Sano T, Baker D, Virag T, Wada A, Yatomi Y, Kobayashi T, Igarashi Y, Tigyi G (2002) Multiple mechanisms linked to platelet activation result in lysophosphatidic acid and sphingosine 1-phosphate generation in blood. J Biol Chem 277:21197-21206.

Sarafidis PA, Lasaridis AN, Nilsson PM, Mouslech TF, Hitoglou-Makedou AD, Stafylas PC, Kazakos KA, Yovos JG, Tourkantonis AA (2005) The effect of rosiglitazone on novel atherosclerotic risk factors in patients with type 2 diabetes mellitus and hypertension. An open-label observational study. Metabolism 54:1236-1242.

Sarraf P, Mueller E, Jones D, King FJ, DeAngelo DJ, Partridge JB, Holden SA, Chen LB, Singer S, Fletcher C, Spiegelman BM (1998) Differentiation and reversal of malignant changes in colon cancer through PPARgamma. Nat Med 4:1046-1052.

Schneider A, Zhang Y, Guan Y, Davis LS, Breyer MD (2003) Differential, inducible gene targeting in renal epithelia, vascular endothelium, and viscera of Mx1Cre mice. Am J Physiol Renal Physiol 284:F411-417.

Schulze C, Smales C, Rubin LL, Staddon JM (1997) Lysophosphatidic acid increases tight junction permeability in cultured brain endothelial cells. J Neurochem 68:991-1000.

Seimon TA, Wang Y, Han S, Senokuchi T, Schrijvers DM, Kuriakose G, Tall AR, Tabas IA (2009) Macrophage deficiency of p38alpha MAPK promotes apoptosis and plaque necrosis in advanced atherosclerotic lesions in mice. J Clin Invest 119:886-898.

Shimada H, Rajagopalan LE (2010) Rho-kinase mediates lysophosphatidic acid-induced IL-8 and MCP-1 production via p38 and JNK pathways in human endothelial cells. FEBS Lett 584:2827-2832.

Shinkuma S, Akiyama M, Inoue A, Aoki J, Natsuga K, Nomura T, Arita K, Abe R, Ito K, Nakamura H, Ujiie H, Shibaki A, Suga H, Tsunemi Y, Nishie W, Shimizu H (2010) Prevalent LIPH founder mutations lead to loss of P2Y5 activation ability of PA-PLA1alpha in autosomal recessive hypotrichosis. Hum Mutat 31:602-610.

Siess W (2002) Athero- and thrombogenic actions of lysophosphatidic acid and sphingosine-1-phosphate. Biochim Biophys Acta 1582:204-215.

Siess W (2006) Platelet interaction with bioactive lipids formed by mild oxidation of low-density lipoprotein. Pathophysiol Haemost Thromb 35:292-304.

Siess W, Tigyi G (2004) Thrombogenic and atherogenic activities of lysophosphatidic acid. J Cell Biochem 92:1086-1094.

Siess W, Zangl KJ, Essler M, Bauer M, Brandl R, Corrinth C, Bittman R, Tigyi G, Aepfelbacher M (1999) Lysophosphatidic acid mediates the rapid activation of platelets and endothelial cells by mildly oxidized low density lipoprotein and accumulates in human atherosclerotic lesions. Proc Natl Acad Sci U S A 96:6931-6936.

Slaaby R, Du G, Altshuller YM, Frohman MA, Seedorf K (2000) Insulin-induced phospholipase D1 and phospholipase D2 activity in human embryonic kidney-293 cells mediated by the phospholipase C gamma and protein kinase C alpha signalling cascade. Biochem J 351 (Pt 3):613-619.

Spector AA (2003) Plaque rupture, lysophosphatidic acid, and thrombosis. Circulation 108:641-643.

Stapleton CM, Mashek DG, Wang S, Nagle CA, Cline GW, Thuillier P, Leesnitzer LM, Li LO, Stimmel JB, Shulman GI, Coleman RA (2011) Lysophosphatidic acid activates peroxisome proliferator activated receptor-gamma in CHO cells that over-express glycerol 3-phosphate acyltransferase-1. PloS one 6:e18932.

Stocker R, Keaney JF, Jr. (2004) Role of oxidative modifications in atherosclerosis. Physiol Rev 84:1381-1478.

Su W, Yeku O, Olepu S, Genna A, Park JS, Ren H, Du G, Gelb MH, Morris AJ, Frohman MA (2009) 5-Fluoro-2-indolyl des-chlorohalopemide (FIPI), a phospholipase D pharmacological inhibitor that alters cell spreading and inhibits chemotaxis. Mol Pharmacol 75:437-446.

Subramanian P, Karshovska E, Reinhard P, Megens RT, Zhou Z, Akhtar S, Schumann U, Li X, van Zandvoort M, Ludin C, Weber C, Schober A (2010) Lysophosphatidic acid receptors LPA1 and LPA3 promote CXCL12-mediated smooth muscle progenitor cell recruitment in neointima formation. Circ Res 107:96-105.

Sugiura T, Nakane S, Kishimoto S, Waku K, Yoshioka Y, Tokumura A, Hanahan DJ (1999) Occurrence of lysophosphatidic acid and its alkyl ether-linked analog in rat brain and comparison of their biological activities toward cultured neural cells. Biochim Biophys Acta 1440:194-204.

Sumida H, Noguchi K, Kihara Y, Abe M, Yanagida K, Hamano F, Sato S, Tamaki K, Morishita Y, Kano MR, Iwata C, Miyazono K, Sakimura K, Shimizu T, Ishii S (2010) LPA4 regulates blood and lymphatic vessel formation during mouse embryogenesis. Blood 116:5060-5070.

Szatmari I, Gogolak P, Im JS, Dezso B, Rajnavolgyi E, Nagy L (2004) Activation of PPARgamma specifies a dendritic cell subtype capable of enhanced induction of iNKT cell expansion. Immunity 21:95-106.

Tabata K, Baba K, Shiraishi A, Ito M, Fujita N (2007) The orphan GPCR GPR87 was deorphanized and shown to be a lysophosphatidic acid receptor. Biochem Biophys Res Commun 363:861-866.

Tai TA, Jennermann C, Brown KK, Oliver BB, MacGinnitie MA, Wilkison WO, Brown HR, Lehmann JM, Kliewer SA, Morris DC, Graves RA (1996) Activation of the nuclear receptor peroxisome proliferator-activated receptor gamma promotes brown adipocyte differentiation. J Biol Chem 271:29909-29914.

Tanaka M, Okudaira S, Kishi Y, Ohkawa R, Iseki S, Ota M, Noji S, Yatomi Y, Aoki J, Arai H (2006) Autotaxin stabilizes blood vessels and is required for embryonic vasculature by producing lysophosphatidic acid. J Biol Chem 281:25822-25830.

Tigyi G (2010) Aiming drug discovery at lysophosphatidic acid targets. Br J Pharmacol 161:241-270.

Tigyi G, Miledi R (1992) Lysophosphatidates bound to serum albumin activate membrane currents in Xenopus oocytes and neurite retraction in PC12 pheochromocytoma cells. J Biol Chem 267:21360-21367.

Tigyi G, Parrill AL (2003) Molecular mechanisms of lysophosphatidic acid action. Prog Lipid Res 42:498-526.

Tokumura A, Fukuzawa K, Akamatsu Y, Yamada S, Suzuki T, Tsukatani H (1978a) Identification of vasopressor phospholipid in crude soybean lecithin. Lipids 13:468-472.

Tokumura A, Fukuzawa K, Tsukatani H (1978b) Effects of synthetic and natural lysophosphatidic acids on the arterial blood pressure of different animal species. Lipids 13:572-574.

Tokumura A, Harada K, Fukuzawa K, Tsukatani H (1983) Biphasic action of platelet-activating factor on isolated guinea-pig ileum. Lipids 18:848-850.

Tokumura A, Iimori M, Nishioka Y, Kitahara M, Sakashita M, Tanaka S (1994) Lysophosphatidic acids induce proliferation of cultured vascular smooth muscle cells from rat aorta. Am J Physiol 267:C204-210.

Tokumura A, Majima E, Kariya Y, Tominaga K, Kogure K, Yasuda K, Fukuzawa K (2002) Identification of human plasma lysophospholipase D, a lysophosphatidic acid-producing enzyme, as autotaxin, a multifunctional phosphodiesterase. J Biol Chem 277:39436-39442.

Tontonoz P, Nagy L, Alvarez JG, Thomazy VA, Evans RM (1998) PPARgamma promotes monocyte/macrophage differentiation and uptake of oxidized LDL. Cell 93:241-252.

Tontonoz P, Spiegelman BM (2008) Fat and beyond: the diverse biology of PPARgamma. Annu Rev Biochem 77:289-312.

Tsuda S, Okudaira S, Moriya-Ito K, Shimamoto C, Tanaka M, Aoki J, Arai H, Murakami-Murofushi K, Kobayashi T (2006) Cyclic phosphatidic acid is produced by autotaxin in blood. J Biol Chem 281:26081-26088.

Tsukahara R, Tsukahahara T, Tigyi G (2011) Regulation of the nuclear hormone receptor PPARgamma by endogenous lysophosphatidic acids. In: Lysophospholipid receptors: Signaling and biochemistry, in press. NJ: Wiley.

Tsukahara T, Tsukahara R, Fujiwara Y, Yue J, Cheng Y, Guo H, Bolen A, Zhang C, Balazs L, Re F, Du G, Frohman MA, Baker DL, Parrill AL, Uchiyama A, Kobayashi T, Murakami-Murofushi K, Tigyi G (2010) Phospholipase D2-dependent inhibition of the nuclear hormone receptor PPARgamma by cyclic phosphatidic acid. Mol Cell 39:421-432.

Tsukahara T, Tsukahara R, Yasuda S, Makarova N, Valentine WJ, Allison P, Yuan H, Baker DL, Li Z, Bittman R, Parrill A, Tigyi G (2006) Different residues mediate recognition of 1-O-oleyllysophosphatidic acid and rosiglitazone in the ligand binding domain of peroxisome proliferator-activated receptor gamma. J Biol Chem 281:3398-3407.

Tzameli I, Fang H, Ollero M, Shi H, Hamm JK, Kievit P, Hollenberg AN, Flier JS (2004) Regulated production of a peroxisome proliferator-activated receptor-gamma ligand during an early phase of adipocyte differentiation in 3T3-L1 adipocytes. J Biol Chem 279:36093-36102.

Uchiyama A, Mukai M, Fujiwara Y, Kobayashi S, Kawai N, Murofushi H, Inoue M, Enoki S, Tanaka Y, Niki T, Kobayashi T, Tigyi G, Murakami-Murofushi K (2007) Inhibition of transcellular tumor cell migration and metastasis by novel carba-derivatives of cyclic phosphatidic acid. Biochim Biophys Acta 1771:103-112.

Umezu-Goto M, Kishi Y, Taira A, Hama K, Dohmae N, Takio K, Yamori T, Mills GB, Inoue K, Aoki J, Arai H (2002) Autotaxin has lysophospholipase D activity leading to tumor cell growth and motility by lysophosphatidic acid production. J Cell Biol 158:227-233.

van Meeteren LA, Ruurs P, Stortelers C, Bouwman P, van Rooijen MA, Pradere JP, Pettit TR, Wakelam MJ, Saulnier-Blache JS, Mummery CL, Moolenaar WH, Jonkers J (2006) Autotaxin, a secreted lysophospholipase D, is essential for blood vessel formation during development. Mol Cell Biol 26:5015-5022.

van Nieuw Amerongen GP, Vermeer MA, van Hinsbergh VW (2000) Role of RhoA and Rho kinase in lysophosphatidic acid-induced endothelial barrier dysfunction. Arterioscler Thromb Vasc Biol 20:E127-133.

Vancura A, Carroll MA, Haldar D (1991) A lysophosphatidic acid-binding cytosolic protein stimulates mitochondrial glycerophosphate acyltransferase. Biochem Biophys Res Commu 175:339-343.

Weatherman RV, Fletterick RJ, Scanlan TS (1999) Nuclear-receptor ligands and ligand-binding domains. Annu Rev Biochem 68:559-581.

Williams JR, Khandoga AL, Goyal P, Fells JI, Perygin DH, Siess W, Parrill AL, Tigyi G, Fujiwara Y (2009) Unique ligand selectivity of the GPR92/LPA5 lysophosphatidate receptor indicates role in human platelet activation. J Biol Chem 284:17304-17319.

Xiao YJ, Schwartz B, Washington M, Kennedy A, Webster K, Belinson J, Xu Y (2001) Electrospray ionization mass spectrometry analysis of lysophospholipids in human ascitic fluids: comparison of the lysophospholipid contents in malignant vs nonmalignant ascitic fluids. Anal Biochem 290:302-313.

Xu J, Kochanek DK, Murphy LS, Tejada-Vera B (2010) Deaths: Final Data for 2007. Natl Vital Stat Rep 58:1-136.

Yanagida K, Masago K, Nakanishi H, Kihara Y, Hamano F, Tajima Y, Taguchi R, Shimizu T, Ishii S (2009) Identification and characterization of a novel lysophosphatidic acid receptor, p2y5/LPA6. J Biol Chem 284:17731-17741.

Yang AH, Ishii I, Chun J (2002) *In vivo* roles of lysophospholipid receptors revealed by gene targeting studies in mice. Biochim Biophys Acta 1582:197-203.

Yang JS, Gad H, Lee SY, Mironov A, Zhang L, Beznoussenko GV, Valente C, Turacchio G, Bonsra AN, Du G, Baldanzi G, Graziani A, Bourgoin S, Frohman MA, Luini A, Hsu VW (2008) A role for phosphatidic acid in COPI vesicle fission yields insights into Golgi maintenance. Nat Cell Biol 10:1146-1153.

Ye X, Hama K, Contos JJ, Anliker B, Inoue A, Skinner MK, Suzuki H, Amano T, Kennedy G, Arai H, Aoki J, Chun J (2005) LPA3-mediated lysophosphatidic acid signalling in embryo implantation and spacing. Nature 435:104-108.

Ye X, Skinner MK, Kennedy G, Chun J (2008) Age-dependent loss of sperm production in mice via impaired lysophosphatidic acid signaling. Biol Reprod 79:328-336.

Yokoyama K, Baker DL, Virag T, Liliom K, Byun H, Tigyi G, Bittman R (2002) Stereochemical properties of lysophosphatidic acid receptor activation and metabolism. Biochim Biophys Acta 1582:295-308.

Yoshida K, Nishida W, Hayashi K, Ohkawa Y, Ogawa A, Aoki J, Arai H, Sobue K (2003) Vascular remodeling induced by naturally occurring unsaturated lysophosphatidic acid *in vivo*. Circulation 108:1746-1752.

Yu C, Markan K, Temple KA, Deplewski D, Brady MJ, Cohen RN (2005) The nuclear receptor corepressors NCoR and SMRT decrease peroxisome proliferator-activated receptor gamma transcriptional activity and repress 3T3-L1 adipogenesis. J Biol Chem 280:13600-13605.

Yu S, Reddy JK (2007) Transcription coactivators for peroxisome proliferator-activated receptors. Biochim Biophys Acta 1771:936-951.

Zernecke A, Schober A, Bot I, von Hundelshausen P, Liehn EA, Mopps B, Mericskay M, Gierschik P, Biessen EA, Weber C (2005) SDF-1alpha/CXCR4 axis is instrumental in neointimal hyperplasia and recruitment of smooth muscle progenitor cells. Circ Res 96:784-791.

Zhang C, Baker DL, Yasuda S, Makarova N, Balazs L, Johnson LR, Marathe GK, McIntyre TM, Xu Y, Prestwich GD, Byun HS, Bittman R, Tigyi G (2004) Lysophosphatidic acid induces neointima formation through PPARgamma activation. J Exp Med 199:763-774.

Zheng Y, Rodrik V, Toschi A, Shi M, Hui L, Shen Y, Foster DA (2006) Phospholipase D couples survival and migration signals in stress response of human cancer cells. J Biol Chem 281:15862-15868.

Zhou Z, Subramanian P, Sevilmis G, Globke B, Soehnlein O, Karshovska E, Megens R, Heyll K, Chun J, Saulnier-Blache JS, Reinholz M, van Zandvoort M, Weber C, Schober A (2011) Lipoprotein-derived lysophosphatidic acid promotes atherosclerosis by releasing CXCL1 from the endothelium. Cell Metab 13:592-600.

APPENDIX. SUPPLEMENTAL INFORMATION FOR CHAPTER 3

A.1 MATERIALS AND METHODS

A.1.1 Materials

Oleoyl cyclic phosphatidic acid (CPA 18:1) and 1-O-octadecenyl cyclic glycerophosphate (CGP 18:1), oleoyl lysophosphatidic acid (LPA 18:1), 1-O-octadecenyl glycerophosphate (AGP 18:1), monooleoyl glycerol (MG), and 1-O-octadecenyl glycerol (AG) were purchased from Avanti Polar Lipids. CPA 18:1 was repurified by thin layer chromatography (TLC) using chloroform-methanol-ammonium hydroxide (3:6:1) on fluorescent indicator-free Silica Gel 60 TLC plates (Whatman), and its purity was determined using negative ion liquid chromatography- mass spectrometry (data not shown). 2-(4,4-difluoro-5,7-dimethyl-4-bora-3a,4a-diaza-*s*-indacene-3-dodecanoyl)-1-hexadecanoyl-*sn*-glycero-3-phosphocholine (β-BODIPY FL C_{12}-HPC) was obtained from Invitrogen Japan. *Rhizopus delemer* lipase and phospholipase D from *Actinomadura* sp. No. 362 were purchased from Seikagaku Co. (Tokyo, Japan). [^{32}P]-AGP 18:1 was synthesized from AG using purified recombinant 1,2-diacylglycerol kinase (Calbiochem). Oleic acid (OA), 4α-phorbol 12-myristate 13-acetate (PMA), WY-14643, and L-165041 were purchased from Sigma. [^{3}H]-ROSI (50 Ci/mmol) was purchased from American Radiolabeled Chemicals, and cold ROSI, TRO and PIO from ALEXIS Biochemicals, Inc. [^{32}P]-Orthophosphoric acid (314-337 TBq/mmol) was purchased from PerkinElmer. Mastoparan was from Bachem. Polyclonal anti-rabbit PPARγ antibody (H-100) was purchased from Santa Cruz Biotechnology Inc. Polyclonal anti-rabbit FABP4 was purchased from Cell Signaling Technology.

A.1.2 Plasmids and Vectors

SV40-β-galactosidase (Promega), pET15b (Novagen) and pcDNA3.1 (Invitrogen) vectors were purchased. WT pcDNA3.1-PPARγ$_1$ (amino acids 1-475) and pET15b-PPARγ$_1$-LBD (amino acids 173-475) were used as templates for mutagenesis as described (Tsukahara et al., 2006). MH-100-PPRE-TK-Luciferase and pCMX-PPARγ-Gal4 vectors were a gift from Dr. Peter Tontonoz (HHMI, UCLA, CA). The construction and application of the pGL3b-PPRE-Luc, pGL3b-PPRE-cd36 plasmids, the PPARα and β/δ reporter gene assays and PLD2 and CI-PLD2 bacmid vectors have been previously described (Colley et al., 1997; Liliom et al., 2006). UAS-Luc, pECE-Gal4-SMRT, and pVP16-PPARγ$_2$ plasmids were a gift from Dr. Ron Cohen (U. Chicago, IL).

A.1.3 Synthesis Cellular Uptake and Visualization of BODIPY-CPA

N-((6-(2,4-dinitrophenyl) amino)hexanoyl)-2-(4,4-difluoro-5,7-dimethyl-4-bora-3a,4a-diaza-*s*-indacene-3-pentanoyl)-1-hexadecanoyl-*sn*-glycero-3-phosphocholine (BODIPY-PC) was deacylated by *Rhizopus delemer* lipase to prepare 2-BODIPY-labeled LPC. 1-BODIPY-labeled LPC was generated through spontaneous acyl migration by incubation at 37ºC for 3 h in 0.1 M TRIS-HCl buffer (pH 9.0). The 1-BODIPY-labeled LPC was converted to BODIPY-CPA by transphosphatidylation using *Actinomadura* phospholipase D as described previously (Tsuda et al., 2006). BODIPY-CPA was added to a final concentration of 3 nmol/well to RAW264.7 cells (1.6×10^6) and cells were incubated for 0.5 to 60 min at 37°C. Cells were centrifuged and washed with ice-cold PBS. The lipids from the cells and medium were separately extracted by the method of Bligh and Dyer, and separated by TLC using chloroform-methanol-acetic acid-1% sodium disulfite (100:40:12:5). Fluorescence images of TLC plates were obtained and quantified with the FOTODYNE Image Analysis system using the Analyst P 5.0 software (FOTODYNE Inc.). For microscopic examination, RAW 264.7 cells were treated with 10 μM BODIPY-CPA and incubated at 37°C for 30 min. Cells were briefly rinsed with PBS and viewed with a NIKON Eclipse 80i fluorescence microscope.

A.1.4 Quantitative Determination of CPA by MS

MDA-MB-231 (3×10^7), 3T3-L1 or RAW 264.7 (3×10^6) cells per sample were used in these experiments. Following serum starvation, cells were treated with 100 nM PMA, 100 nM insulin (Sigma), or vehicle control (1% DMSO) for 30 min at 37°C and washed with PBS and collected by centrifugation (Eppendorf centrifuge, 1,000 rpm, 2 min). Cellular phospholipids were spiked with 100 pmol of CPA 17:0 as internal standard and extracted using chloroform/methanol (200/400 μl), and citrate-phosphate buffer, pH 4.0 (160 μl). Samples were extracted and analyzed by LC-MS as previously described (Baker et al., 2001) with a Thermo-Finnigan LCQ Advantage mass spectrometer. Quantification of the CPA species was done by ratioing the [M- H]- signal intensity for CPA 16:0 and 18:1 to that of the signal intensity of CPA 17:0 internal standard.

LC-MS quantification of CPA in 3T3-L1 or RAW 264.7 cells (3.0×10^6) expressing scrambled shRNA, PLD2 shRNA and WT were pretreated with 30 nM insulin or 100 nM PMA for 30 min. Total lipid was extracted using Bligh & Dyer method with 100 pmol CPA 17:0 (m/z: 405.0) as internal standard and dissolved in 0.1 ml of methanol/ chloroform/ 28% NH_4OH (90:10:0.1) and were immediately analyzed by electrospray ionization LC-MS. LC-MS was performed on an LCMS-2010A mass spectrometer (Shimadzu, Japan) equipped with an Econosphere 3 μm 50 × 4.6 mm silica column (Alltech Associates, IL). The sample was maintained at 250°C with drying gas flow of 1.5 L/min, and data were collected in the negative ion mode from 100 to 1000 *m/z*. The amount of CPA 18:1(m/z: 417.0) produced was estimated by the calibration curve of CPA16:0 (m/z: 391.0) /17:0 (picomoles versus peak area). The final values are shown with the standard errors for the three sets of experiments.

Human PBMC were isolated from Leukopacks by Ficoll-Hystopaque density gradient centrifugation. Monocytes were purified from human PBMC using MACS CD14 microbeads (Miltenyi Biotech). Purity was checked by staining with a FITC conjugated anti-CD14 antibody (Sigma) and FACScan analysis, and routinely found to be higher than 94%. The cells (10^7) were pretreated with or without 750nM FIPI for 30 min followed by treated with 1μg/ml lipoporysaccharide, 100nM PMA, 100nM insulin, or 1mM hydrogen peroxide for 30 min at 37°C. After the treatment the cells were washed with PBS and collected by centrifugation. Total lipids were extracted as described above. The samples were dissolved in 20 μl of chloroform/water/isopropanol/acetonitrile (1:1:1:1) and CPA production was measured by LC- MS/MS. All LC-MS/MS analysis was done with an Applied Biosystems Sciex (Foster City, CA) ABI 4000 QTRAP tandem mass spectrometer equipped with a TurbolonsprayTM interface, a Shimadazu LC-10ADvp pump (Columbia, MD) with a Leap HTS PAL autosampler (Carrboro, NC). Ten microliters of each sample was injected to Tosoh TSK-ODS-100Z column (150mm × 2 mm; silica with 5-μm particle size) with methanol/water (95:5), 5mM ammonium formate solvent with an isocratic flow rate of 0.22ml/min. The data was processed by Analyst software, version 1.5. Various species of CPA were analyzed by multiple reaction monitoring (MRM) in negative ion mode with Q3 (product ion) set at *m/z* 255.1 for CPA16:1, 281.1 for CPA 18:1, and 269.0 for CPA 17:0 (glycerophosphate moiety) (Shan et al., 2008). Q1 was set for the deprotonated molecular ion for all lysophospholipids. Quantification of CPA16:0 and CPA18:1 was done by taking the ratio of peak area to that of CPA 17:0 internal standard.

A.1.5 PLD2 Knockdown

The lentiviral vector pLKO1(clone ID#: TRCN0000076937) containing the validated PLD2 shRNA sequence CCGGGCAGTGTTTCCGAGTCTACTTCTCGAGA AGTAGACTCGGAAACACTGCTTTTTG was purchased from OpenBiosystems (Huntsville, AL.USA). The scrambled shRNA plasmid (#1864) was obtained from Addgene (Cambridge, MA, USA), in which a nonsilencing sequence CCGGCCTAAGGT TAAGTCGCCCTCGCTCTAGCGAGGGCGACTTAACCTTAGGTTTTTG was inserted into lentiviral vector pLKO1. The lentiviruses with scrambled and PLD2 shRNA were produced in UTHSC Viral Vector Core Laboratory (Memphis, TN, USA). Briefly, the shRNAs in pLKO1 were co-transfected into 293FT cells with the packaging plasmids pCMV-VSVG and psPAX2. The supernatant was collected 60 h after transfection and virus particles were collected by ultra-centrifugation. 3T3-L1 and RAW 264.7 cells were transduced by the viruses at 10 MOI. 3T3-L1 and RAW 264.7 stably expressing lenti-mediated shRNA for PLD2 were grown in DMEM containing 10% FBS and puromycin (Sigma) (2.0 μg/ml for 3T3-L1, 3.0 μg/ml for RAW 264.7). The knockdown of PLD2 shRNA was examined by immunoblotting using an antibody specific to PLD2 (gift from Dr. Yoshiko Banno, Gifu University, Japan). RAW264.7 or NIH3T3 cells expressing scrambled shRNA (SC-shRNA) or PLD2 shRNA (PLD2-shRNA) were lysed, the lysates were separated by SDS-PAGE and transferred to a PVDF membrane. The blot was probed with the anti-rabbit anti-PLD2 antibody (1:2000), and incubated with anti-rabbit secondary antibody conjugated to horseradish peroxidase (Promega, Madison,

WI; 1:10000) and visualized using SuperSignal ELISA Pico substrate (Thermo Fisher Scientific Inc., Rockford, IL).

A.1.6 Purification of Recombinant PLD2

Sf-9 insect cells were transduced with recombinant baculoviruses encoding PLD2 or CI-PLD2 at MOI of 10. The cells were grown for 48 h and washed with PBS, lysed on ice by the addition of 3 ml lysis buffer [20 mM TRIS-HCl, pH7.4, 100 mM NaCl, 0.5% Triton X-100, 1 mM PMSF and protease inhibitor cocktail (Sigma)]. After 15 min on ice, the cells were collected by scraping and the lysate was centrifuged at 13,000×g for 30 min at 4°C. The supernatant was mixed with 0.1 ml TALON His-tag Affinity Resin (BD Biosciences) and kept at 4°C with constant agitation for 1 h. PLD2 was eluted after the resin was washed three times with 1 ml of lysis buffer. The purity of the PLD2 preparation was tested by western blotting with a mouse anti-polyhistidine antibody (Sigma) or a rabbit anti-actin (Sigma) primary antibodies, and an anti-mouse or anti-rabbit IgG horseradish peroxidase conjugated secondary antibody (Promega), visualized using the Super Signal kit (Pierce).

A.1.7 *In Vitro* Assay of PLD Activity

Purified PLD2 was incubated with 50 μM [14C]-LPC 16:0 (2.1 GBq/mmol) at 40°C for 1 h in the presence of 10 mM TRIS-HCl, (pH7.2). The reaction was terminated by 30 μl 1-BuOH. The mixture was centrifuged at 12,000×g for 1 min and the upper phase was spotted on Silica Gel 60 TLC plates (Whatman). The plates were developed with chloroform/methanol/acetic acid/1% aqueous sodium metabisulfite (100:40:12:5). Radioactivity was detected using a Cyclone phosphorimager. PLD activity in cell lysates was determined using the Amplex Red PLD kit from Molecular Probes (Eugene, OR).

A.1.8 Oil Red O Stain

RAW 264.7 cells were seeded in Lab-Tek slide-chambers in DMEM at 104 cells per well for 24 h. Acetylated LDL (25 μg/ml) was added. After 24 h, the cells were washed twice with PBS and fixed with 10% formaldehyde in PBS for 10 min. ORO (0.5%) in isopropanol was diluted with 1.5 volumes of distilled water, filtered, and added to the fixed cells for 1 h. Cells were viewed using a Nikon Eclipse 80i microscope. 3T3-L1-derived adipocytes were washed three times with PBS and fixed for 2 min with 10% formaldehyde in PBS. Cells were then washed three-times with wash solution (Chemicon International) and stained with ORO. For the quantification of ORO uptake, cells were extracted using dye extraction solution (Chemicon International), and absorbance was measured at 520 nm in a Shimadzu UV-1700 spectrophotometer.

A.1.9 Induction of Adipocytic Differentiation in 3T3-L1 Cells

Cells were cultured in DMEM supplemented with 10% FBS to reach confluence. 1 μM CPA or vehicle (1% DMSO) was added 24 h prior to induction with 100 nM ROSI with 0.1 - 10 nM insulin. The medium with ligand(s) was replenished every other day. Cytoplasmic lipid droplets were visible by day 5. The cells were cultured following the standard differentiation induction protocol for 14 days. Adipogenesis was determined by staining of lipids with ORO and by RT-PCR and western blotting for the expression of adipocyte marker FABP4.

A.1.10 Animal Experiments

The procedure used in these experiments was approved by the IACUC of the University of Tennessee Health Science Center. The surgical procedure for exposing and cannulating the external and common carotid arteries has been described previously (Zhang et al., 2004). Briefly, 5 μM ROSI or AGP with and without 5 μM CPA or 3 nM insulin were injected into a ligated carotid artery previously rinsed free of blood; the cannula was left in the vessel for 1 h. The cannula was then withdrawn and the external carotid was ligated. The clips isolating the distal and proximal common carotid were released, and blood flow was restored. All animals (groups of 5 for each treatment) received adequate analgesia and preventive antibiotics during recovery. Three weeks post surgery the animals were euthanized, and the carotid arteries were dissected en-block, fixed, and processed for paraffin embedding. Sections 5 μm thick were cut and stained using Masson's trichrome stain (Richard-Allan Scientific Inc.). Intima-to-media ratios were measured using the NIH Image (version 1.62) software.

A.1.11 RNA Extraction and Real-Time Quantitative RT-PCR

C57BL/6 mouse peritoneal macrophages were pretreated with 5 μM CPA or 1μM GW9662 for 15 min and cultured for 12 h in the presence of 5 μM ROSI. 3T3-L1 and RAW 264.7 cells were treated with 30nM insulin or 10μM mastoparan for 30 min followed by treated with vehicle or 10μM ROSI for 24h. RNA was isolated by using TRIzol-LS (Invitrogen) and quantitative real-time RT-PCR analysis was performed using 7300 Fast Real-time PCR system, (Applied Biosystems). Transcript levels were normalized to β-actin or GAPDH for 3T3-L1 and RAW 264.7 cells. Experiments were done using four different pools of macrophages collected from 10 mice. RNA from 3T3-L1 cells was isolated using RNAspin Mini kit (GE Healthcare). Assays of reverse transcription were conducted with specific primer for PPARγ, FABP4 and β-actin and 1 μg of total RNA in 25 μl reaction volume. Reverse transcription was performed at 50 °C for 60 min and the PCR conditions were as follows: 94 °C for 30 s, 50 °C for 60 s, and 72 °C for 60 s with initial activation of enzyme at 94 °C for 1 min for a total of 35 cycles.

A.1.12 PCR Primers Used

qPCR; cd36; forward GCCTCCTTTCCACCTTTTGT, reverse TCTGTACACGG GGATTCCTT, cyp27a1; forward GGCACCTTTCCTGAGCTG, reverse CACCAGTCA CTTCCTTGTGC, hadh; forward GACATCCTGGCAAAATCCAA reverse GCTCAGG GTCTTCTCCACAA, capn3; forward TACGCAGGGATCTTCCACTT, reverse GAAC TCATTGCGGTGGTTG, csf1; forward GAGTCTGTCTTCCACCTGCTG, reverse ACT GGCAGTTCCACCTGTCT, pparγ; forward AGGGCGATCTTGACAGGAA, reverse C ACCTCTTTGCTCTGCTCCT, β-actin; forward TTCTACAATGAGCTGCGTGTG reverse GGGGTGTTGAAGGTCTCAAA, pld1; forvard AGTGCTTCAGACTTGTCCT GGTT, reverse ATGGTAGCGTTTCGAGCTGCTGT, pld2; forward TTGCGGAAGCA CTGTTTCAGTGTG, reverse TTGTTCTCCGCTGTTTCTTGCCAC.

RT- PCR; β-actin; forward GACAACGGCTCCGGCATGTG reverse GGCTGG GGTGTTGAAGGTCTCAA, fabp4; forward AATGTGTGATGCCTTTGTGGG reverse TGGCTCATGCCCTTTCA.

A.2 SUPPORTING FIGURES

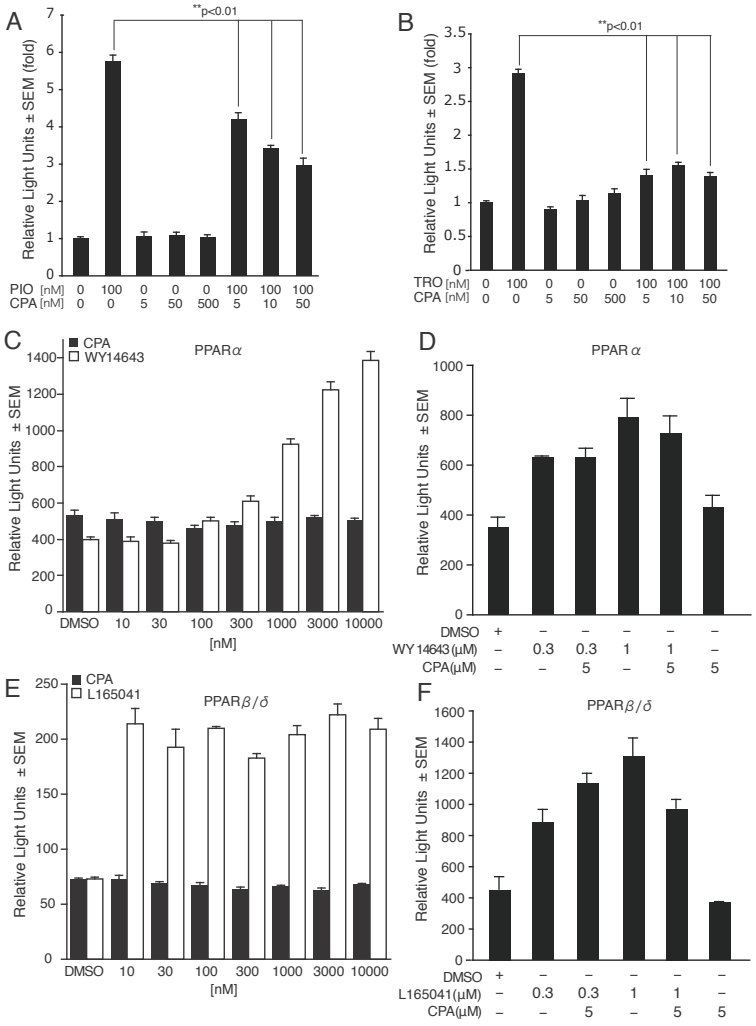

Figure A-1 Inhibition of Pioglitazone (PIO) and Troglitazone (TRO)-induced reporter gene activation by CPA (related to Figure 3-1)

(A and B) CPA dose-dependently suppresses PIO or TRO-induced PPARγ-dependent PPRE-TK- Luc reporter gene activation in B103 cells. The cells were treated for 20 h with ligands and/or different concentrations of CPA as indicated (n=4). Data are representative of two independent transfections. (C-F) CPA does not activate PPARα and PPARβ/δ. CPA did not activate PPARα and β/δ reporter gene expression over a wide-range of concentrations in B103 cells exposed to WY-14643 (C, PPARα-specific agonist) or L-165041 (E, PPARβ/δ-selective agonist) or CPA 18:1 for 20 h. No reporter gene activation was found after treatment with up to 10 μM of CPA, the highest concentration tested, whereas nanomolar concentrations of the synthetic agonists elicited robust expression of the reporter genes. CPA did not inhibit specific agonist induced PPARα or PPARβ/δ activation (D and F).

Figure A-2 PLD2 induces CPA production (related to Figure 3-4)

(A) PMA-induced CPA generation in CHO cells transfected with tet-regulated PLD1 and PLD2 constructs without doxycycline induction. 10^6 Cells biosynthetically labeled with [^{32}P]-orthophosphate were treated with 100 nM PMA for 30 min, and CPA was isolated and separated using 2DTLC and quantified by liquid scintillation counting (n=3). (B) Enzymatic properties of PLD2 using LPC as substrate. Affinity-purified recombinant PLD2 and CI-PLD2 were reacted [^{14}C]-LPC (2.05 GBq/mmol) *in vitro*, and generation of [^{14}C]-CPA was quantified using a [^{14}C]-sensitive phosphorimager screen. The Vmax and Km values were derived from double-reciprocal plots of the data (insets) yielding Vmax=190 pmol/min/mg protein, Km =20 μM for LPC, Data represent the mean ± SEM of values from three experiments. (C-E) Mass spectrometry of CPA production in MDA-MB-231 cells. Cells (3×10^7) were treated with DMSO (vehicle), PMA (100 nM), or insulin (100 nM) for 30 min, spiked with 100 pmol of CPA 17:0 (m/z 405), and CPA was extracted. In vehicle-treated cells (C) CPA was below the detection limit (>10 pmol/3×10^7 cells). In contrast, significant amounts of CPA 16:0 (m/z 391) and CPA 18:1 (m/z 417) were readily detected in PMA- (D) and insulin-treated cells (E). LC- MS/MS quantification of CPA species in unstimulated (F), and insulin (100 nM, G), or PMA (100 nM, I) stimulated human peripheral blood monocytes. The cells were treated for 30 min with the activators and in some cases also pretreated with 750 nM of the PLD2 inhibitor FIPI (H). CPA were analyzed by MRM in negative ion mode monitoring the glycerophosphate moiety at m/z 255.1 for CPA16:1, 281.1 for CPA 18:1, and 269.0 for CPA 17:0 (internal standard). CPA was below the detection limit in unstimulated cells but became detectable after insulin or PMA stimulation. FIPI reduced CPA production.

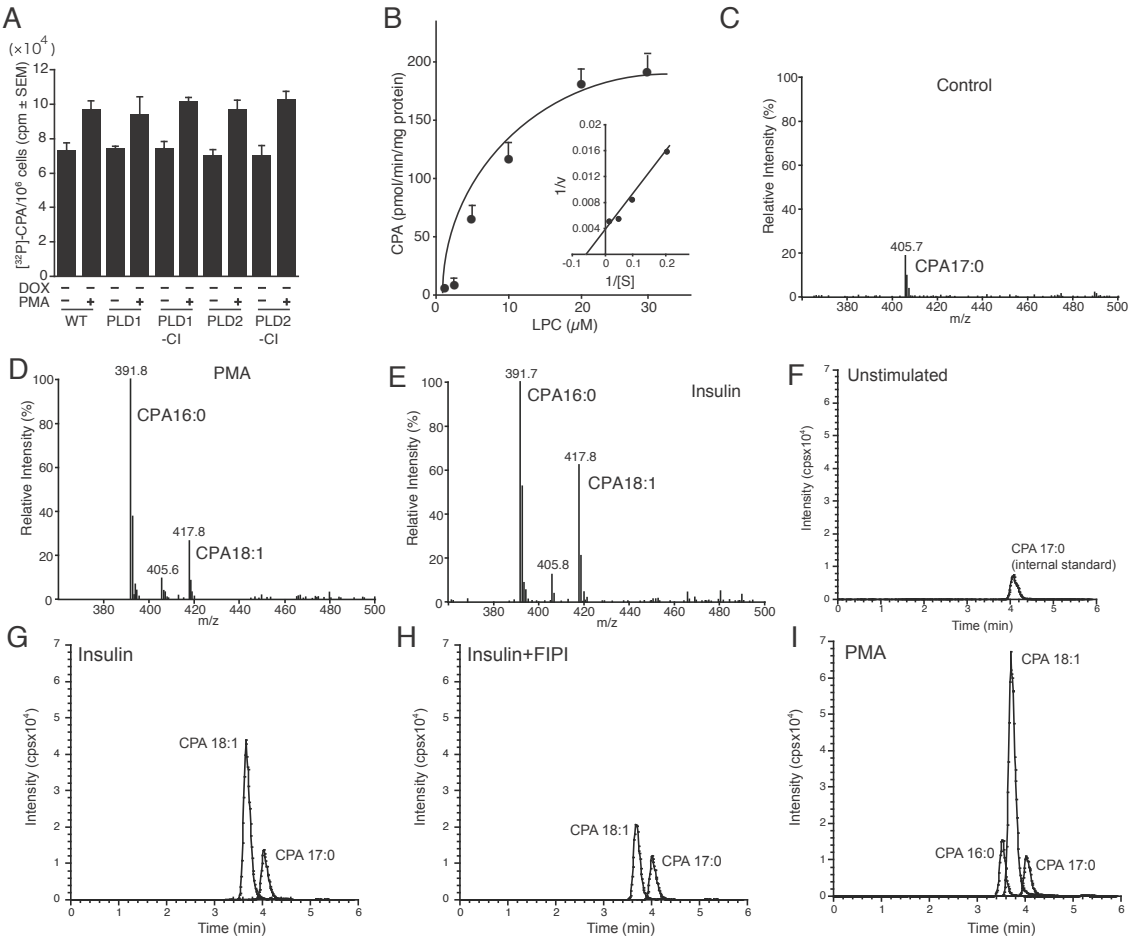
A
(×10^4)
[32P]-CPA/10^6 cells (cpm ± SEM)
DOX
PMA
WT
PLD1
PLD1 -CI
PLD2
PLD2 -CI
B
CPA (pmol/min/mg protein)
LPC (μM)
1/v
1/[S]
C
Control
Relative Intensity (%)
405.7
CPA17:0
m/z
D
PMA
391.8
CPA16:0
417.8
CPA18:1
405.6
E
Insulin
391.7
CPA16:0
417.8
CPA18:1
405.8
F
Unstimulated
Intensity (cpsx10^4)
CPA 17:0
(internal standard)
Time (min)
G
Insulin
CPA 18:1
CPA 17:0
H
Insulin+FIPI
I
PMA
CPA 16:0

Figure A-3 Insulin induced CPA production and PLD2 knock down by shRNA (related to Figure 3-5)

(A-C) Stimulus coupled CPA production in CV-1 cells. Cells (3×10^6) were labeled with [^{32}P]-orthophosphate for 6 h, subsequently exposed to 100 nM insulin or 1% DMSO solvent for 30 min at 37°C, and lipids were extracted and analyzed by 2DTLC and phosphorimaging. (A) [^{32}P]-labeled phospholipids in DMSO treated cells. (B) Primulin staining of the plate shown in panel A spiked with authentic LPA and CPA standards (10 nmols each; A-C designate unidentified phospholipids). (C) [^{32}P]-labeled phospholipids in cells treated with 100 nM insulin. Arrows point to spots co-migrating with the CPA and LPA standard. Note that there in no increase in LPA upon insulin stimulation and as a metabolite of phospholipids synthesis LPA shows a constitutive turnover indicated by the incorporation of the label. In contrast, CPA shows a robust increase upon insulin stimulation. (D and E) shRNA knockdown of PLD2 in RAW 264.7 (D) and 3T3-L1 cells (E). Quantitative RT- PCR showed a selective decrease in pld2 transcripts without significant change in pld1 transcript abundance. (F) Western blotting of PLD2 protein shows diminished levels in the PLD2-shRNA transduced cells compared to WT or scramble shRNA transduced cells.

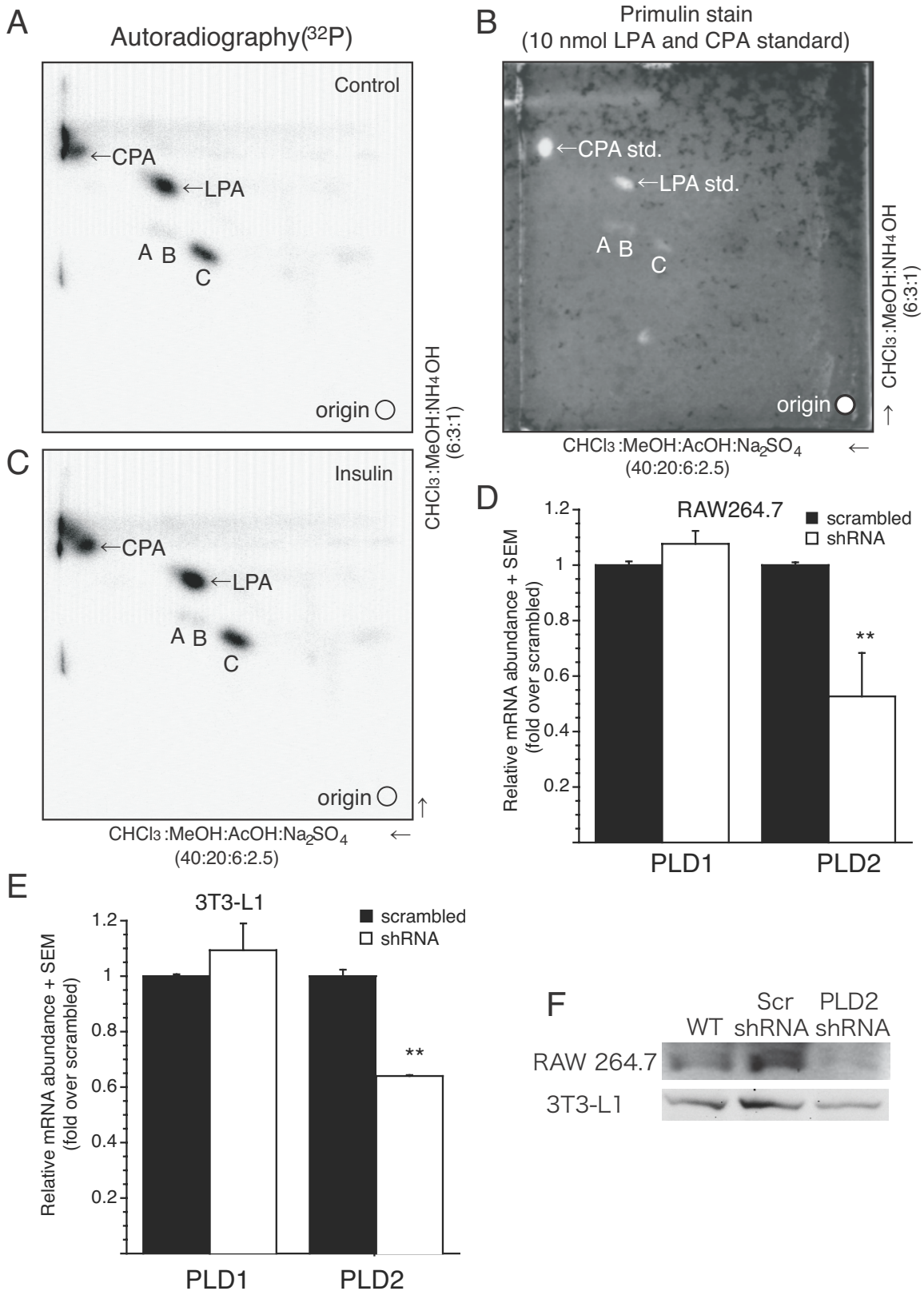
A
Autoradiography(32P)
Control
←CPA
←LPA
A B
C
origin
CHCl3 :MeOH:NH4 OH
(6:3:1)
B
Primulin stain
(10 nmol LPA and CPA standard)
←CPA std.
←LPA std.
A B
C
origin
CHCl3 :MeOH:NH4 OH
(6:3:1)
CHCl3 :MeOH:AcOH:Na2SO4
(40:20:6:2.5)
C
Insulin
←CPA
←LPA
A B
C
origin
CHCl3 :MeOH:AcOH:Na2SO4
(40:20:6:2.5)
D
RAW264.7
scrambled
shRNA
Relative mRNA abundance + SEM
(fold over scrambled)
1.2
1
0.8
0.6
0.4
0.2
**
PLD1
PLD2
E
3T3-L1
scrambled
shRNA
Relative mRNA abundance + SEM
(fold over scrambled)
1.2
1
0.8
0.6
0.4
0.2
**
PLD1
PLD2
F
WT
Scr shRNA
PLD2 shRNA
RAW 264.7
3T3-L1

Figure A-4 CPA and insulin prevent ROSI-induced carotid wall remodeling (related to Figure 3-7)

CPA and insulin inhibit neointima formation induced by ROSI in rat carotid arteries. (A-D) Carotid arteries of anesthetized adult female rats were cannulated and filled with 5 μM ROSI either with or without 5 μM CPA for 1 h; after this treatment, the circulation was restored. Animals were sacrificed 3 weeks later, and the carotid tissue was processed for Masson trichrome staining. (A) In carotids arteries treated with 3% DMSO PBS vehicle no changes in vascular wall morphology were noted. The PPARγ agonist ROSI-induced neointima formation (B) in the common carotid arteries was blocked by co-application of CPA (C, bar, 200 μm). Intima-to-media ratios were determined in the carotids using quantitative image analysis (D). CPA completely abolished ROSI-induced neointima formation. Data represent the mean intima- to-media ratio ± SD of carotid arteries from groups of 5 rats. (E-G) Insulin (3 nM, E) was co-applied with 10 μM ROSI (F) lumenally for 1 h using the described experimental paradigm. Insulin treatment alone induced no vascular remodeling, but it significantly reduced the neointima formation elicited by ROSI. Bar; 200 μm. (G) Data represent the mean intima-to-media ratio ± SD for groups of 5 carotid arteries.

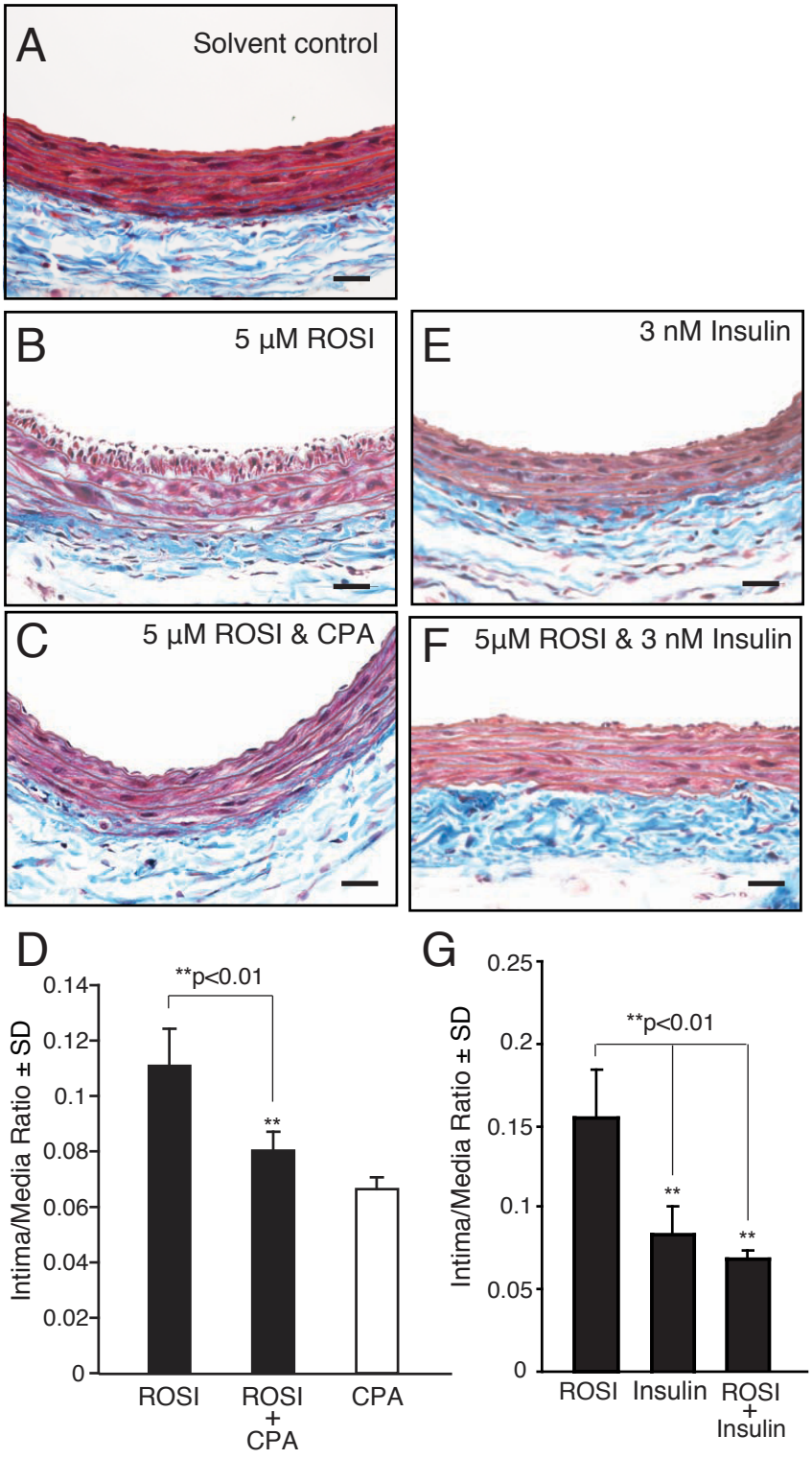
A
Solvent control
B
5 µM ROSI
E
3 nM Insulin
C
5 µM ROSI & CPA
F
5µM ROSI & 3 nM Insulin
D
**p<0.01
Intima/Media Ratio ± SD
0.14
0.12
0.1
0.08
0.06
0.04
0.02
0
**
ROSI
ROSI + CPA
CPA
G
**p<0.01
Intima/Media Ratio ± SD
0.25
0.2
0.15
0.1
0.05
0
**
**
ROSI
Insulin
ROSI + Insulin

VITA

Ryoko Tsukahara was born in 1974 in Kushiro, Japan. She obtained her bachelor degree in Pharmaceutical Sciences from Hokkaido University in Sapporo, Japan in March 1999. She joined the Integrated Program in Biomedical Sciences at the University of Tennessee Health Science Center (UTHSC) in August 2007. She received the J. Paul. Quigley Memorial Scholarship for 2009 and the Dorothy K. and Daniel L. Gerwin Graduate Scholarship for 2010 from the Department of Physiology at UTHSC. She will receive her Doctor of Philosophy degree in December 2011.